

# Investigating 5-HT<sub>2A</sub> receptors – Development of a fluorescent 5HT<sub>2A</sub> receptor agonist and elucidation of the effects of St. John's wort extract STW3-IV, hyperforin and hyperoside on 5HT<sub>2A</sub> receptors

**Dissertation**

zur

Erlangung des Doktorgrades (Dr. rer. nat.)

der Mathematisch-Naturwissenschaftlichen Fakultät

der Rheinischen Friedrich-Wilhelms-Universität Bonn

vorgelegt von

**Stefan Aatz**

aus

Wadern

Bonn 2021



Angefertigt mit Genehmigung der Mathematisch-Naturwissenschaftlichen Fakultät  
der Rheinischen Friedrich-Wilhelms-Universität Bonn.

1. Gutachter: Prof. Dr. Hanns Häberlein

2. Gutachter: Prof. Dr. Gerd Bendas

Tag der Promotion: 14.07.2021

Erscheinungsjahr 2021

Die vorliegende Arbeit wurde in der Zeit von Januar 2016 bis Dezember 2019 am Institut für Biochemie und Molekularbiologie der Rheinischen Friedrich-Wilhelms-Universität Bonn unter der Leitung von Herrn Prof. Dr. Hanns Häberlein angefertigt.

“There’s no shame in admitting what you don’t know.  
The only shame is pretending you know all the answers.”

- Neil deGrasse Tyson -

## Abstract

Serotonin 2A (5-HT<sub>2A</sub>) receptors are involved in the treatment and development of a variety of diseases. It was proven in various pre-clinical and clinical settings that influencing their activity is important in the treatment of depressive disorders. St. John's wort extracts have been used to treat depressive disorders for decades, but their influence on the 5-HT<sub>2A</sub> receptor is still not fully understood. To get a deeper understanding of the influences St. John's wort extracts exhibit on 5-HT<sub>2A</sub> receptors, a fluorescently labeled 5-HT<sub>2A</sub> receptor agonist was synthesized in the first part of this work. Using fluorescence correlation spectroscopy (FCS) measurements, the ligand was characterized for its binding affinity and selectivity to 5-HT<sub>2A</sub> receptors. Additionally, two distinct diffusive states of slow and fast diffusing receptor-ligand complexes were determined. The lateral mobility of 5-HT<sub>2A</sub> receptor-ligand complexes was further investigated in single-particle tracking (SPT) experiments. Furthermore, the agonistic activity of the constructed ligand was determined using the calcium-dependent, fluorescent reporter protein B-GECO1 stably transfected into HEK293 cells together with the 5-HT<sub>2A</sub> receptor.

In the second part of this work, the newly constructed fluorescent ligand was used to investigate the influence of the St. John's wort extract STW3-VI<sup>®</sup> on the 5-HT<sub>2A</sub> receptor. Receptor binding studies using FCS on SH-SY5Y cells showed a dose-dependent increase in 5-HT<sub>2A</sub> receptor binding after preincubation with STW3-VI<sup>®</sup>, whereas two of its active ingredients hyperforin and hyperoside showed no significant effects. Interestingly, the receptor-ligand complexes were redistributed in a dose-dependent manner to their faster diffusing state for STW3-VI<sup>®</sup>, hyperforin and hyperoside. However, this effect was most pronounced for STW3-VI<sup>®</sup>. The receptor-ligand complexes with increased lateral mobility are presumably less able to induce their downstream signaling, due to reduced interactions with their respective G protein. The postulated inhibition of 5-HT<sub>2A</sub> receptor signaling after preincubation with STW3-VI<sup>®</sup> was further investigated by measuring receptor density, internalization after stimulation and signaling activity. Therefore, two luminescence-based HEK293 reporter cell lines were created and stably transfected with the 5-HT<sub>2A</sub> receptor. Receptor density and internalization were investigated using the Nano-Glo<sup>®</sup> HiBiT Extracellular Detection System. Again, STW3-VI<sup>®</sup> dose-dependently inhibited 5-HT<sub>2A</sub> receptor activity by reducing the receptor density and internalization after stimulation with the agonist (±)-TCB-2. Hyperforin and hyperoside displayed neither significant effects on receptor density nor internalization after agonistic stimulation. Lastly, the signaling activity after preincubation with STW3-VI<sup>®</sup>, hyperforin and hyperoside was investigated with the luminescent, calcium-dependent reporter protein aequorin. Intracellular calcium levels after agonistic stimulation with the 5-HT<sub>2A</sub> receptor agonist (±)-TCB-2 were significantly reduced after preincubation with

STW3-VI<sup>®</sup>. This effect again could not be explained by either hyperforin or hyperoside, since both displayed no significant influences on 5-HT<sub>2A</sub> receptor induced calcium signaling.

These findings indicate a correlation between receptor activity and mobility for 5-HT<sub>2A</sub> receptors. STW3-VI<sup>®</sup> clearly demonstrated its inhibitory effect on 5-HT<sub>2A</sub> receptors in the cellular models used within this work. By using different fluorescence- und luminescence-based approaches, deeper insights into the interactions of St. John's wort extract STW3-VI<sup>®</sup> and 5-HT<sub>2A</sub> receptors were made possible. This contributes to the better understanding of 5-HT<sub>2A</sub> receptors themselves, their involvement in the treatment of depressive disorders and the therapeutic effects observed after the administration of St. John's wort extracts.

### Zusammenfassung

Serotonin 2A (5-HT<sub>2A</sub>) Rezeptoren spielen bei der Entwicklung und Behandlung einer Vielzahl von Krankheiten eine wichtige Rolle. In unterschiedlichen präklinischen und klinischen Untersuchungen zu depressiven Erkrankungen wurde nachgewiesen, dass eine Beeinflussung der 5-HT<sub>2A</sub> Aktivität zum Behandlungserfolg beiträgt. Zur Behandlung von depressiven Erkrankungen werden schon seit Jahrzehnten Johanniskrautextrakte eingesetzt, jedoch ist ihr Einfluss auf den 5-HT<sub>2A</sub> Rezeptor noch nicht vollständig aufgeklärt. Um den Einfluss von Johanniskrautextrakten auf den 5-HT<sub>2A</sub> Rezeptor zu untersuchen, wurde im ersten Teil dieser Arbeit ein fluoreszenzmarkierter 5-HT<sub>2A</sub> Rezeptor Agonist synthetisiert. Mittels Fluoreszenz-Korrelations-Spektroskopie (FCS) Messungen wurde dieser Ligand hinsichtlich seiner Bindungsaffinität und Selektivität an 5-HT<sub>2A</sub> Rezeptoren untersucht. Zusätzlich konnten zwei Diffusionszustände von Rezeptor-Ligand-Komplexen mit langsamer und schneller Bewegungsgeschwindigkeit beobachtet werden. Die laterale Mobilität von 5-HT<sub>2A</sub> Rezeptor-Ligand-Komplexen wurde in Single-Particle-Tracking (SPT) Experimenten weiterführend untersucht. Außerdem wurde die agonistische Aktivität des synthetisierten Liganden unter Zuhilfenahme des Calcium-abhängigen, fluoreszierenden Reporterproteins B-GECO1 bestimmt, welches stabil in HEK293-Zellen zusammen dem 5-HT<sub>2A</sub> Rezeptor transfiziert wurde.

Im zweiten Teil dieser Arbeit wurde dieser fluoreszenzmarkierte Ligand genutzt, um den Einfluss des Johanniskrautextraktes STW3-VI<sup>®</sup> auf den 5-HT<sub>2A</sub> Rezeptor zu untersuchen. Rezeptorbindungsstudien an SH-SY5Y-Zellen mittels FCS zeigten einen dosisabhängigen Anstieg der 5-HT<sub>2A</sub> Rezeptorbindung nach Vorinkubation mit STW3-VI<sup>®</sup>, wohingegen die beiden Reinsubstanzen Hyperforin und Hyperosid keinen signifikanten Einfluss zeigten. Die Umverteilung von Rezeptor-Ligand-Komplexen in ihren schnelleren Diffusionszustand nach Vorinkubation mit STW3-VI<sup>®</sup>, Hyperforin und Hyperosid erfolgte erstaunlicherweise

## Abstract

dosisabhängig für alle Vorinkubationten. Am stärksten war dieser Effekt jedoch für STW3-VI<sup>®</sup> ausgeprägt. Die Rezeptor-Ligand-Komplexe mit erhöhter Bewegungsgeschwindigkeit sind vermutlich aufgrund der dadurch reduzierten Interaktionsmöglichkeiten mit ihrem jeweiligen G Protein seltener in der Lage ihre Signaltransduktion zu initiieren. Die aufgestellte These zur Hemmung der 5-HT<sub>2A</sub> Rezeptor Aktivität nach Vorinkubation mit STW3-VI<sup>®</sup> wurde durch Messungen der Rezeptordichte, der Rezeptorinternalisierung nach Stimulation mit (±)-TCB-2 und der Signaltransduktion weiter untersucht. Dazu wurden zwei HEK293-Reporterzelllinien mit stabil transfiziertem 5-HT<sub>2A</sub> Rezeptor für Lumineszenzmessungen erzeugt. Die Rezeptordichte und Rezeptorinternalisierung wurden mittels des Nano-Glo<sup>®</sup> HiBiT Extracellular Detection Systems untersucht. Auch in diesen Experimenten hemmte STW3-VI<sup>®</sup> dosisabhängig die Aktivität des 5-HT<sub>2A</sub> Rezeptors, indem es die Rezeptordichte und auch die Rezeptorinternalisierung nach Stimulation mit dem Agonisten (±)-TCB-2 reduzierte. Hyperforin und Hyperosid zeigten weder auf die Rezeptordichte noch auf die Rezeptorinternalisierung nach agonistischer Stimulation einen signifikanten Einfluss. Abschließend wurde die Signaltransduktion nach Vorinkubation mit STW3-VI<sup>®</sup>, Hyperforin und Hyperosid mittels Aequorin, einem lumineszenten, calciumabhängigen Reporterprotein, untersucht. Die intrazellulären Calciumspiegel nach agonistischer Stimulation mit dem 5-HT<sub>2A</sub> Rezeptor Agonisten (±)-TCB-2 waren nach Vorinkubation mit STW3-VI<sup>®</sup> signifikant erniedrigt. Dieser Effekt konnte wiederum weder durch Hyperforin noch durch Hyperosid erklärt werden. Beide Substanzen zeigten keinen signifikanten Einfluss auf die Signaltransduktion des 5-HT<sub>2A</sub> Rezeptors.

Die hier präsentierten Ergebnisse deuten auf einen Zusammenhang zwischen Rezeptoraktivität und Rezeptormobilität für 5-HT<sub>2A</sub> Rezeptoren hin. STW3-VI<sup>®</sup> zeigte eindeutig eine hemmende Wirkung auf den 5-HT<sub>2A</sub> Rezeptor in den in dieser Arbeit verwendeten Zellmodellen. Durch die Verwendung verschiedener Systeme auf Fluoreszenz- und Lumineszenz-Basis konnten weitergehende Erkenntnisse zur Interaktion des Johanniskrautextraktes STW3-VI<sup>®</sup> mit physiologischen Zielstrukturen gewonnen werden, welche im Rahmen von depressiven Erkrankungen eine wichtige Rolle spielen. Zusammengenommen tragen all diese Ergebnisse zum besseren Verständnis der 5-HT<sub>2A</sub> Rezeptoren selbst, ihrer Beteiligung an der Behandlung depressiver Erkrankungen und der nach Einnahme von Johanniskrautextrakten beobachteten therapeutischen Effekte bei.

## Table of Contents

### Table of Contents

Abstract.....	IV
Zusammenfassung .....	V
Table of Contents .....	VII
List of Abbreviations .....	IX
List of Figures .....	XI
List of Tables .....	XIV
1. Introduction .....	1
1.1 Depressive disorders – impact and treatment approaches .....	1
1.2 Molecular mechanisms of depression .....	2
1.3 The monoamine hypothesis – a tale of many targets.....	3
1.4 Serotonin receptors 1A and 2A .....	5
2. Aim and Approach .....	7
3. Materials .....	9
3.1 Cell lines .....	9
3.2 Solutions .....	10
3.3 Chemicals .....	12
3.4 Software.....	13
4. Methods .....	14
4.1 General procedures .....	14
4.1.1 Cell culture .....	14
4.1.2 High-performance liquid chromatography .....	14
4.1.3 High-resolution mass spectrometry .....	16
4.2 Synthesis of (±)-SAH268 .....	16
4.3 Synthesis of fluorescent ligands .....	16
4.4 Generation of stable cell lines.....	17
4.4.1 Plasmid data .....	17
4.4.2 Transformation of XL1-blue bacteria cultures.....	19
4.4.3 Agarose gel electrophoresis .....	19
4.4.4 Transfection of HEK293 cells .....	20
4.5 FCS measurements.....	21

## Table of Contents

4.6	SPT measurements .....	23
4.7	Calcium measurements for (±)-SAH268-Atto532 .....	24
4.8	Characterization of STW3-VI® via HPLC .....	25
4.9	Influence of STW3-VI®, hyperforin, and hyperoside on the ligand binding and diffusion of 5-HT <sub>2A</sub> receptors .....	25
4.10	Influence of STW3-VI®, hyperforin, and hyperoside on the receptor density and internalization of HiBiT-tagged 5-HT <sub>2A</sub> receptors .....	25
4.11	Influence of STW3-VI®, hyperforin, and hyperoside on the 5-HT <sub>2A</sub> receptor-mediated intracellular Ca <sup>2+</sup> levels .....	26
5.	Results .....	28
5.1	Synthesis of a fluorescent 5-HT <sub>2A</sub> receptor ligand .....	28
5.2	Determination of the 5-HT <sub>2A</sub> receptor binding by FCS .....	36
5.3	Selectivity of the 5-HT <sub>2A</sub> receptor binding for (±)-SAH268-Atto532 .....	49
5.4	(±)-SAH268-Atto532 saturation experiments on SH-SY5Y cells .....	52
5.5	Lateral mobility of 5-HT <sub>2A</sub> receptor-(±)-SAH268-Atto532 complexes on SH-SY5Y cells .....	53
5.6	5-HT <sub>2A</sub> receptor agonistic profile of (±)-SAH268-Atto532 .....	55
5.7	Characterization of STW3-VI® via HPLC .....	57
5.8	Influence of STW3-VI®, hyperforin, and hyperoside on the ligand binding and diffusion of 5-HT <sub>2A</sub> receptors on the surface of SH-SY5Y cells .....	59
5.9	Influence of STW3-VI®, hyperforin, and hyperoside on the receptor density and internalization of HiBiT-tagged 5-HT <sub>2A</sub> receptors on the surface of HEK293 cells .....	63
5.10	Influence of STW3-VI®, hyperforin, and hyperoside on the 5-HT <sub>2A</sub> receptor-mediated intracellular Ca <sup>2+</sup> levels in HEK293 cells .....	66
6.	Discussion .....	70
7.	Conclusion and Outlook .....	85
8.	References .....	86
9.	Supplemental Material .....	97
10.	Danksagung .....	116
11.	Publikationen und Poster .....	117

## List of Abbreviations

### List of Abbreviations

5-HT	5-Hydroxytryptamine (Serotonin)
AcCN	Acetonitrile
ADE	Adverse drug effect
API	Active pharmaceutical ingredient
ATP	Adenosine triphosphate
AUC	Area under the curve
BFP	Blue fluorescent protein
B-GECO1	Blue fluorescent calcium indicator
BiT	Binary technology
B <sub>max</sub>	Total receptor concentration
BOC	tert-Butyloxycarbonyl
BRET	Bioluminescence resonance energy transfer
CaM	Calmodulin
CMV	Human betaherpesvirus 5 (human cytomegalovirus)
DER	Drug-extract-ratio
DMEM	Dulbecco's modified eagle medium
DMF	N,N-Dimethylformamide
EDTA	Ethylenediaminetetraacetic acid
EtOH	Ethanol
FBS	Fetal bovine serum
FCS	Fluorescence correlation spectroscopy
G418	Neomycin
GFP	Green fluorescent protein
GPCR	G protein-coupled receptor
HBSS	Hanks' balanced salt solution
HEK	Human embryonic kidney
HEPES	4-(2-hydroxyethyl)-1-piperazineethanesulfonic acid
HMPC	Committee on Herbal Medicinal Products
HPA	Hypothalamic-pituitary-adrenal
HPLC	High-performance liquid chromatography
HRMS	High-resolution mass spectrometry
K <sub>D</sub>	Dissociation constant
LB	Lysogeny broth

## List of Abbreviations

LSD	Lysergic acid diethylamide
M13	Calmodulin-binding region of chicken myosin light chain kinase
MAO	Monoamine oxidase
m/z	Mass-to-charge ratio
NA	Numerical aperture
NHS	N-Hydroxysuccinimide
P <sub>2</sub> RY <sub>1</sub>	P <sub>2</sub> Y purinoceptor 1
PBS	Phosphate-buffered saline
PCR	Polymerase chain reaction
PDL	Poly-D-lysine
PEI	Polyethylenimine
ppm	Parts per million
P/S	Penicillin/Streptomycin
RLU	Relative light units
ROI	Region of interest
RP	Reversed-phase
SD	Standard deviation
SEM	Standard error of the mean
SERT	Serotonin transporter
SNRI	Serotonin-norepinephrine reuptake inhibitor
SPE	Solid-phase extraction
SPT	Single-particle tracking
SSRI	Selective serotonin reuptake inhibitor
TCA	Tricyclic antidepressant
vbSPT	Variational Bayes single-particle tracking
Zeo	Zeocin

## List of Figures

### List of Figures

Figure 1:	Overview - synthesis of a fluorescent 5-HT <sub>2A</sub> receptor ligand .....	28
Figure 2:	Synthesis of (±)-TCB-2-Alexa532 .....	29
Figure 3:	HRMS spectrum for (±)-TCB-2-Alexa532 .....	29
Figure 4:	Synthesis of (±)-TCB-2-Alexa647 .....	30
Figure 5:	HRMS spectra for (±)-TCB-2-Alexa647 .....	30
Figure 6:	Synthesis of (±)-TCB-2-Atto532 .....	31
Figure 7:	HRMS spectra for (±)-TCB-2-Atto532 .....	31
Figure 8:	Synthesis of (±)-SAH268 .....	32
Figure 9:	HRMS spectra for (±)-SAH268 .....	32
Figure 10:	Synthesis of (±)-SAH268-Alexa532 .....	33
Figure 11:	HRMS spectra for (±)-SAH268-Alexa532 .....	33
Figure 12:	Synthesis of (±)-SAH268-Alexa647 .....	34
Figure 13:	HRMS spectra for (±)-SAH268-Alexa647 .....	34
Figure 14:	Synthesis of (±)-SAH268-Atto532 .....	35
Figure 15:	HRMS spectra for (±)-SAH268-Atto532 .....	35
Figure 16:	Autocorrelation curves determined by FCS measurements .....	36
Figure 17:	Exemplary autocorrelation curves for (±)-TCB-2-Alexa532 on C6 cells .....	38
Figure 18:	Exemplary autocorrelation curves for (±)-TCB-2-Alexa647 on C6 cells .....	39
Figure 19:	Exemplary autocorrelation curves for (±)-SAH268-Alexa532 on C6 cells .....	41
Figure 20:	Exemplary autocorrelation curves for (±)-SAH268-Alexa647 on C6 cells .....	42
Figure 21:	Exemplary autocorrelation curves for (±)-SAH268-Atto532 on C6 cells .....	43
Figure 22:	Exemplary autocorrelation curves for (±)-SAH268-Atto532 on SH-SY5Y cells .....	45
Figure 23:	Exemplary autocorrelation curves for (±)-SAH268-Alexa647 on SH-SY5Y cells .....	46
Figure 24:	Exemplary autocorrelation curves for (±)-TCB-2-Atto532 on SH-SY5Y cells .....	47
Figure 25:	Displacement experiments for (±)-SAH268-Atto532 .....	50
Figure 26:	5-HT-receptor selectivity for (±)-SAH268-Atto532 .....	51
Figure 27:	FCS saturation experiments for (±)-SAH268-Atto532 on SH-SY5Y cells .....	52
Figure 28:	Single-particle tracking and further analysis of (±)-SAH268-Atto532 receptor-ligand complexes on SH-SY5Y cells .....	53

## List of Figures

Figure 29:	Principle of cytosolic Ca <sup>2+</sup> detection using B-GECO1 .....	55
Figure 30:	Calcium measurements for (±)-SAH-268-Atto532 .....	56
Figure 31:	HPLC chromatogram of STW3-VI® at 210nm (insert at 590 nm).....	58
Figure 32:	Influence of STW3-VI®, hyperforin and hyperoside on the 5-HT <sub>2A</sub> receptor binding of (±)-SAH268-Atto532.....	62
Figure 33:	Illustration of HiBiT-tagged 5-HT <sub>2A</sub> receptor detection in the plasma membrane of HEK293 cells.....	63
Figure 34:	Influence of STW3-VI®, hyperforin and hyperoside on the receptor density of HiBiT-tagged 5-HT <sub>2A</sub> receptors on the surface of HEK293 cells .....	64
Figure 35:	Influence of STW3-VI®, hyperforin and hyperoside on the internalization of HiBiT-tagged 5-HT <sub>2A</sub> receptors on the surface of HEK293 cells .....	65
Figure 36:	Schematic representation of intracellular Ca <sup>2+</sup> level detection by chemiluminescence using aequorin.....	67
Figure 37:	Influence of STW3-VI®, hyperforin and hyperoside on the intracellular Ca <sup>2+</sup> levels in HEK293 cells after stimulation with (±)-TCB-2 .....	68
Figure 38:	Influence of STW3-VI®, hyperforin and hyperoside on the intracellular Ca <sup>2+</sup> levels in HEK293 cells after stimulation with ionomycin and ATP .....	69
Figure S 1:	Plasmid card of CMV-B-GECO1.....	97
Figure S 2:	Plasmid card of pCDNA3.1Zeo(+) .....	97
Figure S 3:	Plasmid card of pCDNA3.1Zeo(+)-B-GECO1.....	98
Figure S 4:	Enzymatic digestion of pCDNA3.1Zeo(+)-B-GECO1 .....	98
Figure S 5:	Plasmid card of pCDNA5-FRT-hu5HTR2a .....	99
Figure S 6:	Plasmid card of pCDNA3 .....	99
Figure S 7:	Plasmid card of pCDNA3-hu5HTR2a .....	100
Figure S 8:	Enzymatic digestion of pCDNA3-hu5HTR2a .....	100
Figure S 9:	Plasmid card of pCDNA3.cytGAP.....	101
Figure S 10:	Plasmid card of pCDNA3.1Zeo(+)-Aequorin.....	101
Figure S 11:	Enzymatic digestion of pCDNA3.1Zeo(+)-Aequorin .....	102
Figure S 12:	Plasmid card of pCDNA3.1Zeo(+)-HiBiT-ADRB2.....	102
Figure S 13:	Plasmid card of pCDNA3.1Zeo(+)-HiBiT-hu5HTR2a .....	103
Figure S 14:	Enzymatic digestion of pCDNA3.1Zeo(+)-HiBiT-hu5HTR2a .....	103
Figure S 15:	Plasmid card of 5HT2C-RNA2-Flag.....	104
Figure S 16:	Plasmid card of pCDNA3-HiBiT-hu5HTR2c .....	104

## List of Figures

Figure S 17: Enzymatic digestion of pCDNA3-HiBiT-hu5HTR2c .....	105
Figure S 18: Plasmid card of HTR7-Tango .....	105
Figure S 19: Plasmid card of pCDNA3.1Zeo(+)-HiBiT-hu5HTR7 .....	106
Figure S 20: Enzymatic digestion of pCDNA3.1Zeo(+)-HiBiT-hu5HTR7 .....	106
Figure S 21: Plasmid card of pTet-NewMCS.....	107
Figure S 22: Plasmid card of Exp-pcDNA3.2delCMV(EF1 $\alpha$ -tTA/TetO-mCh-Rs1).....	107
Figure S 23: Plasmid card of pTet-NewMCS-HiBiT-hu5HTR2a .....	108
Figure S 24: Enzymatic digestion of pTet-NewMCS-HiBiT-hu5HTR2a .....	108
Figure S 25: Miraprep protocol .....	109
Figure S 26: Electroporation protocol for HEK293 cells by amaxa GmbH.....	110
Figure S 27: Single-cell cloning protocol byCorning Inc.....	111
Figure S 28: Nano-Glo® HiBiT Extracellular Detection System protocol by Promega GmbH .....	112
Figure S 29: Determination of second messenger generation of 5-HT <sub>2C</sub> and 5-HT <sub>7</sub> receptors .....	113

## List of Tables

### List of Tables

Table 1:	Bought cell lines .....	9
Table 2:	Stably transfected cell lines .....	9
Table 3:	Bought solutions.....	10
Table 4:	Self-made solutions .....	11
Table 5:	Chemicals .....	12
Table 6:	Software .....	13
Table 7:	Overview of employed HPLC methods.....	15
Table 8:	Synthesis conditions for fluorescent ligands.....	17
Table 9:	Transfection by electroporation.....	20
Table 10:	FCS data for (±)-TCB-2-Alexa532 on C6 cells .....	38
Table 11:	FCS data for (±)-TCB-2-Alexa647 on C6 cells .....	40
Table 12:	FCS data for (±)-SAH268-Alexa532 on C6 cells .....	41
Table 13:	FCS data for (±)-SAH268-Alexa647 on C6 cells .....	42
Table 14:	FCS data for (±)-SAH268-Atto532 on C6 cells.....	43
Table 15:	FCS data for (±)-SAH268-Atto532 on SH-SY5Y cells .....	45
Table 16:	FCS data for (±)-SAH268-Alexa647 on SH-SY5Y cells.....	46
Table 17:	FCS data for (±)-TCB-2-Atto532 on SH-SY5Y cells .....	48
Table 18:	SPT data for (±)-SAH268-Atto532 receptor-ligand complexes on SH-SY5Y cells.....	54
Table 19:	FCS data for (±)-SAH268-Atto532 receptor-ligand complexes on SH-SY5Y cells after preincubation with STW3-VI®, hyperforin, and hyperoside.....	60
Table S 1:	HPLC determination of hyperoside and hyperforin reference standards .....	115
Table S 2:	Calculation of hyperoside and hyperforin in STW3-VI® .....	115

### 1. Introduction

#### 1.1 Depressive disorders – impact and treatment approaches

People suffering from depressive disorders display a variety of different symptoms. Some examples are depressed mood, insomnia/hypersomnia, feelings of worthlessness and even recurring thoughts of death as well as suicidal thoughts and many more<sup>1</sup>. Depressive disorders are very complex and frequent diseases. They belong to the leading causes of disabilities in modern society recorded for the years 1990, 2007 and 2017. Roughly 260 million people worldwide suffer from depressive disorders, with females being affected more often than males<sup>2,3</sup>. Although being one of the most frequent causes of disabilities, the therapy of mental disorders (including depressive disorders) is highly affected by the development stage of the country patients live in. Overall, the share of patients receiving mental health services and follow-up treatment was highly affected by the countries' health care budget<sup>4</sup>. Depressive disorders are not only a burden for the affected patients but also the economy due to their high direct and indirect costs<sup>5</sup>. Because of the strong impact on patients' personal life and the whole society, it is evident that depressive disorders should not be left untreated.

The treatment of depressive disorders is commonly carried out with psychotherapy, pharmaceutical antidepressants and electroconvulsive therapy (ECT) or a combination of those depending on the severity of symptoms<sup>6</sup>. Selective serotonin reuptake inhibitors (SSRI), e.g. escitalopram, citalopram or sertraline, and serotonin-norepinephrine reuptake inhibitors (SNRI), such as duloxetine, replaced tricyclic antidepressants (TCA), for instance amitriptyline or desipramine, as first in line therapeutic options mainly because of their improved adverse drug effect (ADE) profile rather than their better efficacy<sup>1,7</sup>. Extracts of *Hypericum perforatum* L. (St. John's wort) are used to treat depressive patients and their beneficial effects are documented in many randomized controlled trials, although not all trials showed superiority compared to placebo intervention. Overall, studies from German-speaking countries showed more favorable effects compared to other countries, which may be caused by the high acceptance of herbal medicinal products in those countries<sup>8,9</sup>. In general, they were found to be superior to placebo and similar in efficacy compared with standard antidepressants, e.g. the widely-used SSRI escitalopram, citalopram or sertraline, while having a highly favorable ADE profile<sup>10</sup>. Due to this reliable research data and the long-lasting experience with St. John's wort extracts, they are included as the only phytopharmaceutical in the S3-Leitlinie/Nationale Versorgungs Leitlinie "Unipolare Depression". A variation in the contents of the active ingredients in extracts from different manufacturers and products is to be concerned. Consequently, only products with a proven efficacy in clinical trials are recommended for prescription in mild to moderate depressive disorders<sup>6</sup>. Another safety concern is their

## Introduction

pharmacokinetic interaction with other drugs by inducing cytochrome P450 enzyme activity. In a recent phase I, open-label, nonrandomized, single-sequence study no pharmacokinetic interactions between a St. John's wort extract low on hyperforin and a variety of cytochrome P450 enzymes or P-glycoprotein were observed<sup>11</sup>. As already observed, the active ingredient hyperforin seems to be responsible for the interaction with cytochrome P450 enzymes. A St. John's wort extract low on hyperforin may be favorable in terms of pharmacokinetic safety. Overall, a deeper understanding of the mode of action of St. John's wort extracts is crucial for a safer and broader use in daily practice.

### 1.2 Molecular mechanisms of depression

In order to come to a better understanding of the mode of action of antidepressants, the underlying mechanisms leading to depressive disorders have to be outlined first. Until today, there is no satisfactory explanation or model explaining all facets of depressive disorders. However, there are several mechanisms commonly associated with the development of depressive disorders<sup>12</sup>.

One of the first theories was the monoamine hypothesis. It was observed that reduced levels of the monoamines serotonin (5-HT), norepinephrine, and dopamine could trigger depressive disorders and elevating monoamine levels through therapy showed antidepressant effects. Since this discovery, many substance classes (e.g. TCA, SSRI, SNRI) were developed and are widely used in clinical practice to this day<sup>12</sup>. Unfortunately, this theory does not explain the delayed onset of classic antidepressants of up to four weeks compared to hallucinogens such as LSD or psilocybin, where no such onset was observed in recent pilot trials<sup>13</sup>. The variability of responses to the same antidepressant for different patients or even the different depressive episodes for the same patient are also not explained by the monoamine hypothesis<sup>14</sup>. Hence, many factors seem to influence the development and progression of depressive disorders.

One of those factors is the influence on the hypothalamic-pituitary-adrenal (HPA) axis. Chronic stress leads to a more active HPA axis resulting in increased plasma cortisol levels<sup>15</sup>. The activity of the HPA axis is controlled by a negative feedback mechanism. Corticotropin-releasing hormone is the main activator of the HPA axis and its release is in turn regulated by cortisol. This negative feedback mechanism is strongly affected by the immunophilin FK506 binding protein 51 (FKBP51). Increased levels of FKBP51, caused by genetic polymorphism, lead to a higher risk for anxiety related and depressive disorders by inhibiting the negative feedback mechanism<sup>16</sup>. Prolonged hyperactivity of the HPA axis is also linked to an activation of macrophages and microglia leading to chronic inflammation, another factor believed to be of interest in the development of depression. Chronic inflammation is the subject of

antidepressant research with increasing interest, even leading to the examination of non-steroidal anti-inflammatory drugs in the treatment of depression<sup>12,17</sup>. One important factor in the development and progression of inflammation are reactive oxygen species (ROS). They are mainly produced by cells belonging to the adaptive immune system, leading to dysfunction of endothelia and signaling proteins<sup>18</sup>. St. John's wort extracts displayed high antioxidant activity, which could also benefit their antidepressant action by inhibiting chronic inflammation through inactivation of ROS<sup>19</sup>. Changes in neuroplasticity through hyperactivity of the HPA axis or inflammation are also directly linked to the development of depressive disorders. Neuroplasticity is a recently discovered process during which neurons are able to adapt to changes in their environment or can even be generated anew from pluripotent stem cells by neurogenesis<sup>12,20</sup>. Structural changes of the brain through functional plasticity where functions of the brain are transferred from damaged regions to still intact regions, or through structural plasticity where synapses, neurons, axons etc. are broken down or build again, as well as influence of genetic predisposition, stressful life events and environmental changes and the interaction of genetics and environment, the so-called epigenetics, are further aspects associated with depressive disorders<sup>12,21,22</sup>.

Despite the discoveries in recent years in terms of neuroplasticity, genetics and the other fields of research mentioned above, the clinical practice of antidepressant treatment is dominated by substances influencing monoamines, in most cases serotonin, its transporters and receptors<sup>6,23</sup>.

### 1.3 The monoamine hypothesis – a tale of many targets

The first antidepressants imipramine and iproniazide were discovered back in the 1950s. Imipramine inhibits the reuptake of serotonin and norepinephrine from the synaptic cleft and iproniazide irreversibly inhibits monoamine oxidases (MAO). This discovery caused researches to conclude that a dysregulation of monoamine signaling was one of the main causes for developing depressive disorders. From this time onward, many pharmaceutical agents have been discovered and used in clinical practice<sup>24</sup>. During the 1980s substances were identified which selectively inhibited serotonin reuptake by blocking the serotonin transporter (SERT), the so-called SSRI. Fluoxetine was the first clinically approved SSRI and was followed by many others, even leading to SNRI, a completely new substance class discovered in the 1990s. SNRI block the norepinephrine transporter (NET) in addition to blocking SERT. SSRI and SNRI are still the first in line option for treating depressive disorders because of their proven efficacy and favorable ADE profile compared to TCA or MAO inhibitors<sup>7,25,26</sup>. Their targets SERT and NET have been studied extensively, and it was also

## Introduction

proven that St. John's wort extracts inhibit serotonin reuptake, mainly through one of its ingredients: hyperforin<sup>27,28</sup>.

Apart from blocking serotonin and/or norepinephrine reuptake, also other targets are influenced by SSRI and SNRI. For example, the SSRI sertraline strongly inhibits dopamine reuptake, fluoxetine is a highly active antagonist for serotonin 2C receptors (5-HT<sub>2C</sub>) and sertraline shows rather high affinities for muscarinic acetylcholine receptor M<sub>1</sub> (M<sub>1</sub>) and  $\alpha$ <sub>1</sub> adrenergic receptor ( $\alpha$ <sub>1</sub>). Citalopram and its more potent pure enantiomer escitalopram only show weak affinities for targets beside SERT, with a least a thousand-fold selectivity for SERT over other targets<sup>29,30</sup>. Strictly speaking, SSRI and SNRI are not selective, with escitalopram and citalopram being an exception. But they mostly affect only a small number of targets besides SERT and/or NET<sup>26,31</sup>. In contrast to SSRI and SNRI, TCA have been known for many years to exert their antidepressant effect by mainly antagonizing different receptors in addition to blocking serotonin reuptake. The main receptors targeted by TCA are the histamine H<sub>1</sub> receptor (H<sub>1</sub>), M<sub>1</sub>,  $\alpha$ <sub>1</sub> and also the serotonin 1A and 2A receptors (5-HT<sub>1A</sub> and 5-HT<sub>2A</sub>)<sup>32</sup>. This broad range of influences can be problematic. It leads to an inferior ADE profile of TCA compared to SSRI, but also help to understand which receptors and neurotransmitter systems are affected by antidepressants and are likely of importance in the treatment of depressive disorders. Additionally, inhibiting MAO and thereby reducing the degradation of monoamines also proved effective in the treatment of depression. MAO inhibitors with iproniazide were the first type of antidepressant drugs discovered. On the one hand, selective inhibition of the isoform MAO-A by e.g. moclobemid leads to elevated serotonin and norepinephrine levels as MAO-A preferably metabolizes serotonin and norepinephrine. Therefore, selective and non-selective MAO-A inhibitors are used in the treatment of depressive disorders. On the other hand, an inhibition of MAO-B by e.g. selegilin in combination with L-3,4-dihydroxyphenylalanine (L-DOPA) is often used in the therapy of Parkinson's disease<sup>33</sup>. Due to their high potential of ADE, mainly by interacting with SSRI and SNRI causing serotonin syndrome, and the necessary restrictions in diet and other medications, their usage in the treatment of depressive disorders has to be monitored closely. Overall, if supervised by experienced personnel, they are a promising option for a combination therapy in treatment resistant depression<sup>34</sup>.

### 1.4 Serotonin receptors 1A and 2A

The family of serotonin receptors consists of 14 receptors, 13 of which belong to class A G protein-coupled receptors (GPCR) and one ligand-gated ion channel (5-HT<sub>3</sub> receptor)<sup>35</sup>. The diversity of GPCR as the largest class of membrane-associated receptors and their involvement in many physiological processes makes them one of the most important targets in drug discovery<sup>36</sup>.

For example, in recent years the 5-HT<sub>1A</sub> and 5-HT<sub>2A</sub> receptors have been studied extensively for their involvement in the development and treatment of depressive disorders and other diseases such as Parkinson's disease<sup>37</sup>. 5-HT<sub>1A</sub> receptors can act in two distinct ways. On the one hand, they act as heteroreceptors, which means that their selective stimulation leads to an inhibition of the activity of non-serotonergic neurons. For example, they reduce L-DOPA induced dyskinesia by influencing dopaminergic signaling<sup>38</sup>. On the other hand they act as autoreceptors, controlling the release of serotonin from serotonergic neurons. Their stimulation facilitates the release of serotonin leading to anxiolytic and antidepressant-like effects<sup>37,39</sup>. Overall, a stimulation of 5-HT<sub>1A</sub> receptors seems to be beneficial in the treatment of depressive disorders. The influence of hyperforin, hyperoside and hypericin on the lateral mobility and signaling of 5-HT<sub>1A</sub> receptors was investigated in a prior work<sup>40</sup>. Additionally, St. John's wort extracts increased 5-HT<sub>1A</sub> and, in contrast to TCA, also 5-HT<sub>2A</sub> receptor density<sup>41</sup>.

Standing out of the family of serotonin receptors is the 5-HT<sub>2A</sub> receptor due to its involvement in many different processes. It is associated with the development and treatment of anxiety, schizophrenia, and depressive disorders<sup>37,42</sup>. Blocking 5-HT<sub>2A</sub> receptors and thereby modulating the release of other neurotransmitters such as dopamine with TCA or the downregulation of 5-HT<sub>2A</sub> receptors seen after treatment with SSRI is both linked to their antidepressant effects<sup>37,43</sup>. Additionally, 5-HT<sub>2A</sub> receptor activation causes desensitization of 5-HT<sub>1A</sub> receptors which is relevant in the regulation of mood<sup>44</sup>. Antipsychotic effects of drugs like clozapine (atypical antipsychotic) for the treatment of delusions and hallucinations in schizophrenic or bipolar patients is exerted by 5-HT<sub>2A</sub> receptor antagonism<sup>45</sup>. The functional crosstalk between the 5-HT<sub>2A</sub> receptor and the metabotropic glutamate receptors (mGluR2) received extensive attention in recent years. It is believed to be a major factor in the mechanism of action of atypical antipsychotics<sup>46</sup>. One of the most outstanding features of the 5-HT<sub>2A</sub> receptor is its involvement in the hallucinogenic effects of lysergic acid diethylamide (LSD) or psilocybin. The main part of the hallucinogenic action of those and related substances is mainly mediated through agonism of 5-HT<sub>2A</sub> receptors<sup>47,48</sup>. After initial clinical research involving LSD in the treatment of depression in the 1950s and 1960s, it received the status of a controlled substance around 1970 and research ended. In recent years a growing body of studies and evidence supports the antidepressant effects of LSD and its related molecule

## Introduction

psilocybin in small pilot trials<sup>49</sup>. The effects are often observed after the first drug administration in comparison to a delay of sometimes four or six weeks for classic antidepressants. The reasons for that are still not fully discovered<sup>13</sup>. Nevertheless, randomized controlled trials for LSD or psilocybin in the treatment of depressive disorders are still lacking. Interestingly, 5-HT<sub>2A</sub> receptors are also relevant for the infection of glial cells by the human polyomavirus (JCV)<sup>50</sup>. The 5-HT<sub>2A</sub> receptor with its involvement in many physiological processes is an important target in the research of depressive disorders. Furthermore, the question if and how St. John's wort extracts and/or their main ingredients influence this particular receptor is still not fully answered.

## 2. Aim and Approach

This work aims to investigate how St. John's wort extract STW3-VI® and/or its active ingredients hyperforin and hyperoside mediate parts of their antidepressant action via the 5-HT<sub>2A</sub> receptor. To study the effects in real-time fluorescence correlation spectroscopy (FCS) was chosen as a suitable technique. In comparison to more commonly used techniques like radioligand binding studies FCS allows to measure real-time receptor-ligand interactions in a dynamic system with living cells on a single-molecule level. For radioligand binding studies, the cells have to be treated, lysed, filtered through a membrane, washed several times and analyzed afterwards. Interaction between ligand and receptor could be disrupted mainly during lysis, filtration and washing. The challenging part of applying FCS is the construction of a fluorescent ligand that is still selective and binds with high affinity to the 5-HT<sub>2A</sub> receptor. In that regard, constructing a radioligand is a lot easier because one only has to replace a single atom of the chosen molecule with its radioactive counterpart. This process does not affect selectivity or binding affinity.

Due to the complexity of ligand construction, this work is divided into two major parts. The first part covers the synthesis and characterization of a fluorescent 5-HT<sub>2A</sub> receptor agonist. As mentioned before, such a tool is useful to investigate real-time receptor dynamics and receptor-ligand interaction by using single-molecule techniques like fluorescence correlation spectroscopy (FCS) and single-particle tracking (SPT)<sup>51,52</sup>. In contrast to commonly used GFP-labeled or SNAP-tagged receptors in molecular drug research, fluorescent ligands are required for detecting receptor-ligand complexes exclusively<sup>53,54</sup>. Many fluorescent ligands for serotonergic receptors were successfully produced in recent years (e.g. 5-HT<sub>1A</sub>, 5-HT<sub>2B</sub>, 5-HT<sub>2C</sub>, 5-HT<sub>3</sub>, 5-HT<sub>4</sub>, and 5-HT<sub>6</sub> receptors), but until today a selective, fluorescent 5-HT<sub>2A</sub> receptor ligand is still missing<sup>55-60</sup>. The construction of a fluorescent 5-HT<sub>2A</sub> receptor agonist demonstrated to be dependent on the choice of starting molecule and the chosen fluorophore. Whether the constructed ligand bound selectively to the 5-HT<sub>2A</sub> receptor was investigated by FCS with two different approaches. First, the displaceability of the observed receptor binding was measured with selective ligands for different serotonin receptors (5-HT<sub>1A</sub>, 5-HT<sub>2A</sub>, 5-HT<sub>2C</sub>, and 5-HT<sub>7</sub>). Second, human embryonic kidney cells (HEK293) were stably transfected with the aforementioned serotonin receptors and investigated for detectable receptor binding of the constructed ligand. Ligand and receptor characteristics  $K_D$  and  $B_{max}$  were determined by saturation experiments using FCS. The lateral mobility and diffusion behavior of the receptor-ligand complexes on the cell surface was visualized by SPT. The agonistic activity of the constructed ligand was proven by measurements of the intracellular Ca<sup>2+</sup> levels using HEK293 cells stably transfected with the 5-HT<sub>2A</sub> receptor and B-GECO1, a fluorescent, calcium-dependent, proteinaceous reporter<sup>61</sup>.

## Aim and Approach

The second part of this work covers the investigation of the influence of St. John's wort extract (STW3-VI®) and their active ingredients hyperforin and hyperoside on 5-HT<sub>2A</sub> receptors using different techniques. The ligand constructed in the first part of this work was used in FCS studies with SH-SY5Y cells to assess whether the ligand binding and lateral mobility of 5-HT<sub>2A</sub> receptors are affected by a six days preincubation period with said substances. After investigating the ligand binding and later lateral mobility of 5-HT<sub>2A</sub> receptors, further experiments regarding receptor density, internalization, and signaling were conducted. Receptor density and trafficking after stimulation were investigated in HEK293 cells stably transfected with the HiBiT-tagged human 5-HT<sub>2A</sub> receptor. After the addition of the LgBiT, a functional NanoLuc® luciferase is formed emitting chemiluminescence after binding and converting its substrate. The HiBiT-system allows to only detect receptors in the plasma membrane due to the substrate not being able to enter the cell. Lastly, the influence of the preincubations with STW3-VI®, hyperforin and hyperoside on the signaling of 5-HT<sub>2A</sub> receptors after stimulation was investigated. Therefore, a chemiluminescence-based system was employed. HEK293 cells were stably transfected with the human 5-HT<sub>2A</sub> receptor and the calcium-dependent luciferase aequorin<sup>62</sup>.

### 3. Materials

#### 3.1 Cell lines

**Table 1: Bought cell lines**

Name	Cell type	Supplied by	Reference number
C6	Rat glioma cells	Deutsche Sammlung von Mikroorganismen und Zellkulturen (DSMZ) GmbH Braunschweig, Germany	ACC 550
SH-SY5Y	Human neuroblastoma cells	DSMZ	ACC 209
HEK293	Human embryonic kidney cells	DSMZ	ACC 305

**Table 2: Stably transfected cell lines**

Name	Expressed genetic information	Transfection method (see 4.4.4)
HEK293-B-GECO1	- Blue fluorescent proteinaceous calcium indicator (B-GECO1)	Polyethylenimine
HEK293-B-GECO1-5HT2a	- Blue fluorescent proteinaceous calcium indicator (B-GECO1) - Human 5-HT <sub>2A</sub> receptor	Polyethylenimine
HEK293-HiBiT-5HT2a	- HiBiT-tagged human 5-HT <sub>2A</sub> receptor	Electroporation
HEK293-Aequorin-HiBiT-5HT2c	- Apoaequorin part of the calcium-dependent luciferase aequorin - HiBiT-tagged human 5-HT <sub>2C</sub> receptor	Electroporation
HEK293-GloSensor-HiBiT-5HT7	- cAMP-dependent firefly luciferase (GloSensor) - HiBiT-tagged human 5-HT <sub>7</sub> receptor	Electroporation
HEK293-Aequorin-Tetoff-HiBiT-5HT2a	- Apoaequorin part of the calcium-dependent luciferase aequorin - HiBiT-tagged human 5-HT <sub>2A</sub> receptor, expression levels are controllable by tetracyclines (doxycycline)	Electroporation

## Materials

### 3.2 Solutions

**Table 3: Bought solutions**

Name	Abbreviation	Supplied by	Reference number
Dulbecco's modified eagle medium / nutrient mixture F-12, no glutamine	DMEM/F-12, no glutamine	Life Technologies Ltd.; Paisley, UK	21331046
Dulbecco's modified eagle medium, high glucose, no glutamine, no phenol red	DMEM, high glucose, no glutamine, no phenol red	Life Technologies	31053028
Dulbecco's modified eagle medium	DMEM	Life Technologies	31885049
Dulbecco's modified eagle medium, no glutamine, without phenol red	DMEM, no glutamine, no phenol red	Life Technologies	11054020
Fetal bovine serum	FBS	Life Technologies	10270
GlutaMAX™ Supplement	GlutaMAX™	Life Technologies	35050061
Hygromycin B Gold™	Hygromycin	InvivoGen, Toulouse, France	ant-hg-1
Nano-Glo® HiBiT Extracellular Detection System	HiBiT Assay	Promega GmbH, Mannheim, Germany	N2420
Penicillin-Streptomycin 10,000 U/ml	P/S	Life Technologies	15140122
Phosphate buffered saline	PBS	Life Technologies	10010056
Trypsin EDTA 0.05%, phenol red	T/E	Life Technologies	25300104
Zeocin™ Selection Reagent	Zeocin	Life Technologies	R25001

## Materials

**Table 4: Self-made solutions**

Name	Abbreviation	Composition
Electroporation buffer for HEK293 cells	-	5 mM KCl 15 mM MgCl <sub>2</sub> 15 mM HEPES 50 mM NaCl 150 mM Na <sub>2</sub> HPO <sub>4</sub> /NaH <sub>2</sub> PO <sub>4</sub> pH 7.2
Locke's solution	Locke	150 mM NaCl 5.6 mM KCl 2.3 mM CaCl <sub>2</sub> 1.0 mM MgCl <sub>2</sub> 3.6 mM NaHCO <sub>3</sub> 5.0 mM HEPES 20 mM Glucose pH 7.4
Lysogeny broth-medium	LB-medium	1% (w/v) Bacto™ Tryptone 0.5% (w/v) Bacto™ Yeast extract 1% (w/v) NaCl pH 7.0
Phosphate buffered saline	PBS	137 mM NaCl 2.7 mM KCl 10 mM Na <sub>2</sub> HPO <sub>4</sub> 1.5 mM K <sub>2</sub> HPO <sub>4</sub> pH 7.4
Tris, acetic acid, EDTA buffer	TAE buffer	40 mM Tris 20 mM acetic acid 1 mM EDTA

## Materials

### 3.3 Chemicals

**Table 5: Chemicals**

Name	Supplied by	Reference number
Acetonitrile	VWR International, Radnor, Pennsylvania, USA	20060.320
Alexa Fluor™ 532 NHS Ester	Life Technologies	A20101MP
Alexa Fluor™ 647 NHS Ester	Life Technologies	A20006
Atto532-NHS-Ester	Atto-Tec GmbH, Siegen, Germany	AD 532-21
6-(Boc-amino)hexyl bromide	CHEMPUR Feinchemikalien und Forschungsbedarf GmbH, Karlsruhe, Germany	fl-37106-1
Caesium hydroxide	Sigma-Aldrich, Darmstadt, Germany	21000
Coelenterazine	Carl Roth GmbH + Co. KG, Karlsruhe, Germany	4094.4
Ionomycin, calcium salt	Biomol GmbH, Hamburg, Germany	Cay-11932
Neomycin (G418)	Merck, Darmstadt, Germany	345810
SB 242084	Tocris Bioscience, Bristol, UK	2901
SB-269970 hydrochloride	Sigma-Aldrich	S7389
(±)-TCB-2 hydrobromide	Tocris Bioscience	2592
WAY-100135	Sigma-Aldrich	W1895

## 3.4 Software

**Table 6: Software**

Name	Supplied by	Version
Axiovision®	Carl Zeiss Microscopy GmbH, Jena, Germany	Rev. 4.8
Agilent ChemStation	Agilent Technologies Inc., Santa Clara, CA, USA	Rev. B04.01
Fiji (ImageJ)	National Institutes of Health, Bethesda, MD, USA	1.52n
GraphPad Prism	GraphPad Software Inc., San Diego, CA, USA	6.01
MATLAB®	The MathWorks, Inc. Natick, MA, USA	R2009a and R2016b
Tecan i-control®	Tecan Trading AG, Maennedorf, Switzerland	1.10
Xcalibur®	Thermo Fisher Scientific Inc., Grand Island, NY, USA	4.2.28.14

### 4. Methods

#### 4.1 General procedures

##### 4.1.1 Cell culture

Rat glioma cells (C6), obtained from Leibniz Institute DSMZ (Braunschweig, Germany), were cultivated in DMEM/F-12, no glutamine (Life Technologies Ltd.; Paisley, UK) supplemented with 2 mM GlutaMAX™ (Life Technologies), 100 units/ml penicillin, 100 µg/ml streptomycin (Life Technologies) and 5% fetal bovine serum (Life Technologies). C6 cells were maintained by ten-fold dilutions with fresh medium every 2-3 days in 10 cm dishes.

Human neuroblastoma cells (SH-SY5Y), obtained from Leibniz Institute DSMZ, were cultivated in DMEM, high glucose, no glutamine, no phenol red (Life Technologies) supplemented with 100 units/ml penicillin, 100 µg/ml streptomycin and 15% fetal bovine serum. SH-SY5Y cells were maintained by three-fold dilutions with fresh medium every 3-4 days in 10 cm dishes.

Human embryonic kidney cells (HEK293) obtained from Leibniz Institute DSMZ were cultivated in DMEM (Life Technologies) supplemented with 100 units/ml penicillin, 100 µg/ml streptomycin and 10% fetal bovine serum. HEK293 cells and all generated clones were maintained by ten-fold dilutions with fresh medium every 3-4 days in 10 cm dishes.

All cells were cultured at 37 °C and 5% CO<sub>2</sub>.

##### 4.1.2 High-performance liquid chromatography

High-performance liquid chromatography (HPLC) analyses were performed on an Agilent Series 1200 HPLC system equipped with a degasser (G1322A), a quaternary pump (G1311A), an autosampler (G1329A), and a photodiode array detector (G1315D), operated by Agilent ChemStation Rev. B.04.01. The following methods were used (Table 7).

Methods

Table 7: Overview of employed HPLC methods.

No.	Column	$\lambda$ [nm]	Eluent composition (v/v)		Gradient (linear)									
			A	B	time [min]	Eluent [%]		flow [m/min]						
						A	B							
1	LiChrospher® RP 18 (5 $\mu$ m, 125 x 4 mm)	210 532	AcCN 1 H <sub>2</sub> O 22 pH 2 (H <sub>3</sub> PO <sub>4</sub> )	AcCN	0	100	0	1.0						
					25	52	48	1.0						
					40	0	100	1.0						
2		210 647			0	100	0	1.0						
					40	0	100	1.0						
3		210 532			0	80	20	1.0						
	20		50	50	1.0									
4	LiChrospher® RP 18 (5 $\mu$ m, 125 x 4 mm)	210 647	AcCN 1 H <sub>2</sub> O 22 pH 2 (H <sub>3</sub> PO <sub>4</sub> )	AcCN	0	100	0	1.0						
					8	82.5	17.5	1.0						
					14	82.5	17.5	1.0						
					20	70	30	1.0						
5		LiChrospher® RP 18 (5 $\mu$ m, 125 x 4 mm)			210 532	AcCN 1 H <sub>2</sub> O 22 pH 2 (H <sub>3</sub> PO <sub>4</sub> )	AcCN	0	85	15	1.0			
								10	75	25	1.0			
								20	50	50	1.0			
6					210 254 280			0	100	0	1.0			
								30	25	75	1.0			
7					Symmetry™ C18 (5 $\mu$ m, 150 x 3.9 mm)			210 254 590	AcCN 19 H <sub>2</sub> O 80 H <sub>3</sub> PO <sub>4</sub> 1	AcCN 59 MeOH 40 H <sub>3</sub> PO <sub>4</sub> 1	0	100	0	0.5
											8	100	0	0.5
											15	92.5	7.5	0.5
	37		50	50							0.5			
	52	0	100	0.5										
	52	0	100	1.0										
	85	0	100	1.0										

### 4.1.3 High-resolution mass spectrometry

High-resolution mass spectrometry (HRMS) analyses were performed with an LTQ Orbitrap Velos mass spectrometer (Thermo Fisher Scientific, Bremen, Germany) by direct infusion nano spray (TriVersa NanoMate, Advion, Harlow, UK). Chips with 400  $\mu\text{m}$  nozzles were used with 1.6 kV in positive mode. MS1 spectra were recorded in the Orbitrap mass analyzer with a resolution of 60,000. A lock mass (polysiloxane  $[\text{M}+\text{H}]^+$ , 445.120024 mass-to-charge ratio ( $m/z$ )) was applied for internal calibration resulting in a typical mass error  $<1$  ppm. Data were manually inspected and  $m/z$  values compared to the theoretical values of the analytes after averaging several spectra in Xcalibur® software Version 4.2.28.14 (Thermo Fisher Scientific).

### 4.2 Synthesis of ( $\pm$ )-SAH268

2.2 mg (6.23  $\mu\text{mol}$ ) of ( $\pm$ )-TCB-2 hydrobromide together with 0.9 mg (6.23  $\mu\text{mol}$ ) CsOH, 1.8 mg of 0.4 nm molecular sieve (both dried for 24 h at 120  $^{\circ}\text{C}$ ) and 2.05 mg (7.32  $\mu\text{mol}$ ) 6-(BOC-amino)hexyl bromide were dissolved in 300  $\mu\text{l}$  dried DMF and stirred for 21 h at room temperature to receive ( $\pm$ )-SAH267. The reaction mixture was not further worked up but mixed with 150  $\mu\text{l}$  aq. 85%  $\text{H}_3\text{PO}_4$  and stirred for additionally 6 h at room temperature to generate ( $\pm$ )-SAH268. ( $\pm$ )-SAH268 was isolated using HPLC method 6 (Table 7). Collected fractions of ( $\pm$ )-SAH268 were pooled and adjusted to pH 12 using ammonium hydroxide solution (27%). Subsequent solvent extraction with 3 x 10 ml ethyl acetate and evaporation in vacuo yielded ( $\pm$ )-SAH268 as yellowish oil, which was dissolved in  $\text{H}_2\text{O}$ . The overall yield was 31%.

### 4.3 Synthesis of fluorescent ligands

All fluorescent ligands were synthesized using the same protocol only varying in the molar equivalents and purification procedures used. A general protocol is described below. Further information regarding a specific ligand is provided in Table 8.

( $\pm$ )-TCB-2 / ( $\pm$ )-SAH268 and a fluorescent dye (Alexa532-NHS, Alexa647-NHS or, Atto532-NHS) were reacted in an aqueous solution of 0.1 M  $\text{NaHCO}_3$  for 24 h at room temperature. All chemicals were prepared in stock solutions with defined concentrations in the range of 1 to 100 mM of which the required amount was taken (Table 8 column 2). All reaction mixtures were separated by HPLC with a distinct method (Table 8 column 3). Fractions containing the fluorescent ligand were pooled and  $\text{H}_3\text{PO}_4$  was removed by solid-phase extraction (SPE) on a LiChrolut® RP-18 cartridge (Merck; Darmstadt, Germany) using distilled water. The fluorescent ligand was eluted using a defined solvent mixture (Table 8 column 4). Solvents were removed by evaporation in vacuo. The residue of the fluorescent ligand was dissolved in

## Methods

H<sub>2</sub>O and the aqueous solution was prepared in a defined concentration suitable for further measurements.

**Table 8: Synthesis conditions for fluorescent ligands.**

Reaction partners	Molar equivalents	HPLC method (Table 7)	SPE solvent
(±)-TCB-2 / Alexa532-NHS	2 : 1	1	80% AcCN
(±)-TCB-2 / Alexa647-NHS	5 : 1	2	50% EtOH
(±)-SAH268 / Alexa532-NHS	1 : 2	3	50% AcCN
(±)-SAH268 / Alexa647-NHS	2 : 1	4	50% AcCN
(±)-SAH268 / Atto532-NHS	1 : 1	5	80% AcCN
(±)-TCB-2 / Atto532-NHS	6 : 1	5	80% AcCN

### 4.4 Generation of stable cell lines

#### 4.4.1 Plasmid data

##### 1) pCDNA3.1Zeo(+)-B-GECO1

The plasmid CMV-B-GECO1 was a gift from Robert Campbell (Addgene plasmid # 32448)<sup>61</sup>. To enable cell clone selection by Zeocin, the information for B-GECO1 was transferred from this plasmid into the pCDNA3.1Zeo(+) vector (Life Technologies), using BamHI/XhoI restriction endonuclease sites of both plasmids.

##### 2) pCDNA3-hu5HTR2a

The plasmid pCDNA5-FRT-hu5HTR2a was a gift from Alexander Glassmann. From this plasmid, the genetic information for the human 5-HT<sub>2A</sub> receptor was extracted and inserted into the pCDNA3 vector (Life Technologies), using BamHI/XhoI restriction endonuclease sites of both plasmids.

##### 3) pCDNA3.1Zeo(+)-Aequorin

The plasmid pCDNA3.cytGAP was a gift from Teresa Alonso (Addgene plasmid # 78734)<sup>63</sup>. From this plasmid, the genetic information for the calcium-dependent Luciferase Aequorin was amplified via PCR (forward primer: 5'-GATCGTTCGACATGGGTACCGGTAAACTTACATC-3', reverse primer: 5'-TAGAAGGCACAGTCGAGG-3'). To enable cell clone selection by Zeocin, the information for Aequorin was inserted into the pCDNA3.1Zeo(+) vector using NheI/NotI restriction endonuclease sites. The PCR conditions were as follows: initial activation of the Q5<sup>®</sup> High-Fidelity DNA Polymerase for 60 s at 98 °C, followed by 25 cycles of 10 s denaturation at

## Methods

98 °C, 10 s annealing at 63 °C and extension for 30 sec at 72 °C. The program ended with a 2 min fill in step at 72 °C.

### 4) pCDNA3.1Zeo(+)-HiBiT-hu5HTR2a

The already existing plasmid pCDNA3.1Zeo(+)-HiBiT-ADRB2 was used as a template. The sequence of the human  $\beta$ 2-adrenergic receptor (ADRB2) was exchanged with the human 5-HT<sub>2A</sub> receptor via NheI/XhoI endonuclease sites.

### 5) pCDNA3-HiBiT-hu5HTR2c

5HT2C-RNA2-Flag was a gift from Stefan Stamm (Addgene plasmid # 79679)<sup>64</sup>. The information for the human 5-HT<sub>2C</sub> receptor was amplified via PCR (forward primer: 5'-CTC-GGATCCACCATGGTGAACC -3', reverse primer: 5'-AGACTCGAGTCACACACTGCTAATC-CTTTC-3') and exchanged for the human 5-HT<sub>2A</sub> receptor via BamHI/XhoI endonuclease sites in pCDNA3.1Zeo(+)-HiBiT-hu5HTR2a. Afterwards, the N-terminally HiBiT-tagged human 5-HT<sub>2c</sub> receptor was transferred into the pCDNA3 vector via EcoRV/XhoI endonuclease sites for selection with Neomycin (G418). The PCR conditions were as follows: initial activation of the Q5<sup>®</sup> High-Fidelity DNA Polymerase for 60 s at 98 °C, followed by 25 cycles of 10 s denaturation at 98 °C, 10 s annealing at 58 °C and extension for 30 sec at 72 °C. The program ended with a 2 min fill in step at 72 °C.

### 6) pCDNA3.1Zeo(+)-HiBiT-hu5HTR7

HTR7-Tango was a gift from Bryan Roth (Addgene plasmid # 66415)<sup>65</sup>. The information for the human 5-HT<sub>7</sub> receptor was amplified via PCR (forward primer: 5'-CTCGCTAGCGGGATC-CATGATGGACGTTAACAGC-3', reverse primer: 5'-AGACTCGAGTCAGTCATGGATCATT-ACCTTC-3') and exchanged for the human 5-HT<sub>2A</sub> receptor in the pCDNA3.1Zeo(+)-HiBiT-hu5HTR2a vector via NheI/XhoI endonuclease sites. The PCR conditions were the same as for pCDNA3-HiBiT-hu5HTR2c.

### 7) pTet-NewMCS-HiBiT-hu5HTR2a

The already existing plasmid pTet-NewMCS (based on Exp-pcDNA3.2delCMV(EF1 $\alpha$ -tTA/TetO-mCh-Rs1) (the plasmid was a gift from Edward Hsiao (Addgene plasmid # 26797)<sup>66</sup> was used as a template. Into this vector, the genetic information for the HiBiT-tagged human 5-HT<sub>2A</sub> receptor was inserted via Bsu15I/Spel restriction endonuclease sites.

All constructs were amplified by transformation into XL1-blue bacteria and subsequent isolation of plasmid DNA. The integrity of all constructs was confirmed by agarose gel electrophoresis and cycle sequencing performed by GATC (part of Eurofins Genomics,

## Methods

Ebersberg, Germany). Plasmid cards for all mentioned constructs and agarose gel electrophoresis for constructed plasmids are available in the supplementary information (Figure S 1 to Figure S 24). Ligation was performed for 1 h at room temperature by combining 1 Unit T4-DNA ligase with 20 ng vector-DNA and 3-fold amount of the insert-DNA fragment in 1x ligase buffer.

### 4.4.2 Transformation of XL1-blue bacteria cultures

The amplification of the DNA constructs described above was achieved by mixing approx. 1 ng of DNA with 100 µl competent XL-1 blue bacteria. The mixture was kept on ice for 30 min. A heat shock was performed by heating the mixture for 30 s to 42 °C and suddenly cooling it on ice for 1 min. Subsequently, 900 µl of pre-warmed LB medium was added to the bacteria–DNA mix and the mixture was incubated in a shaker at 37 °C for 1 h. Afterwards, the bacteria were harvested by centrifugation at 3,000 x g for 5 min at RT. After resuspension in 50 µl LB medium, 10 to 25 µl were spread on agar-LB-medium plates (1.5% w/v agar in LB-medium) containing appropriate antibiotics (50 µg/ml ampicillin or 25 µg/ml kanamycin) and incubated at 37 °C overnight. Single clones arising from single bacterial cells were picked and inoculated each in 5 ml antibiotic containing LB-medium and incubated at 37 °C for 8 h in an orbital shaker. Afterwards, 500 µl of pre-culture was added to 50 ml fresh, antibiotic-containing LB-medium and allowed to grow at 37 °C overnight in an orbital shaker. Plasmid DNA was isolated according to the step-by-step Miraprep protocol from Pronobis et. al. (Figure S 25)<sup>67</sup>. Resulting plasmids were digested with the suitable restriction enzymes and the correct insert size was verified by agarose gel electrophoresis in comparison to a DNA standard ladder.

### 4.4.3 Agarose gel electrophoresis

An agarose gel (1 %) was prepared by suspending the required amount of agarose in 1 x TAE buffer and heating in a microwave oven until the solution became clear. After cooling the solution down to approximately 55 °C, ethidium bromide was added in a final concentration of 1 µg/ml and the mixture was allowed to polymerize in a prepared casting tray with a comb of suitable size. After being completely polymerized, the gel was placed into an electrophoresis chamber filled with a 1 x TAE buffer. The digested DNA samples were mixed with the sample buffer and slowly loaded into the wells before an electric current was applied (3-10 V/cm<sup>2</sup>) for 30 min. Finally, DNA fragments were detected using an UV detector.

#### 4.4.4 Transfection of HEK293 cells

##### 1) Polyethylenimine (PEI) transfection

HEK293 cells were transfected using Polyethylenimine (PEI). The cells were seeded in 6 well plates and allowed to attach to the surface for at least 24 h. The medium was changed prior to transfection to 1.8 ml fully supplemented culture medium. Three µg DNA was mixed with 9.87 µl of 1 mg/ml PEI solution in 200 µl 150 mM NaCl. The mixtures were added dropwise to the wells and incubated for 24 h at 37° C and 5% CO<sub>2</sub>. After 24 h, the medium was changed to selection medium containing 150 µg/ml Zeocin for HEK293-B-GECO1 and 700 µg/ml Neomycin (G418) and 150 µg/ml Zeocin for HEK293-B-GECO1-5HT2a. After two weeks of selection, single colonies were isolated using trypsin solution and metal cloning rings and transferred into distinct wells of a 12 well plate. The resulting clones were tested for functionality and one clone for each cell line was chosen for measurements and further on cultured in 10 cm dishes.

##### 2) Transfection by electroporation

**Table 9: Transfection by electroporation.** Transfected HEK293 cell lines and their corresponding antibiotic resistances

Cell line	Antibiotic resistance
HEK293-HiBiT-5HT2a	150 µg/ml Zeocin
HEK293-Aequorin-HiBiT-5HT2c	150 µg/ml Zeocin + 700 µg/ml G418
HEK293-GloSensor-HiBiT-5HT7*	150 µg/ml Zeocin + 100 µg/ml Hygromycin
HEK293-Aequorin-Tetoff-HiBiT-5HT2a	150 µg/ml Zeocin + 700 µg/ml G418

\*HEK293-GloSensor cells have been transfected and characterized in our workgroup and are comparable to Binkowski et. al.<sup>68</sup>

HEK293 cells were transfected by Amaxa electroporation technology, Nucleofector® II. For each transfection 1 x 10<sup>6</sup> cells were diluted in 100 µl of a self-made electroporation buffer with 1 µg DNA and transfected with the program Q-001 according to the manufacturer's protocol (Amaxa GmbH, Koeln, Germany) (Figure S 26). After transfection, the cells were seeded in 6 well plates and allowed to attach to the surface for at least 24 h. The medium was changed to selection medium containing the appropriate antibiotic (150 µg/ml Zeocin, 700 µg/ml G418, 100 µg/ml Hygromycin or a combination of them; see Table 9). After two weeks of selection single-cell colonies were isolated using a single cell cloning protocol (Corning Inc., New York, USA) (Figure S 27). The resulting clones were tested for functionality and one clone was chosen for measurements and further on cultured in 10 cm dishes.

#### 4.5 FCS measurements

##### Experimental setup

FCS measurements were performed with a ConfoCor 1 instrument (Carl Zeiss Microscopy GmbH; Jena, Germany). For excitation, the 514 nm line of an argon-ion laser (LGK 7812 ML 2, Lasos; Jena, Germany) was focused through a water immersion objective (C Apochromat, 63x, NA 1.2, Carl Zeiss Microscopy GmbH) into the sample localized in an illuminated open volume element of 0.2 fl (laser power:  $p_{514\text{nm}} = 2.4 \text{ kW/cm}^2$ ). The emitted fluorescence was collected by the same objective. After passing a dichroic mirror (FT540, Andover, Salem, USA), a band-pass filter (EF530-600, Andover), and a pinhole with a diameter of 40  $\mu\text{m}$ , the emitted photons were detected by an avalanche single-photon counting module (SPCM) (SPCM-AQ Series, EG & G Optoelectronics Canada Inc.; Vaudreuil, Quebec, Canada). Using the MATLAB Software (version R2009a, The MathWorks Inc., Natick, MA) autocorrelation curves were evaluated with the autocorrelation function:

$$(1) \quad G(\tau) = 1 + \frac{\sum_{j=1}^n Q_j^2 N_j}{\left[ \sum_{j=1}^n Q_j N_j \right]^2} \frac{1}{1 + \tau/\tau_{D_j}} \sqrt{\frac{1}{1 + (\omega_0/z_0)^2 \tau/\tau_{D_j}}}$$

with

$$(2) \quad \tau_{D_j} = \frac{\omega_0^2}{4D_j}$$

and

$$(3) \quad Q_j = \sigma_j \eta_j g_j$$

where  $N_j$  is the average number of molecules of the species  $j$  in the volume element,  $\tau_{D_j}$  is the diffusion time constant of the species  $j$ ,  $\tau$  is the correlation time,  $\omega_0$  is the radius of the observation volume in the focal plane,  $z_0$  is the radius of the observation volume in the  $z$ -direction,  $D_j$  is the translational diffusion coefficient of the species  $j$ ,  $Q_j$  is the quantum yield factor,  $\sigma_j$  is the absorption coefficient,  $\eta_j$  is the fluorescence quantum yield and  $g_j$  is the fluorescence detection efficiency of the species  $j$ .

## Methods

### Cell measurements

C6 / SH-SY5Y cells were seeded in a density of 50,000 cells per cm<sup>2</sup> on 18 mm glass coverslips (Menzel-Gläser, Germany) in their respective fully supplemented culture media two days prior to the experiment. On the day of the experiment, C6 / SH-SY5Y cells reached a density of 75-90% and were washed with Locke's solution (Locke / HEPES 5 mM, NaCl 154 mM, KCl 5.6 mM, MgCl<sub>2</sub> 1 mM, Na<sub>2</sub>CO<sub>3</sub> 3.6 mM, glucose 20 mM, CaCl<sub>2</sub> 2.3 mM, pH 7.4) at 37 °C. Coverslips were mounted on a coverslip carrier with 300 µl of Locke and the respective fluorescent ligand was added in the desired concentration. The focal plane of the open volume element was positioned to the upper plasma membrane by motor aided scanning through the cell in the z-direction. At the position of half-maximal fluorescence, simultaneous detection of fast diffusing free ligand and slow diffusing ligand bound to the receptor was possible. The diffusion time constant for the free diffusing ligand was measured after 30 min incubation of C6 / SH-SY5Y cells by positioning the open volume element in the solution above the cells.

### Ligand binding and non-specific binding

C6 / SH-SY5Y cells were incubated for 30 min at room temperature with the respective fluorescent ligand in the desired concentration. Fluorescence fluctuation in the plasma membrane and in the solution above was measured 10 times for 30 s each per cell. Non-specific binding was measured on the same cell after a further 30 minutes incubation with 10 µM (±)-TCB-2.

### Displacement experiments

Experiments were performed by 30 min incubation of SH-SY5Y cells with 10 nM (±)-SAH268-Atto532 and measurement of the total binding. After the addition of 10 µM (±)-TCB-2, 5 µM WAY-100635, 5 µM SB-242084 and 5 µM SB-269970, respectively, incubation was continued for further 30 min to displace (±)-SAH268-Atto532 binding. (±)-SAH268-Atto532 binding and displacement were determined at the same cell. Remaining binding after displacement was normalized to the binding before displacement and plotted for every condition. Statistical significance was determined by Student's unpaired t-test with a p-value < 0.05.

### Selectivity of the (±)-SAH268-Atto532-binding to 5HT<sub>2A</sub> receptors

HEK293-HiBiT-5HT<sub>2a</sub>, HEK293-Aequorin-HiBiT-5HT<sub>2c</sub>, and HEK293-GloSensor-HiBiT-5HT<sub>7</sub> cells were seeded in a density of 50,000 cells per cm<sup>2</sup> on 18 mm glass coverslips in their fully supplemented culture medium. Beforehand, the coverslips were coated using 500 µl of 0.1 mg/ml PDL solution for 30 min at 37 °C and washed three times with 500 µl PBS. Binding experiments were performed by 30 min incubation of cells with 10 nM (±)-SAH268-Atto532 and measurement of total binding. Afterwards, 10 µM (±)-TCB-2 was added and incubated for

## Methods

further 30 min to displace ( $\pm$ )-SAH268-Atto532 binding. ( $\pm$ )-SAH268-Atto532 binding and displacement were determined at the same cell. Remaining binding after displacement was normalized to the binding before displacement. Statistical significance was determined by Student's unpaired t-test with a p-value < 0.05.

### Saturation experiment

SH-SY5Y cells were incubated with concentrations between 5 nM and 200 nM ( $\pm$ )-SAH268-Atto532 for 30 min at room temperature. Fluorescence fluctuation in the plasma membrane and in the solution above was measured 10 times for 30 s each per cell. Total binding represents the sum of receptor-ligand fractions with the diffusion time constants  $T_{diff2}$  and  $T_{diff3}$  for each concentration. The fraction of bound ( $\pm$ )-SAH268-Atto532 was plotted against the total concentration of ( $\pm$ )-SAH268-Atto532 used in the saturation experiment.  $K_D$  and  $B_{max}$  were obtained by computer-assisted curve fitting (GraphPad Prism, San Diego, CA, USA) using a nonlinear fit for one site-specific binding with Hill slope.

## 4.6 SPT measurements

### Experimental setup

All SPT data were recorded with an EMCCD camera (iXon DV-860DCS-BV, Andor Technology), being part of a custom-built inverted wide-field epifluorescence microscope (TE2000-S, Nikon) equipped with a water immersion objective (Plan APO VC, 60x, 1.2 NA, Nikon) and a 200-mm-focal length tube lens. Due to a 4x-magnification lens (VM Lens C-x, Nikon), the setup had an effective magnification of 240x, translating to an image width of 10  $\mu\text{m}$  with a pixel width of 0.1  $\mu\text{m}$ . A 532 nm continuous wave laser (LasNova GLK 2350 T01, 532 nm, 50 mW) was used for excitation. Laser intensity was regulated using an acousto-optic tunable filter (AA Opto-Electronic) and set to 0.733 kW/cm<sup>2</sup> in the object plane.

### Cell measurements

SH-SY5Y cells were seeded in a density of 50,000 cells per cm<sup>2</sup> on 18 mm glass coverslips in their fully supplemented cell culture medium two days prior to the experiment. On the day of the experiment, SH-SY5Y cells reached a density of 75-90% and were washed with Locke at 37 °C. The coverslips were mounted on a coverslip carrier with 300  $\mu\text{l}$  of Locke and 2 nM ( $\pm$ )-SAH268-Atto532 was added. To avoid photobleaching before image acquisition, cells were searched and focused to the epical plasma membrane in transmitted light, before opening the laser shutter and starting the recording. Image sequences were acquired with a frame-rate of 20 Hz.

## Methods

### Spot detection and tracking

Two-dimensional particle tracks from image data were generated and further diffusion analysis was conducted using the MATLAB software (version R2016b). Direct import of the images and further processing were accomplished by the u-track package with the following settings: 1.32 px spot radius, 3 frame rolling window time-averaging for local maxima detection, 2 frame minimum track segment length, 1 frame maximum gap length, other settings on default<sup>69</sup>.

Identification of discrete diffusive states from particle tracks was carried out using variational Bayes single particle tracking with the help of the vbSPT Matlab package<sup>70</sup>. Tracks were thereby segmented and variably classified to one of three states according to their diffusion speed. Higher order models were recognized by the program but not used, since they resulted in degenerate states of insignificant occupancy and indistinct diffusion behaviour. The following settings in the runinput-file were used: timestep = 0.05, dim = 2, trjLmin = 4, runs = 36, maxHidden = 4, bootstrapNum = 100, fullBootstrap = 0.

### 4.7 Calcium measurements for ( $\pm$ )-SAH268-Atto532

#### Experimental setup

Fluorescence imaging was conducted with an Axiovert<sup>®</sup> 200 M microscope, equipped with a Colibri.2<sup>®</sup> LED system including a 365 nm LED, LD Achromplan 40x, NA 0.60 Corr objective, AxioCamMR3<sup>®</sup> camera, and filter set 49 (Excitation: G 365, Beam Splitter: FT 395 Emission: BP 445/50). The system was operated with Axiovision<sup>®</sup> Rev. 4.8. All parts mentioned were from Carl Zeiss Microscopy GmbH, Jena, Germany.

#### Cell measurements

HEK293-B-GECO1 and HEK293-B-GECO1-5HT2a cells were seeded in a density of 12,500 cells per cm<sup>2</sup> on 18 mm glass coverslips in DMEM, no glutamine, no phenol red (Life Technologies Ltd.; Paisley, UK) supplemented with 10% FBS and 2 mM L-glutamine two days prior to the experiment. Beforehand, the coverslips were coated using 500  $\mu$ l of 0.1 mg/ml PDL solution for 30 min at 37 °C and washed three times with 500  $\mu$ l PBS. On the day of the experiment, the cells reached a density of 75-90% and were washed with Locke at 37 °C. The coverslips were mounted on a coverslip carrier with 300  $\mu$ l of Locke. After focusing on the cellular layer, pictures were taken every 3 s with an illumination time of 1 s and LED power of 50%. After ten seconds (between pictures 4 and 5) the compound of interest (1.4  $\mu$ M ionomycin, 10  $\mu$ M ( $\pm$ )-TCB-2 or 5  $\mu$ M ( $\pm$ )-SAH268-Atto532, each dissolved in Locke and Locke itself) was applied to the cells and pictures were taken for additional 60 s.

## Methods

### Data analysis

Acquired image sequences were analyzed with the optional Time Series Analyzer v3 plugin for the Fiji software package. Cells were randomly chosen and overlaid with ROI. The mean fluorescence intensity for the chosen ROI was determined for every picture of the sequence. The background was subtracted from all values by positioning an ROI of the same size in cell-free areas of the picture. Mean fluorescence intensity after 9 s was set to 100% for each cell measured. Then mean fluorescence intensity for each time-point was normalized to this value. Statistical significance was determined by Student's unpaired t-test with a p-value < 0.05.

### 4.8 Characterization of STW3-VI<sup>®</sup> via HPLC

STW3-VI<sup>®</sup> was dissolved in 50% EtOH in a concentration of 1.0 mg/ml and analyzed by HPLC method 7 (Table 7). Identification of rutin, hyperoside, isoquercetin, quercetin, quercitrin, amentoflavone, hyperforin, pseudohypericin, and hypericin was carried out by comparison of UV spectra of reference substances and their corresponding retention times (Figure 31). Concentrations for hyperforin and hyperoside were determined to be 36.8 µM for hyperforin and 53.3 µM for hyperoside (calculations in supplemental material). STW3-VI<sup>®</sup> was used for preincubations in the concentrations of 0.02, 0.002 and 0.0002 mg/ml. Hyperforin and hyperoside were used in concentrations of 1.0, 0.1 and 0.01 µM.

### 4.9 Influence of STW3-VI<sup>®</sup>, hyperforin, and hyperoside on the ligand binding and diffusion of 5-HT<sub>2A</sub> receptors

SH-SY5Y cells were preincubated for at least six days with 1.0, 0.1 and 0.01 µM hyperforin and hyperoside or with 0.02, 0.002 and 0.0002 mg/ml STW3-VI<sup>®</sup> and with the highest concentration of 0.5% ethanol used in the experiment as a control. On day four of the preincubation period, SH-SY5Y cells were seeded in a density of 50,000 cells per cm<sup>2</sup> on 18 mm glass coverslips in fully supplemented culture medium containing the respective test substance. Measurement and data analysis were conducted as described in 4.5.

### 4.10 Influence of STW3-VI<sup>®</sup>, hyperforin, and hyperoside on the receptor density and internalization of HiBiT-tagged 5-HT<sub>2A</sub> receptors

#### Experimental setup

Luminescence measurements were conducted on a Tecan Infinite<sup>®</sup> M200 PRO plate reader operated by Tecan i-control ver. 1.10 (Tecan Trading AG, Maennedorf, Switzerland).

## Methods

### Cell measurements

HEK293-HiBiT-5HT<sub>2A</sub> cells were preincubated for at least six days with 1.0  $\mu$ M hyperforin and hyperoside or with 0.02, 0.002 and 0.0002 mg/ml STW3-VI<sup>®</sup> and with the highest concentration of 0.5% ethanol used in the experiment as a control. The cells were seeded in a density of 50,000 cells per cm<sup>2</sup> on a white 96-well plate with a transparent flat bottom for luminescence measurements (Greiner Bio One International GmbH, Frickenhausen, Germany) three days prior to the experiment. Beforehand, the plates were coated using 50  $\mu$ l of 0.1 mg/ml PDL solution for 30 min at 37 °C and washed three times with 50  $\mu$ l PBS. On the day of the experiment, the cells were treated either with 1.0  $\mu$ M of ( $\pm$ )-TCB-2 for 15 min or with buffer as control. Afterwards, the experiment was undertaken according to the manufacturer's protocol for Nano-Glo<sup>®</sup> HiBiT Extracellular Detecton System (Promega GmbH, Walldorf, Germany) (Figure S 28). Emitted light was measured in relative light units (RLU) every 2 min with an integration time of 1 s for the duration of 60 min.

### Data analysis

RLU values at assay time point  $t = 30$  min were considered optimal in terms of reproducibility during method implementation. First, the influence of different preincubations on the amount of 5-HT<sub>2A</sub> receptors in the cellular membrane under non-stimulating conditions was evaluated. Therefore, the RLU values for cells preincubated with STW3-VI<sup>®</sup>, hyperforin and hyperoside were normalized to non-preincubated control cells. Second, the influence of the preincubations on the ( $\pm$ )-TCB-2 induced internalization of 5-HT<sub>2A</sub> receptors was assessed. RLU values for cells treated with 1.0  $\mu$ M ( $\pm$ )-TCB-2 for 15 min were normalized to non-treated cells for each experimental condition (non-preincubated cells and all preincubations) at the assay time point  $t = 30$  min. Statistical significance was determined by Student's unpaired t-test with a p-value  $< 0.05$ .

### 4.11 Influence of STW3-VI<sup>®</sup>, hyperforin, and hyperoside on the 5-HT<sub>2A</sub> receptor-mediated intracellular Ca<sup>2+</sup> levels

#### Experimental setup

Luminescence measurements were conducted on a Tecan Infinite<sup>®</sup> M200 PRO plate reader operated by Tecan i-control ver. 1.10.

### Cell measurements

HEK293-Aequorin-Tetoff-HiBiT-5HT<sub>2A</sub> cells were preincubated for at least six days with 1.0  $\mu$ M hyperforin and hyperoside or with 0.02, 0.002 and 0.0002 mg/ml STW3-VI<sup>®</sup> and with the highest concentration of 0.5% ethanol used in the experiment as a control. The cells were

## Methods

seeded in a density of 25,000 cells per cm<sup>2</sup> on a white 96-well plate with a transparent flat bottom for luminescence measurements three days prior to the experiment. Beforehand, the plates were coated using 50 µl of 0.1 mg/ml PDL solution for 30 min at 37 °C and washed three times with 50 µl PBS. Two hours before assay start, the culture medium was replaced with 99 µl Locke. Afterwards, 1 µl of 500 µM coelenterazine stock solution was added to each well. Right before assay start, another 95 µl Locke was added to the wells. The injection system was loaded with 400 µM (±)-TCB-2 solution and 5 µl of it were injected, resulting in 10 µM (±)-TCB-2 per well. RLU were measured every 2 s with an integration time of 1 s for the duration of 50 s, 8 s before injection and another 42 s after injection.

### Data analysis

For the resulting measurement curve of RLU over time [s] the area under the curve (AUC) was determined via trapezoidal rule.

$$Area = \frac{1}{2} * (a + c) * h$$

An exemplary calculation of the trapezoid between t = 8 s and t = 10 s with:

$$a = RLU_{8s} \quad c = RLU_{10s}$$

$$h = 10 s - 8 s = 2 s$$

$$Area_{8s,10s} = \frac{1}{2} * (RLU_{8s} + RLU_{10s}) * 2 s$$

For calculating the AUC all trapezoidal areas have to be summed up (26 time points result in 25 trapezoids, therefore m = 25).

$$AUC = \sum_n^m = \sum_{n=1}^{25} Area_{2n-2,2n}$$

Resulting AUC values for each preincubation were normalized to non-preincubated control cells. Statistical significance was determined by Student's unpaired t-test with a p-value < 0.05.

## 5. Results

### 5.1 Synthesis of a fluorescent 5-HT<sub>2A</sub> receptor ligand

The general synthetic approach for a selective fluorescent 5-HT<sub>2A</sub> receptor agonist started from the racemic mixture of the 5-HT<sub>2A</sub> receptor agonist (±)-TCB-2. Different succinimidylester-activated fluorophores were coupled to the primary amine group of (±)-TCB-2. The rhodamine-based dyes Alexa-Fluor532-NHS and Atto532-NHS, as well as the cyanine-based dye Alexa-Fluor647-NHS were employed. The binding to 5-HT<sub>2A</sub> receptors of the resulting molecule could be impacted by coupling a large fluorophore to (±)-TCB-2. Furthermore, converting the primary amine of (±)-TCB-2 to an acid amide by reacting it with NHS esters, leads to a nitrogen atom, which cannot be further protonated in aqueous solution. It is described in the literature that a protonable amine in the phenylalkylamine moiety is important for the agonistic binding of 5-HT<sub>2A</sub> ligands<sup>71,72</sup>. Therefore, additionally to labelling (±)-TCB-2 with fluorophores differing in their detection wavelengths and general chemical structure, an aminohexyl-linker was introduced to (±)-TCB-2. The resulting (±)-SAH268 with a secondary amine, which can still be protonated in aqueous solution, was also coupled to Alexa-Fluor532-NHS, Alexa-Fluor647-NHS and Atto532-NHS via its primary amine function.

An overview for the synthesized ligands is provided in Figure 1.

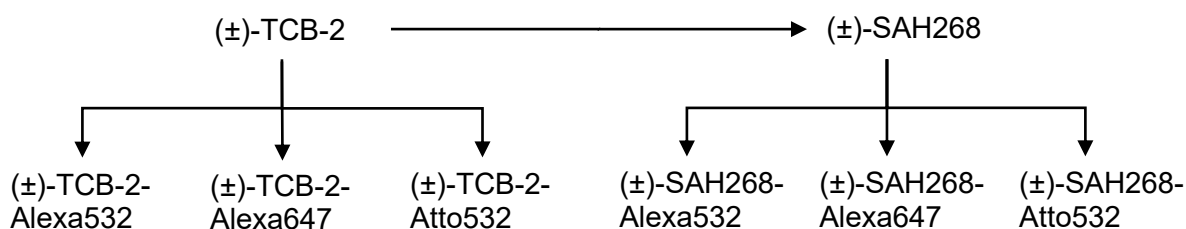


**Figure 1: Overview - synthesis of a fluorescent 5-HT<sub>2A</sub> receptor ligand**

In the first step, (±)-TCB-2 was coupled to Alexa-Fluor532-NHS in aqueous 0.1 M NaHCO<sub>3</sub> solution overnight at room temperature (Figure 2). The used molecular equivalents and purification conditions are displayed in Table 8.

## Results

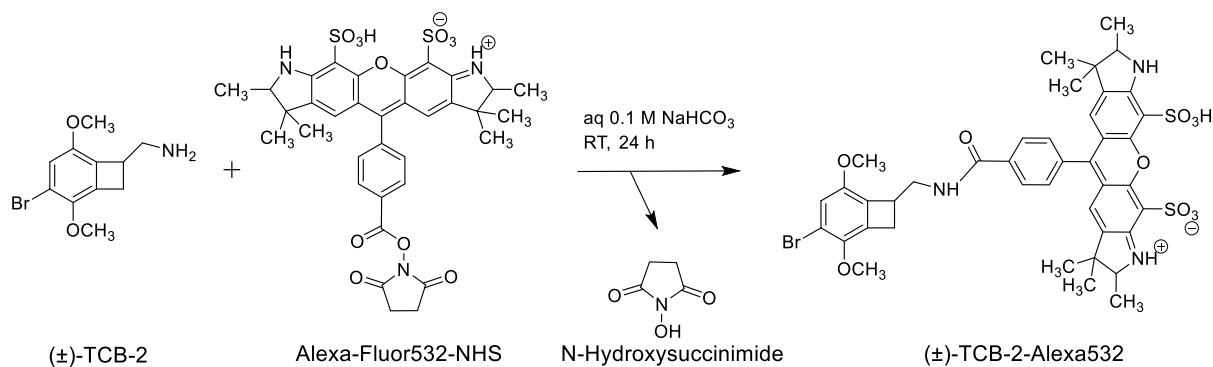


**Figure 2: Synthesis of (±)-TCB-2-Alexa532.** Alexa-Fluor532-NHS was directly coupled to the primary amine of (±)-TCB-2 in aqueous 0.1 M NaHCO<sub>3</sub> solution overnight at room temperature, forming the desired amide (±)-TCB-2-Alexa532 and N-Hydroxysuccinimide (NHS) as a leaving group.

After purification, (±)-TCB-2-Alexa532 with the sum formula C<sub>41</sub>H<sub>42</sub>BrN<sub>3</sub>O<sub>10</sub>S<sub>2</sub> was detected using high-resolution mass spectrometry as a Na<sup>+</sup>-adduct with m/z = 902.13837 [M+Na]<sup>+</sup>. It was identified by comparing the detected m/z and the typical isotopic pattern resulting from the bromide atom to a simulated spectrum with a calculated value of m/z = 902.13872 [M+Na]<sup>+</sup> (Figure 3).

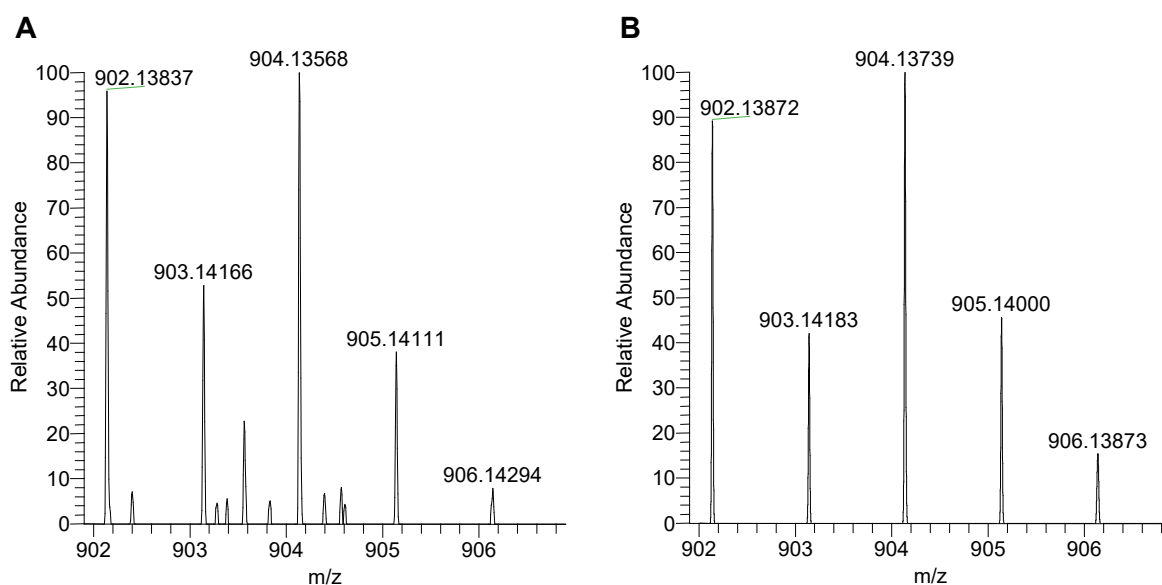


**Figure 3: HRMS spectrum for (±)-TCB-2-Alexa532.** Measured spectrum (A) and simulated spectrum with a resolution of R = 60,000 (B).

In the second step, Alexa-Fluor647-NHS was coupled to (±)-TCB-2 in aqueous 0.1 M NaHCO<sub>3</sub> solution overnight at room temperature (Figure 4). With Alexa-Fluor647-NHS, a fluorophore with a cyanine-based structure compared to Alexa-Fluor532-NHS with a rhodamine-based structure was used. The used molecular equivalents and purification conditions are displayed in Table 8.

## Results

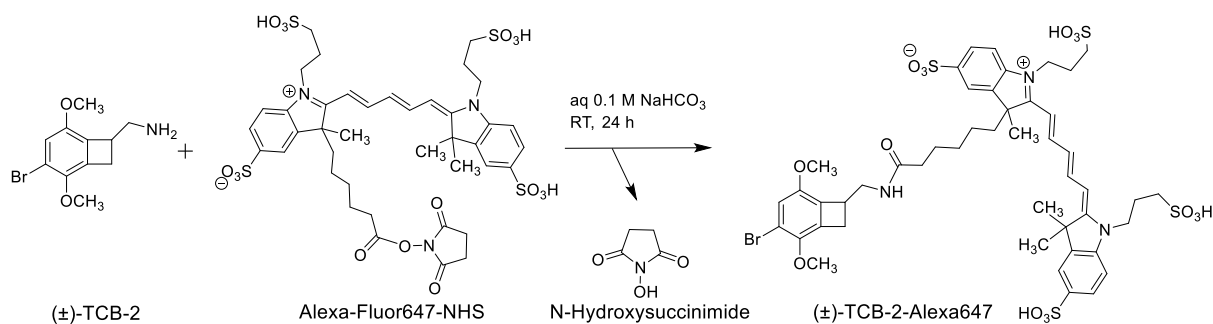


**Figure 4: Synthesis of (±)-TCB-2-Alexa647.** Alexa-Fluor647-NHS was directly coupled to the primary amine of (±)-TCB-2 in aqueous 0.1 M NaHCO<sub>3</sub> solution overnight at room temperature, forming the desired amide (±)-TCB-2-Alexa647 and NHS as a leaving group.

(±)-TCB-2 Alexa647 with the sum formula C<sub>47</sub>H<sub>58</sub>BrN<sub>3</sub>O<sub>15</sub>S<sub>4</sub> was detected using high-resolution mass spectrometry as a H<sup>+</sup>-adduct with m/z = 1112.20223 [M+H]<sup>+</sup>. It was identified by comparing the detected m/z and the isotopic pattern to a simulated spectrum with a calculated value of m/z = 1112.20069 [M+H]<sup>+</sup> (Figure 5).

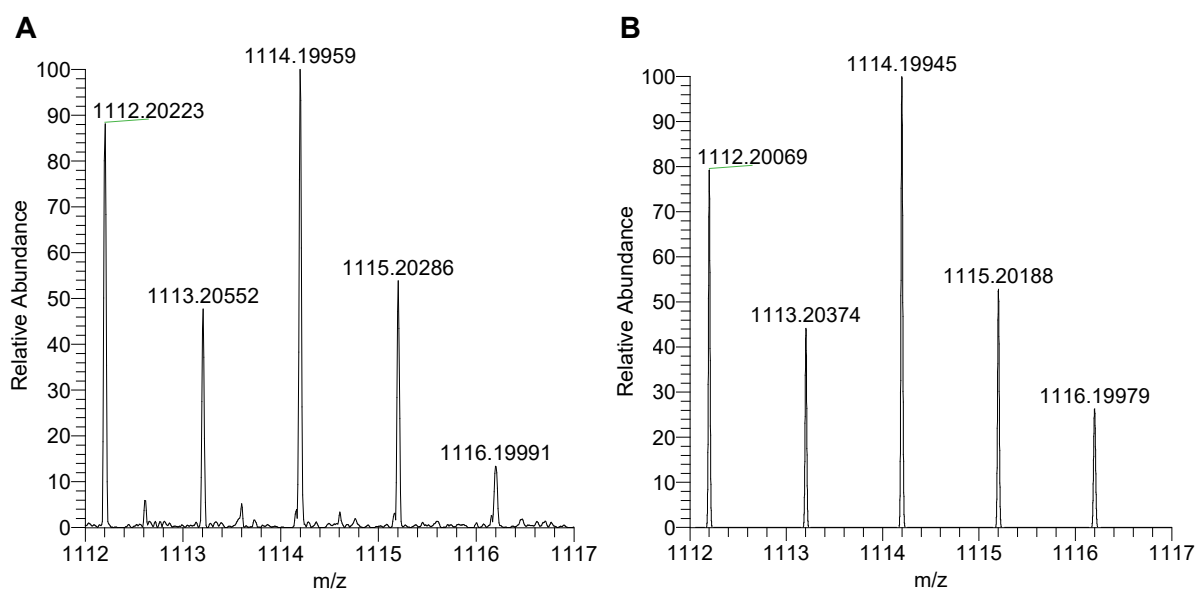


**Figure 5: HRMS spectra for (±)-TCB-2-Alexa647.** Measured spectrum (A) and simulated spectrum with a resolution of R = 60,000 (B).

For the completion of the first set of fluorescent ligands, Atto532-NHS was coupled to (±)-TCB-2 in aqueous 0.1 M NaHCO<sub>3</sub> solution overnight at room temperature (Figure 6). Atto532-NHS and Alexa-Fluor532-NHS are both rhodamine-based fluorophores, but Atto532-NHS differs from Alexa-Fluor532-NHS in the heterocyclic ring system and the distance of the fluorophore to the NHS-group. The used molecular equivalents and purification conditions are displayed in Table 8.

## Results

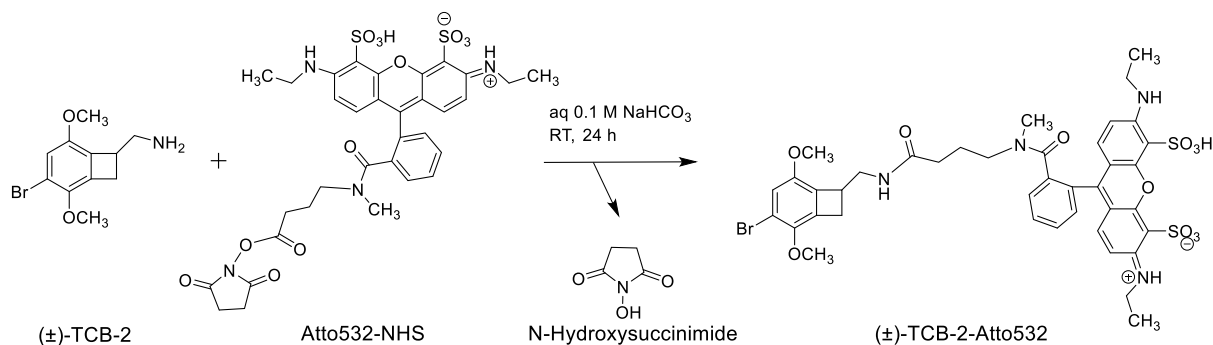


**Figure 6: Synthesis of (±)-TCB-2-Atto532.** Atto532-NHS was directly coupled to the primary amine of (±)-TCB-2 in aqueous 0.1 M NaHCO<sub>3</sub> solution overnight at room temperature, forming the desired amide (±)-TCB-2-Atto532 and NHS as a leaving group.

(±)-TCB-2-Atto532 with the sum formula C<sub>40</sub>H<sub>43</sub>BrN<sub>4</sub>O<sub>11</sub>S<sub>2</sub> was detected using high-resolution mass spectrometry as a H<sup>+</sup>-adduct with  $m/z = 899.16394$  [M+H]<sup>+</sup>. It was identified by comparing the detected  $m/z$  and the isotopic pattern to a simulated spectrum with a calculated value of  $m/z = 899.16259$  [M+H]<sup>+</sup> (Figure 7).

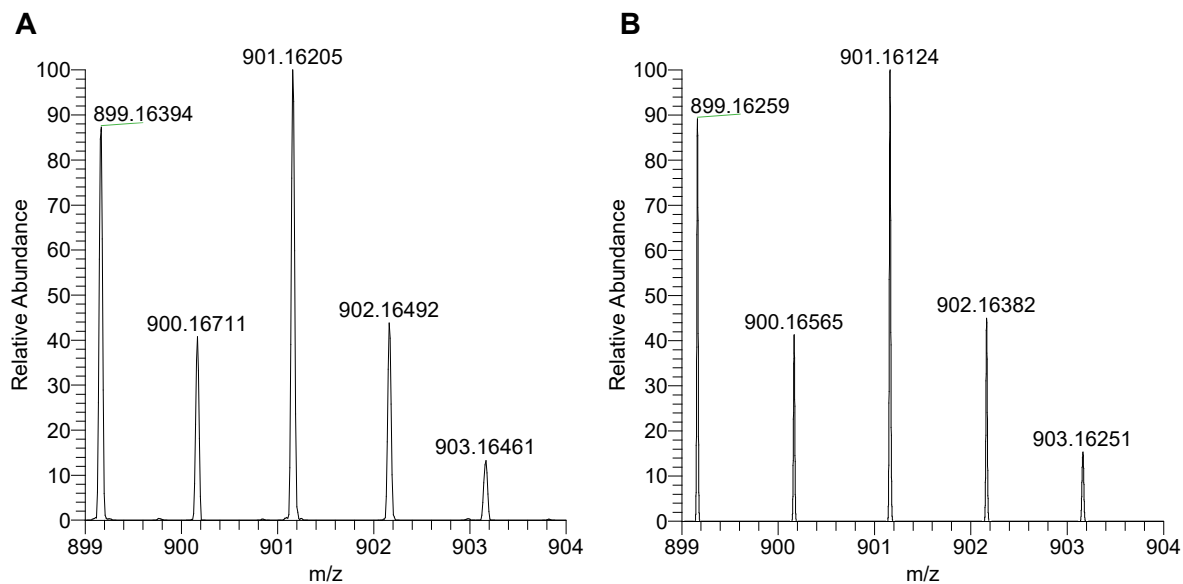


**Figure 7: HRMS spectra for (±)-TCB-2-Atto532.** Measured spectrum (A) and simulated spectrum with a resolution of R = 60,000 (B).

As already mentioned, a protonable amine in the phenylalkylamine moiety is necessary for the agonistic binding of 5-HT<sub>2A</sub> receptor ligands. By direct coupling of (±)-TCB-2 via NHS esters, an acid amide is formed from the primary amine, whose nitrogen atom cannot be further protonated in aqueous solution. To address this problem, an aminohexyl linker was introduced to (±)-TCB-2 to allow coupling to an NHS-activated dye and to ensure protonation on an aliphatic nitrogen (Figure 8). In addition, the linker should also facilitate an improved binding to the 5-HT<sub>2A</sub> receptor.

## Results

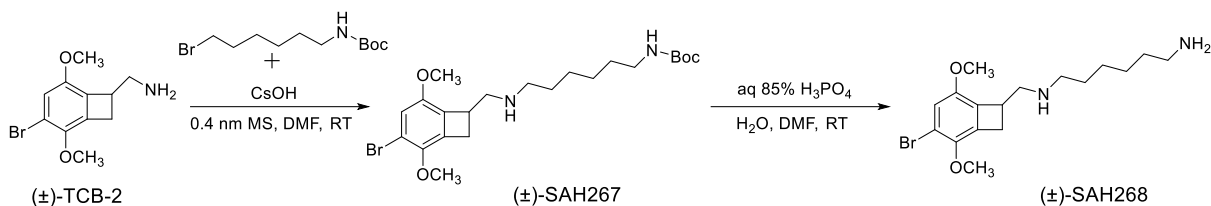


**Figure 8: Synthesis of (±)-SAH268.** Starting from (±)-TCB-2, in a cesium-catalyzed reaction a Boc-protected aminohexyl linker was introduced to the primary amine of (±)-TCB-2, which was deprotected in the following reaction by aqueous phosphoric acid, finally leading to (±)-SAH268.

(±)-SAH268 with the sum formula C<sub>17</sub>H<sub>27</sub>BrN<sub>2</sub>O<sub>2</sub> was detected using high-resolution mass spectrometry as a H<sup>+</sup>-adduct with  $m/z = 371.13289$  [M+H]<sup>+</sup>. It was identified by comparing the detected  $m/z$  and the isotopic pattern to a simulated spectrum with a calculated value of  $m/z = 371.13287$  [M+H]<sup>+</sup> (Figure 9).

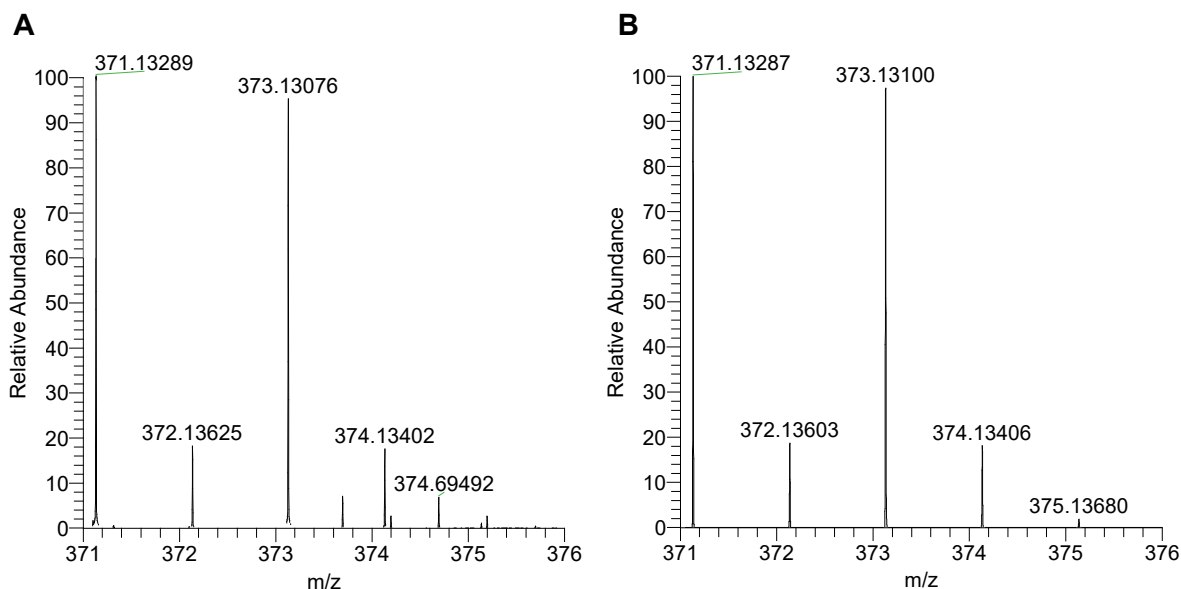


**Figure 9: HRMS spectra for (±)-SAH268.** Measured spectrum (A) and simulated spectrum with a resolution of  $R = 60,000$  (B).

Following the reasoning for the (±)-TCB-2-based fluorescent ligands, (±)-SAH268 was coupled to Alexa-Fluor532-NHS (Figure 10), Alexa-Fluor647-NHS (Figure 12) and Atto532-NHS (Figure 14) in aqueous 0.1 M NaHCO<sub>3</sub> solution overnight at room temperature. The used molecular equivalents and purification conditions are displayed in Table 8 for all those reactions.

## Results

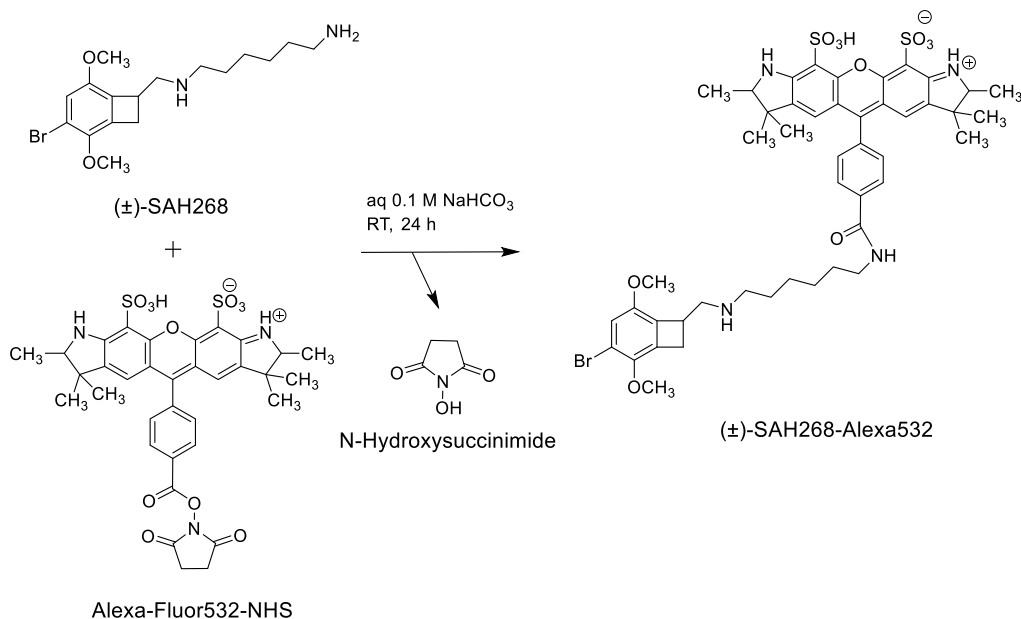


**Figure 10: Synthesis of (±)-SAH268-Alexa532.** Alexa-Fluor532-NHS was directly coupled to the primary amine of (±)-SAH268 in aqueous 0.1 M NaHCO<sub>3</sub> solution overnight at room temperature, forming the desired amide (±)-SAH268-Alexa532 and NHS as a leaving group.

(±)-SAH268-Alexa532 with the sum formula C<sub>47</sub>H<sub>55</sub>BrN<sub>4</sub>O<sub>10</sub>S<sub>2</sub> was detected using high-resolution mass spectrometry as a H<sup>+</sup>-adduct with  $m/z = 979.26025$  [M+H]<sup>+</sup>. It was identified by comparing the detected  $m/z$  and the isotopic pattern to a simulated spectrum with a calculated value of  $m/z = 979.26157$  [M+H]<sup>+</sup> (Figure 11).

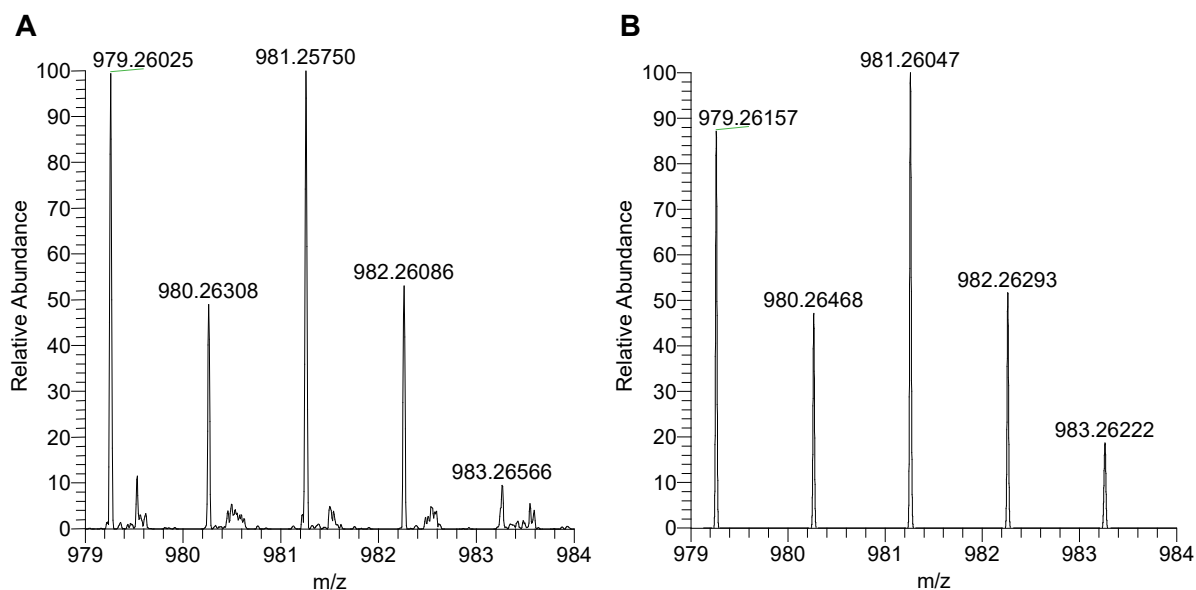


**Figure 11: HRMS spectra for (±)-SAH268-Alexa532.** Measured spectrum (A) and simulated spectrum with a resolution of  $R = 60,000$  (B).

## Results

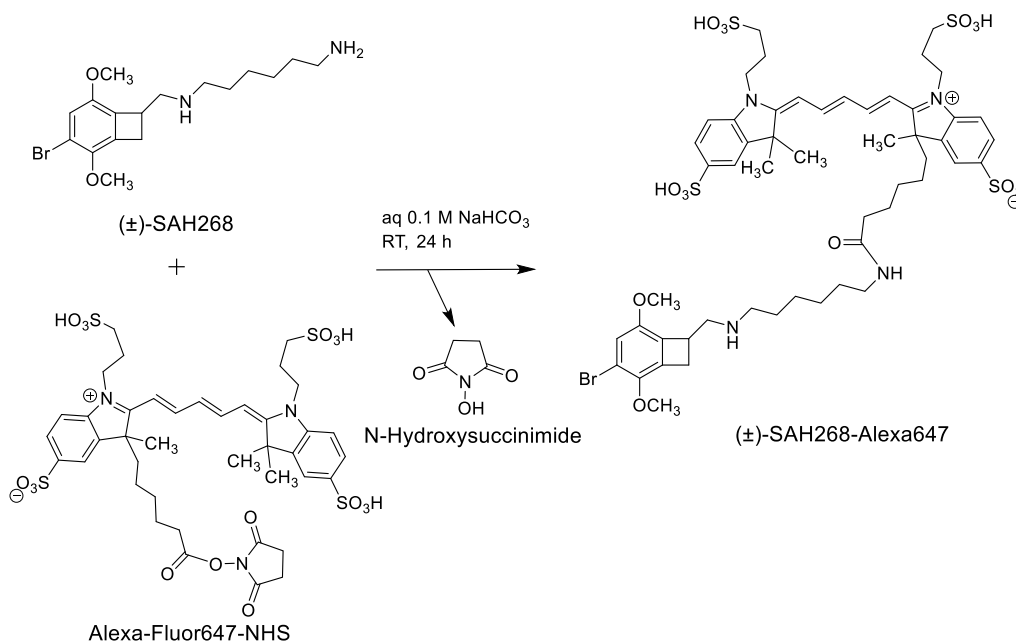


**Figure 12: Synthesis of (±)-SAH268-Alexa647.** Alexa-Fluor647-NHS was directly coupled to the primary amine of (±)-SAH268 in aqueous 0.1 M NaHCO<sub>3</sub> solution overnight at room temperature, forming the desired amide (±)-SAH268-Alexa647 and NHS as a leaving group.

(±)-SAH268-Alexa647 with the sum formula C<sub>53</sub>H<sub>71</sub>BrN<sub>4</sub>O<sub>15</sub>S<sub>4</sub> was detected using high-resolution mass spectrometry as a H<sup>+</sup>-adduct with m/z = 1211.30495 [M+H]<sup>+</sup>. It was identified by comparing the detected m/z and the isotopic pattern to a simulated spectrum with a calculated value of m/z = 1211.30549 [M+H]<sup>+</sup> (Figure 13).

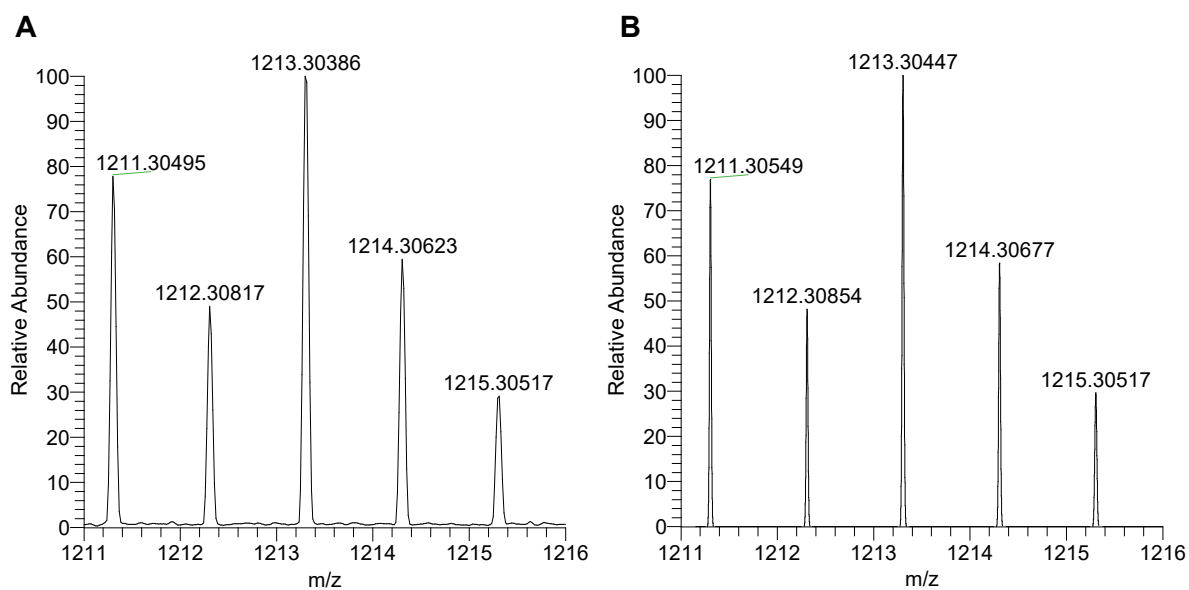


**Figure 13: HRMS spectra for (±)-SAH268-Alexa647.** Measured spectrum (A) and simulated spectrum with a resolution of R = 60,000 (B).

## Results

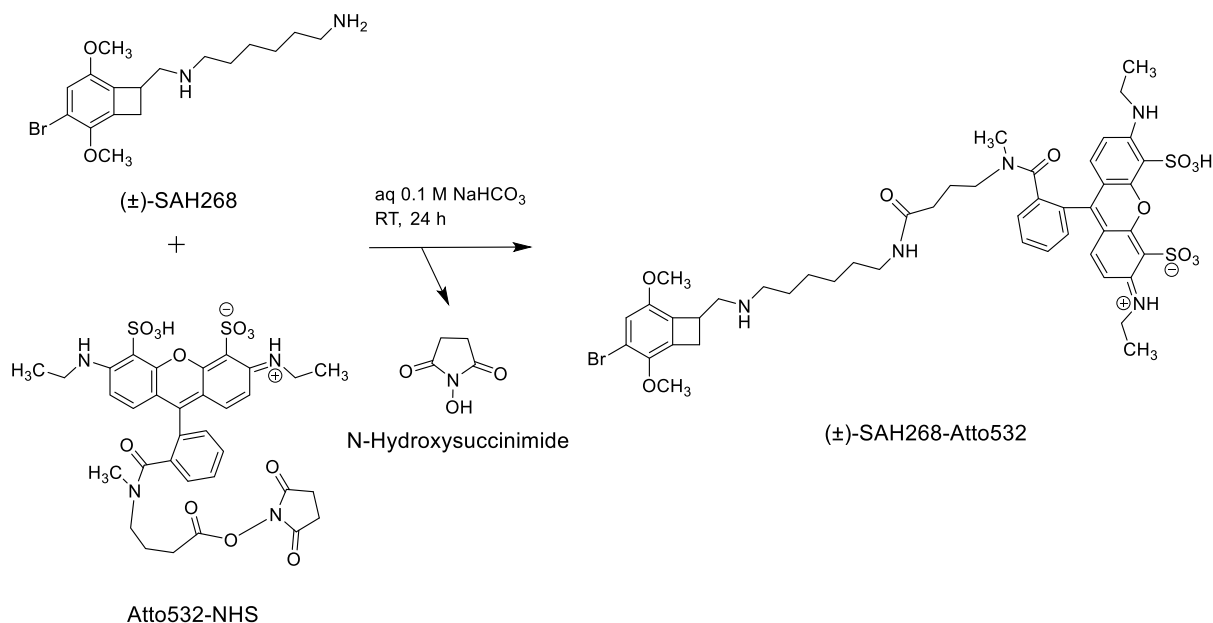


**Figure 14: Synthesis of (±)-SAH268-Atto532.** Atto532-NHS was directly coupled to the primary amine of (±)-SAH268 in aqueous 0.1 M NaHCO<sub>3</sub> solution overnight at room temperature, forming the desired amide (±)-SAH268-Atto532 and NHS as a leaving group.

(±)-SAH268-Atto532 with the sum formula C<sub>46</sub>H<sub>57</sub>BrN<sub>5</sub>O<sub>11</sub>S<sub>2</sub> was detected using high-resolution mass spectrometry as a H<sup>+</sup>-adduct with  $m/z = 998.26773$  [M+H]<sup>+</sup>. It was identified by comparing the detected  $m/z$  and the isotopic pattern to a simulated spectrum with a calculated value of  $m/z = 998.26739$  [M+H]<sup>+</sup> (Figure 15).

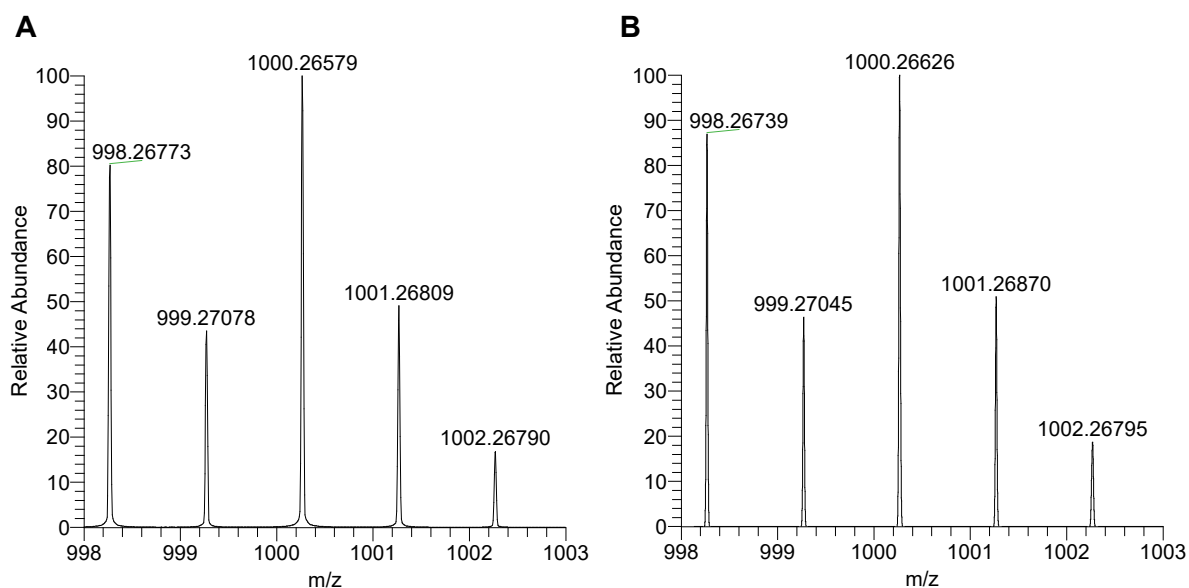


**Figure 15: HRMS spectra for (±)-SAH268-Atto532.** Measured spectrum (A) and simulated spectrum with a resolution of  $R = 60,000$  (B).

## 5.2 Determination of the 5-HT<sub>2A</sub> receptor binding by FCS

The synthesized fluorescent ligands described in 5.1 were examined for their binding affinity to 5-HT<sub>2A</sub> receptors. This was accomplished by employing fluorescence correlation spectroscopy (FCS) as technique on single-molecule level. FCS measures fluorescence fluctuation in a defined, very small observation volume. Fluorescent molecules can be distinguished by the time they remain in the observation volume, the so-called diffusion time constant  $T_{diff}$ . Fast diffusing molecules, e.g. free diffusing fluorophores in solution, only remain in the observation volume for a short time, whereas slower diffusing molecules, e.g. fluorescent ligands bound to parts of the plasma membrane remain in the observation volume for a longer duration. The detected fluorescence fluctuation over time is converted into an autocorrelation curve. The turning point(s) of the autocorrelation curve represent the mean diffusion time constant(s). Exemplary autocorrelation curves for measurements of only free diffusing fluorescent molecules in solution and for a mixture of free diffusing and bound fluorescent molecules in a plasma membrane are shown in Figure 16.

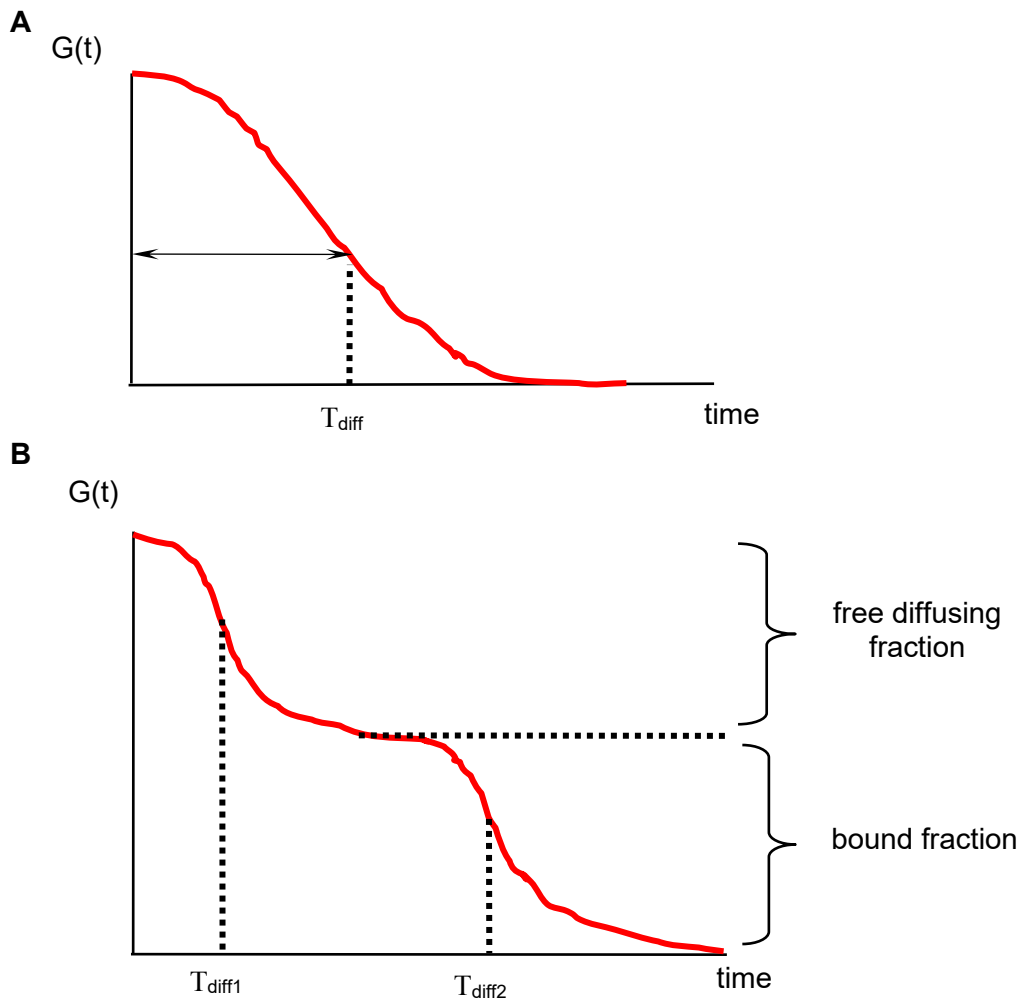


**Figure 16: Autocorrelation curves determined by FCS measurements.** Exemplary autocorrelation curves for only free diffusing (A) and a mixture of free diffusing and bound (B) fluorescent molecules.

## Results

For receptor-ligand complexes it is possible to record more than one  $T_{diff}$ . Different  $T_{diff}$  each characterize a distinct diffusive state for a receptor-ligand complex. GPCR commonly occur in different diffusive states represented by their distinct diffusion coefficients, which can be calculated using the measured  $T_{diff}$  and formula (2) shown in 4.5. The evaluation of the autocorrelation curves was accomplished by a three-component model, where both fractions of  $T_{diff2}$  and  $T_{diff3}$  account for the fluorescent ligand bound to the plasma membrane and  $T_{diff1}$  represents the free diffusing ligand. In case one of the synthesized ligands displayed binding affinity by showing elevated amounts of fluorescent molecules belonging to  $T_{diff2}$  and  $T_{diff3}$ , a 1000-fold excess of ( $\pm$ )-TCB-2 was added. If the autocorrelation curve remained nearly unchanged after the addition, the observed binding affinity was considered not selective for 5-HT<sub>2A</sub> receptors. If the excess of ( $\pm$ )-TCB-2 was able to shift the autocorrelation curve to the left, by displacing fluorescent ligand from its binding, the binding affinity was considered selective for 5-HT<sub>2A</sub> receptors. Nevertheless, a complete displacement of fluorescent ligand from its binding is not expected, due to the remaining non-specific binding, which is always observed.

The first ligand tested for its binding affinity to 5-HT<sub>2A</sub> receptors on C6 cells was ( $\pm$ )-TCB-2-Alexa532. After 30 min incubation with 10 nM ( $\pm$ )-TCB-2-Alexa532, three distinct  $T_{diff}$  were identified.  $T_{diff1}$  with 0.067 ms represents free and therefore fast diffusing ( $\pm$ )-TCB-2-Alexa532 in solution above the plasma membrane. Slower diffusing particles with  $T_{diff2} = 2.08$  ms and  $T_{diff3} = 83.33$  ms account for ( $\pm$ )-TCB-2-Alexa532 specifically bound to 5-HT<sub>2A</sub> receptors or non-specifically bound to other components of the plasma membrane. The corresponding fractions and diffusion coefficients are provided in Table 10. The addition of a 1,000-fold excess of ( $\pm$ )-TCB-2 was not able to significantly displace the bound fractions of ( $\pm$ )-TCB-2-Alexa532, neither in  $T_{diff2}$  nor in  $T_{diff3}$ . This can be seen in Figure 17, where the blue autocorrelation curve for the measurement after displacement was not shifted towards the grey dotted curve for the measurement in solution next to cells, but remained nearly identical to the black curve measured before displacement.

## Results

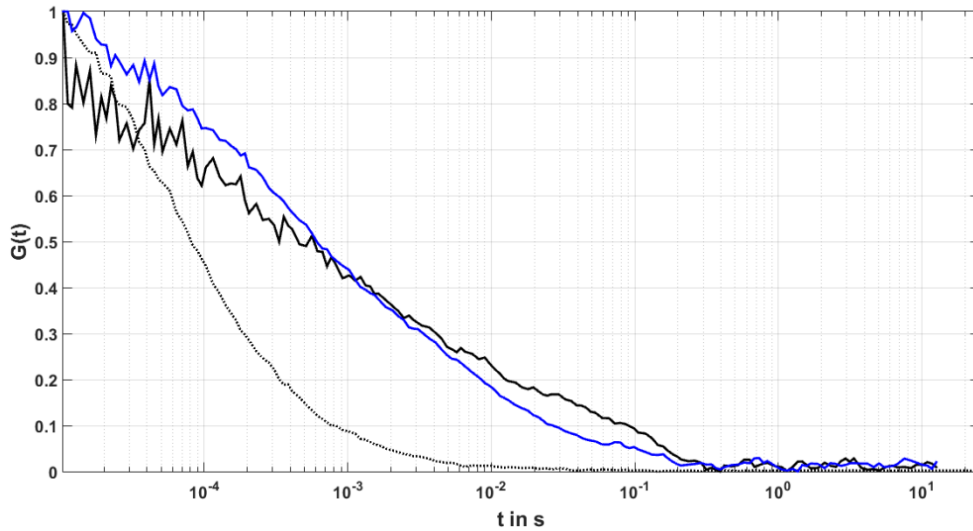


**Figure 17: Exemplary autocorrelation curves for (±)-TCB-2-Alexa532 on C6 cells.** Incubation of C6 cells with 10 nM (±)-TCB-2-Alexa532 for 30 min and subsequent FSC measurement on their surface (black line). Measurement after the addition of 10  $\mu$ M (±)-TCB-2 and incubation for another 30 min (blue line). The grey dotted line represents 10 nM (±)-TCB-2-Alexa532 measured in solution next to cells.

**Table 10: FCS data for (±)-TCB-2-Alexa532 on C6 cells.** Diffusion time constants ( $T_{diff}$ ), their respective fractions and diffusion coefficients ( $D_{diff}$ ) for (±)-TCB-2-Alexa532 on the surface of C6 cells presented as mean  $\pm$  SD.

	$T_{diff1}$ [ms]	$T_{diff2}$ [ms]	$T_{diff3}$ [ms]	fraction $T_{diff1}$ [%]	fraction $T_{diff2}$ [%]	fraction $T_{diff3}$ [%]	$D_{diff1}$ [ $\mu$ m <sup>2</sup> /s]	$D_{diff2}$ [ $\mu$ m <sup>2</sup> /s]	$D_{diff3}$ [ $\mu$ m <sup>2</sup> /s]
10 nM (±)-TCB-2- Alexa532	0.067* $\pm$ 0.005	2.08 $\pm$ 0.96	83.33 $\pm$ 75.20	36.9 $\pm$ 6.2	41.5 $\pm$ 5.5	22.6 $\pm$ 7.5	149.25 $\pm$ 11.14	4.81 $\pm$ 2.22	0.12 $\pm$ 0.11
10 nM (±)-TCB-2- Alexa532 + 10 $\mu$ M (±)-TCB-2	0.067* $\pm$ 0.005	1.71 $\pm$ 0.06	14.82 $\pm$ 13.08	27.3 $\pm$ 3.5	35.3 $\pm$ 17.0	37.4 $\pm$ 15.3	149.25 $\pm$ 11.14	5.85 $\pm$ 0.21	0.68 $\pm$ 0.60

\* determined by measuring 10 nM (±)-TCB-2-Alexa532 in solution next to cells

(±)-TCB-2-Alexa532 displayed high amounts of non-specific binding to the plasma membrane of C6 cells and is not suitable for further 5-HT<sub>2A</sub> receptor binding studies.

## Results

Following ( $\pm$ )-TCB-2-Alexa532, ( $\pm$ )-TCB-2-Alexa647 was tested for its binding affinity to 5-HT<sub>2A</sub> receptors on C6 cells. After 30 min incubation with 20 nM ( $\pm$ )-TCB-2-Alexa647, two distinct  $T_{diff}$  were identified:  $T_{diff1}$  with 0.067 ms and  $T_{diff2}$  with 58.44 ms. The corresponding fractions and diffusion coefficients are provided in Table 11. Neither the black nor the blue autocorrelation curve differed significantly from the grey dotted curve measured in solution next to cells (Figure 18). ( $\pm$ )-TCB-2-Alexa647 displayed no notable selective binding.

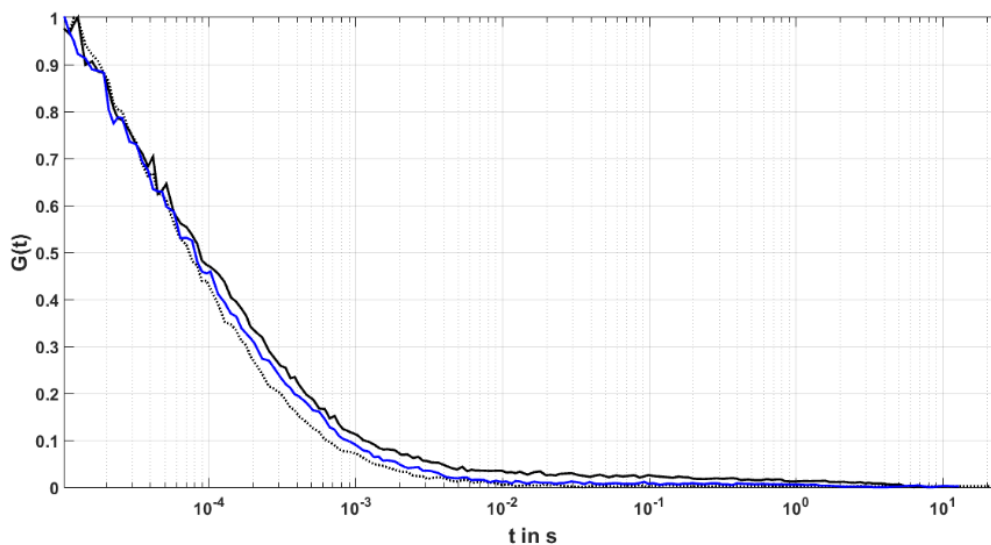


**Figure 18: Exemplary autocorrelation curves for ( $\pm$ )-TCB-2-Alexa647 on C6 cells.** Incubation of C6 cells with 20 nM ( $\pm$ )-TCB-2-Alexa647 for 30 min and subsequent FSC measurement on their surface (black line). Measurement after the addition of 20  $\mu$ M ( $\pm$ )-TCB-2 and incubation for another 30 min (blue line). The grey dotted line represents 20 nM ( $\pm$ )-TCB-2-Alexa647 measured in solution next to cells.

## Results

**Table 11: FCS data for (±)-TCB-2-Alexa647 on C6 cells.** Diffusion time constants ( $T_{diff}$ ), their respective fractions and diffusion coefficients ( $D_{diff}$ ) for (±)-TCB-2-Alexa647 on the surface of C6 cells presented as mean  $\pm$  SD.

	$T_{diff1}$ [ms]	$T_{diff2}$ [ms]	$T_{diff3}$ [ms]	fraction $T_{diff1}$ [%]	fraction $T_{diff2}$ [%]	fraction $T_{diff3}$ [%]	$D_{diff1}$ [ $\mu\text{m}^2/\text{s}$ ]	$D_{diff2}$ [ $\mu\text{m}^2/\text{s}$ ]	$D_{diff3}$ [ $\mu\text{m}^2/\text{s}$ ]
20 nM (±)-TCB-2- Alexa647	0.067* $\pm$ 0.006	58.44 $\pm$ 70.13	n.a.	89.0 $\pm$ 4.8	11.0 $\pm$ 4.8	n.a.	149.25 $\pm$ 11.14	0.17 $\pm$ 0.20	n.a.
20 nM (±)-TCB-2- Alexa647 + 20 $\mu\text{M}$ (±)-TCB-2	0.058* $\pm$ 0.002	84.87 $\pm$ 35.40	n.a.	92.0 $\pm$ 0.2	8.0 $\pm$ 0.2	n.a.	172.41 $\pm$ 5.95	0.11 $\pm$ 0.05	n.a.

\* determined by measuring 20 nM (±)-TCB-2-Alexa647 in solution next to cells  
n.a. = not applicable

(±)-TCB-2-Alexa647 displayed no notable selective binding and is not suitable for further studies 5-HT<sub>2A</sub> receptor binding studies.

Two fluorescent ligands with the fluorophore directly coupled to (±)-TCB-2 were not suitable for FCS investigations. Therefore, (±)-SAH268-Alexa532 was tested for its binding affinity to 5-HT<sub>2A</sub> receptors on C6 cells in the next step. After 30 min incubation with 10 nM (±)-SAH268-Alexa532, three distinct  $T_{diff}$  were identified:  $T_{diff1}$  with 0.053 ms,  $T_{diff2}$  with 1.32 ms and  $T_{diff3}$  with 210.30 ms. The corresponding fractions and diffusion coefficients are provided in Table 12. A 1,000-fold excess of (±)-TCB-2 slightly but not significantly reduced the bound fractions  $T_{diff2}$  and  $T_{diff3}$  in total from 53.9% to 45.4%. Nevertheless, the shift of the blue autocorrelation curve to the grey dotted one is not detectable (Figure 19). The detected binding of (±)-SAH268-Alexa532 was not displaceable by (±)-TCB-2.

## Results

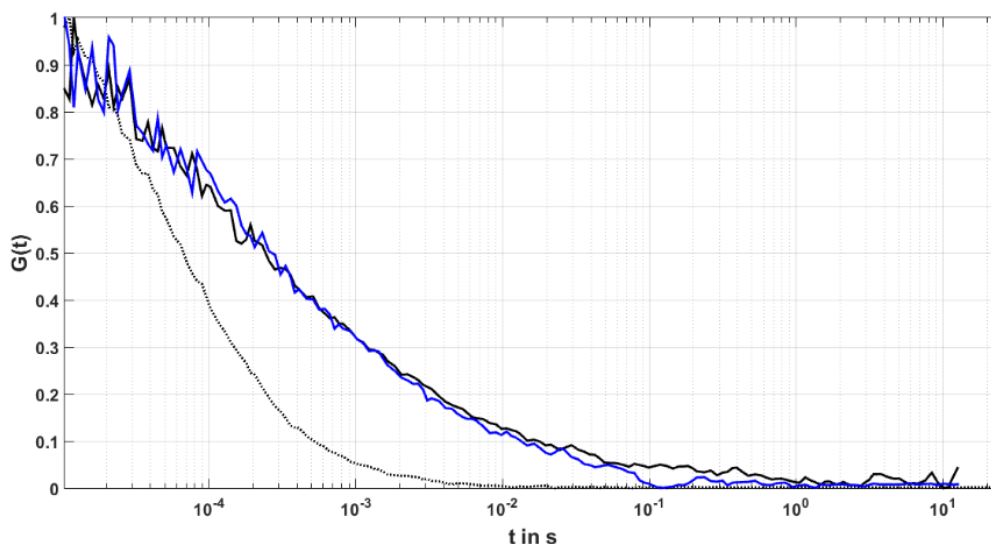


**Figure 19: Exemplary autocorrelation curves for (±)-SAH268-Alexa532 on C6 cells.** Incubation of C6 cells with 10 nM (±)-SAH268-Alexa532 for 30 min and subsequent FCS measurement on their surface (black line). Measurement after the addition of 10 μM (±)-TCB-2 and incubation for another 30 min (blue line). The grey dotted line represents 10 nM (±)-SAH268-Alexa532 measured in solution next to cells.

**Table 12: FCS data for (±)-SAH268-Alexa532 on C6 cells.** Diffusion time constants ( $T_{diff}$ ), their respective fractions and diffusion coefficients ( $D_{diff}$ ) for (±)-SAH268-Alexa532 on the surface of C6 cells presented as mean  $\pm$  SD.

	$T_{diff1}$ [ms]	$T_{diff2}$ [ms]	$T_{diff3}$ [ms]	fraction $T_{diff1}$ [%]	fraction $T_{diff2}$ [%]	fraction $T_{diff3}$ [%]	$D_{diff1}$ [ $\mu\text{m}^2/\text{s}$ ]	$D_{diff2}$ [ $\mu\text{m}^2/\text{s}$ ]	$D_{diff3}$ [ $\mu\text{m}^2/\text{s}$ ]
10 nM (±)-SAH268- Alexa532	0.053* $\pm$ 0.003	1.32 $\pm$ 0.27	210.30 $\pm$ 333.08	46.1 $\pm$ 6.6	32.0 $\pm$ 6.2	21.9 $\pm$ 9.3	188.68 $\pm$ 10.68	7.58 $\pm$ 1.55	0.05 $\pm$ 0.08
10 nM (±)-SAH268- Alexa532 + 10μM (±)-TCB-2	0.053* $\pm$ 0.003	1.26 $\pm$ 0.76	17.38 $\pm$ 6.08	54.6 $\pm$ 21.2	29.6 $\pm$ 16.2	15.8 $\pm$ 5.1	188.68 $\pm$ 10.68	7.94 $\pm$ 4.79	0.58 $\pm$ 0.20

\* determined by measuring 10 nM (±)-SAH268-Alexa532 in solution next to cells

Since the observed binding for (±)-SAH268-Alexa532 was non-displaceable and thereby non-specific, it cannot be employed for further 5-HT<sub>2A</sub> receptors binding studies.

## Results

Thereafter, ( $\pm$ )-SAH268-Alexa647 was tested for its binding affinity to 5-HT<sub>2A</sub> receptors on C6 cells. After 30 min incubation with 20 nM ( $\pm$ )-SAH268-Alexa647, two distinct  $T_{diff}$  were identified:  $T_{diff1}$  with 0.067 ms and  $T_{diff2}$  with 26.33 ms. The corresponding fractions and diffusion coefficients are provided in Table 13. Since the bound fraction of ( $\pm$ )-SAH268-Alexa647 was 3.2%, the courses of the autocorrelation curves for ( $\pm$ )-SAH268-Alexa647 in solution next to cells and in the plasma membrane of C6 cells are almost identical (Figure 20). Consequently, no further displacement experiments were undertaken.

The synthesis of ( $\pm$ )-SAH268-Alexa647 yielded a ligand with no notable selective binding to the 5-HT<sub>2A</sub> receptor. Therefore, ( $\pm$ )-SAH268-Alexa647 is not suited for further FCS studies.

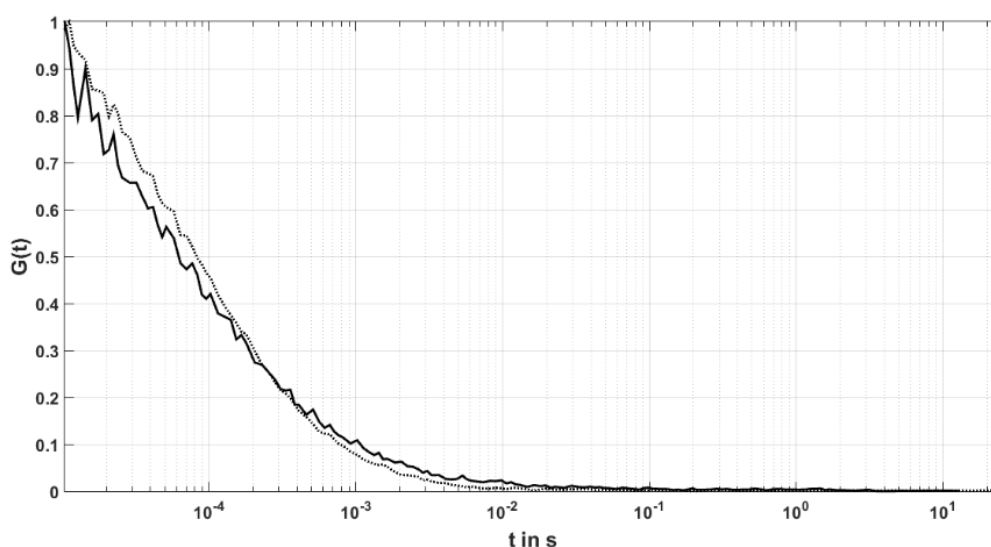


**Figure 20: Exemplary autocorrelation curves for ( $\pm$ )-SAH268-Alexa647 on C6 cells.** Incubation of C6 cells with 20 nM ( $\pm$ )-SAH268-Alexa647 for 30 min and subsequent FCS measurement on their surface (black line). The grey dotted line represents 20 nM ( $\pm$ )-SAH268-Alexa647 measured in solution next to cells.

**Table 13: FCS data for ( $\pm$ )-SAH268-Alexa647 on C6 cells.** Diffusion time constants ( $T_{diff}$ ), their respective fractions and diffusion coefficients ( $D_{diff}$ ) for ( $\pm$ )-SAH268-Alexa647 on the surface of C6 cells presented as mean  $\pm$  SD.

	$T_{diff1}$ [ms]	$T_{diff2}$ [ms]	$T_{diff3}$ [ms]	fraction $T_{diff1}$ [%]	fraction $T_{diff2}$ [%]	fraction $T_{diff3}$ [%]	$D_{diff1}$ [ $\mu\text{m}^2/\text{s}$ ]	$D_{diff2}$ [ $\mu\text{m}^2/\text{s}$ ]	$D_{diff3}$ [ $\mu\text{m}^2/\text{s}$ ]
20 nM ( $\pm$ )-SAH268- Alexa647	0.077* $\pm$ 0.002	26.33 $\pm$ 48.36	n.a.	96.8 $\pm$ 1.2	3.2 $\pm$ 1.2	n.a.	129.87 $\pm$ 3.37	0.38 $\pm$ 0.70	n.a.

\* determined by measuring 20 nM ( $\pm$ )-SAH268-Alexa647 in solution next to cells

n.a. = not applicable

## Results

Since none of the fluorescent ligands with Alexa-Fluor fluorophores was suitable for FCS binding studies, ( $\pm$ )-SAH268-Atto532 was tested for its binding affinity to 5-HT<sub>2A</sub> receptors on C6 cells. After 30 min incubation with 10 nM ( $\pm$ )-SAH268-Atto532, two distinct  $T_{diff}$  were identified:  $T_{diff1}$  with 0.067 ms and  $T_{diff2}$  with 26.33 ms. The corresponding fractions and diffusion coefficients are provided in Table 14. Since the bound fraction of ( $\pm$ )-SAH268-Atto532 was 10.4%, the courses of the autocorrelation curves for ( $\pm$ )-SAH268-Atto532 in solution next to cells and in the plasma membrane of C6 cells are only slightly different (Figure 21). Consequently, no further displacement experiments were undertaken.

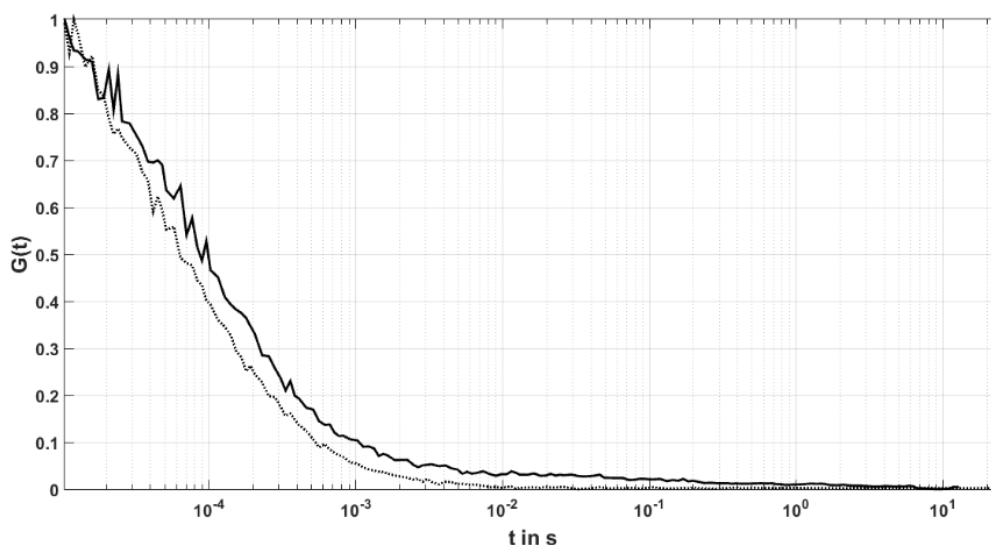


**Figure 21: Exemplary autocorrelation curves for ( $\pm$ )-SAH268-Atto532 on C6 cells.** Incubation of C6 cells with 10 nM ( $\pm$ )-SAH268-Atto532 for 30 min and subsequent FCS measurement on their surface (black line). The grey dotted line represents 10 nM ( $\pm$ )-SAH268-Atto532 measured in solution next to cells.

**Table 14: FCS data for ( $\pm$ )-SAH268-Atto532 on C6 cells.** Diffusion time constants ( $T_{diff}$ ), their respective fractions and diffusion coefficients ( $D_{diff}$ ) for ( $\pm$ )-SAH268-Atto532 on the surface of C6 cells presented as mean  $\pm$  SD.

	$T_{diff1}$ [ms]	$T_{diff2}$ [ms]	$T_{diff3}$ [ms]	fraction $T_{diff1}$ [%]	fraction $T_{diff2}$ [%]	fraction $T_{diff3}$ [%]	$D_{diff1}$ [ $\mu\text{m}^2/\text{s}$ ]	$D_{diff2}$ [ $\mu\text{m}^2/\text{s}$ ]	$D_{diff3}$ [ $\mu\text{m}^2/\text{s}$ ]
10 nM ( $\pm$ )-SAH268- Atto532	0.058*	39.47	n.a.	89.6	10.4	n.a.	172.41	0.25	n.a.
	$\pm$ 0.002	$\pm$ 55.15		$\pm$ 2.9	$\pm$ 2.9		$\pm$ 5.95	$\pm$ 0.35	

\* determined by measuring 10 nM ( $\pm$ )-SAH268-Atto532 in solution next to cells  
n.a. = not applicable

## Results

C6 cells are known to genuinely express 5-HT<sub>2A</sub> receptors. However, those cells were isolated from *Rattus norvegicus* and therefore express murine 5-HT<sub>2A</sub> receptors. Remarkably, the fluorescently labeled (±)-TCB-2 and (±)-SAH268 derivatives showed either a high non-specific binding to the plasma membrane of C6 cells or no notable selective binding to the 5-HT<sub>2A</sub> receptor. The non-specific binding could be attributed to the fluorophore, whereas the absence of selective binding to the 5-HT<sub>2A</sub> receptor could be attributed to the differences between murine and human 5-HT<sub>2A</sub> receptors. They differ in only three amino acids in the transmembrane region associated with ligand binding. The different amino acids are isoleucine and valine at position 150, threonine and alanine at position 82 and alanine and serine at position 242. Alanine/Serine-242 seems to be mainly responsible for the differences in ligand binding for the two species<sup>73,74</sup>. Consequently, the human neuroblastoma cell line SH-SY5Y was used to investigate whether (±)-SAH268-Atto532 displays binding affinity to human 5-HT<sub>2A</sub> receptors. After 30 min incubation with 10 nM (±)-SAH268-Alexa532, three distinct  $T_{diff}$  were identified:  $T_{diff1}$  with 0.063 ms,  $T_{diff2}$  with 1.27 ms and  $T_{diff3}$  with 55.40 ms. The corresponding fractions and diffusion coefficients are provided in Table 15. After another 30 min incubation with 10  $\mu$ M (±)-TCB-2, the bound fractions  $T_{diff2}$  and  $T_{diff3}$  were reduced from 43.5% to 10.8% in total, which is equal to the non-specific binding measured for (±)-SAH268-Alexa532 on C6 cells (Table 14). The displacement of the bound fractions of (±)-SAH268-Alexa532 by (±)-TCB-2 is indicated by a clear left shift of the blue autocorrelation curve towards the grey dotted curve, since increased amounts of free diffusing ligand are detected (Figure 22). (±)-SAH268-Atto532 showed 5-HT<sub>2A</sub> receptor binding in SH-SY5Y cells.

## Results

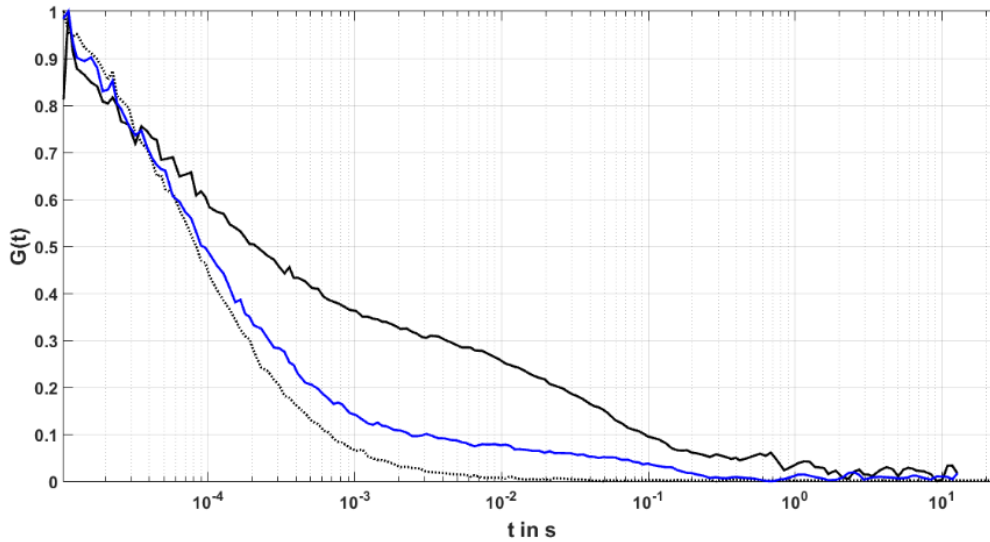


**Figure 22: Exemplary autocorrelation curves for (±)-SAH268-Atto532 on SH-SY5Y cells.** Incubation of SH-SY5Y cells with 10 nM (±)-SAH268-Atto532 for 30 min and subsequent FCS measurement on their surface (black line). Measurement after the addition of 10 μM (±)-TCB-2 and incubation for another 30 min (blue line). The grey dotted line represents 10 nM (±)-SAH268-Atto532 measured in solution next to cells.

**Table 15: FCS data for (±)-SAH268-Atto532 on SH-SY5Y cells.** Diffusion time constants ( $T_{diff}$ ), their respective fractions and diffusion coefficients ( $D_{diff}$ ) for (±)-SAH268-Atto532 on the surface of SH-SY5Y cells presented as mean  $\pm$  SD.

	$T_{diff1}$ [ms]	$T_{diff2}$ [ms]	$T_{diff3}$ [ms]	fraction $T_{diff1}$ [%]	fraction $T_{diff2}$ [%]	fraction $T_{diff3}$ [%]	$D_{diff1}$ [ $\mu\text{m}^2/\text{s}$ ]	$D_{diff2}$ [ $\mu\text{m}^2/\text{s}$ ]	$D_{diff3}$ [ $\mu\text{m}^2/\text{s}$ ]
10 nM (±)-SAH268- Atto532	0.063* $\pm$ 0.008	1.27 $\pm$ 0.19	55.40 $\pm$ 22.96	56.5 $\pm$ 12.4	19.6 $\pm$ 10.1	23.9 $\pm$ 4.8	158.73 $\pm$ 20.16	7.90 $\pm$ 1.20	0.18 $\pm$ 0.07
10 nM (±)-SAH268- Atto532 + 10 μM (±)-TCB-2	0.063* $\pm$ 0.008	1.93 $\pm$ 0.93	43.72 $\pm$ 11.17	89.2 $\pm$ 2.5	3.7 $\pm$ 0.5	7.1 $\pm$ 2.1	158.73 $\pm$ 20.16	5.18 $\pm$ 2.50	0.23 $\pm$ 0.06

\* determined by measuring 10 nM (±)-SAH268-Atto532 in solution next to cells

After (±)-SAH268-Atto532 demonstrated displaceable binding on SH-SY5Y cells, (±)-SAH268-Alexa647 needed to be examined on SY-SY5Y cells to assess whether the dye moiety influences the 5-HT<sub>2A</sub> receptor binding. After 30 min incubation with 30 nM (±)-SAH268-

## Results

Alexa647, two distinct  $T_{diff}$  were identified:  $T_{diff1}$  with 0.079 ms and  $T_{diff2}$  with 8.36 ms. The corresponding fractions and diffusion coefficients are provided in Table 16. Since the bound fraction of ( $\pm$ )-SAH268-Alexa647 was 4.7%, the courses of the autocorrelation curves for ( $\pm$ )-SAH268-Alexa647 in solution next to cells and in the plasma membrane of SH-SY5Y cells are only slightly different (Figure 23). Therefore, no further displacement experiments were undertaken.

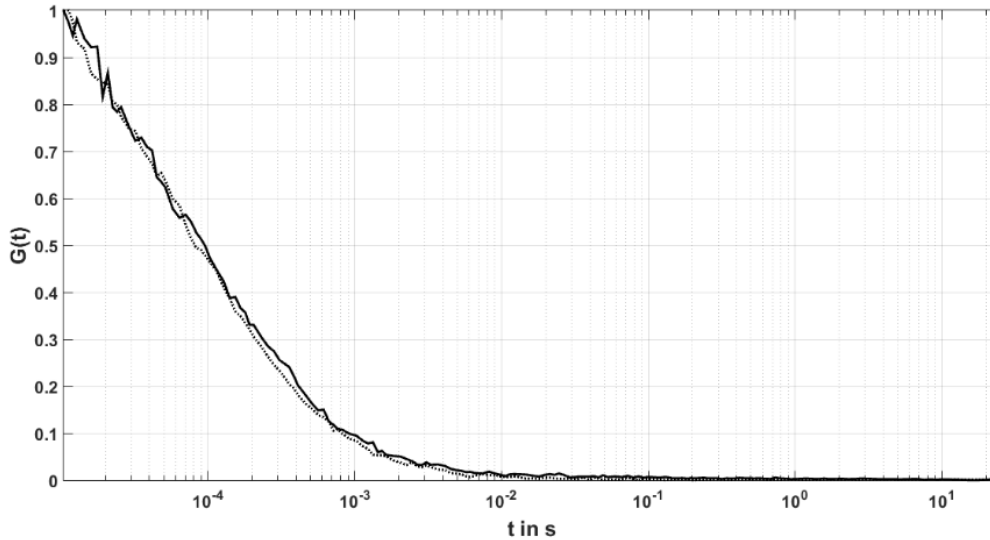


**Figure 23: Exemplary autocorrelation curves for ( $\pm$ )-SAH268-Alexa647 on SH-SY5Y cells.** Incubation of SH-SY5Y cells with 30 nM ( $\pm$ )-SAH268-Alexa647 for 30 min and subsequent FSC measurement on their surface (black line). The grey dotted line represents 30 nM ( $\pm$ )-SAH268-Alexa647 measured in solution next to cells.

**Table 16: FCS data for ( $\pm$ )-SAH268-Alexa647 on SH-SY5Y cells.** Diffusion time constants ( $T_{diff}$ ), their respective fractions and diffusion coefficients ( $D_{diff}$ ) for ( $\pm$ )-SAH268-Alexa647 on the surface of SH-SY5Y cells presented as mean  $\pm$  SD.

	$T_{diff1}$ [ms]	$T_{diff2}$ [ms]	$T_{diff3}$ [ms]	fraction $T_{diff1}$ [%]	fraction $T_{diff2}$ [%]	fraction $T_{diff3}$ [%]	$D_{diff1}$ [ $\mu\text{m}^2/\text{s}$ ]	$D_{diff2}$ [ $\mu\text{m}^2/\text{s}$ ]	$D_{diff3}$ [ $\mu\text{m}^2/\text{s}$ ]
30 nM ( $\pm$ )-SAH268- Alexa647	0.079* $\pm$ 0.002	8.36 $\pm$ 5.33	n.a.	95.3 $\pm$ 4.1	4.7 $\pm$ 4.1	n.a.	126.58 $\pm$ 3.20	1.20 $\pm$ 0.76	n.a.

\* determined by measuring 30 nM ( $\pm$ )-SAH268-Alexa647 in solution next to cells

n.a. = not applicable

## Results

(±)-SAH268-Alexa647 showed no notable selective binding to 5-HT<sub>2A</sub> receptors on SH-SY5Y cells with 4.7%, in contrast to (±)-SAH268-Atto532 with 43.5%. (±)-SAH268-Alexa647 is not suitable for further 5-HT<sub>2A</sub> receptors binding studies.

Lastly, the introduction of an aminohexyl linker to (±)-TCB-2 resulting in (±)-SAH268 needed to be reviewed critically. Therefore, (±)-TCB-2-Atto532 was tested for its binding affinity to 5-HT<sub>2A</sub> receptors on SH-SY5Y-cells. After 30 min incubation with 10 nM (±)-TCB-2-Atto532, two distinct  $T_{diff}$  were identified:  $T_{diff1}$  with 0.052 ms and  $T_{diff2}$  with 14.55 ms. The corresponding fractions and diffusion coefficients are provided in Table 17. Since the bound fraction of (±)-TCB-2-Atto532 was 11.0%, the courses of the autocorrelation curves for (±)-TCB-2-Atto532 in solution next to cells and in the plasma membrane of SH-SY5Y cells are only slightly different (Figure 24).

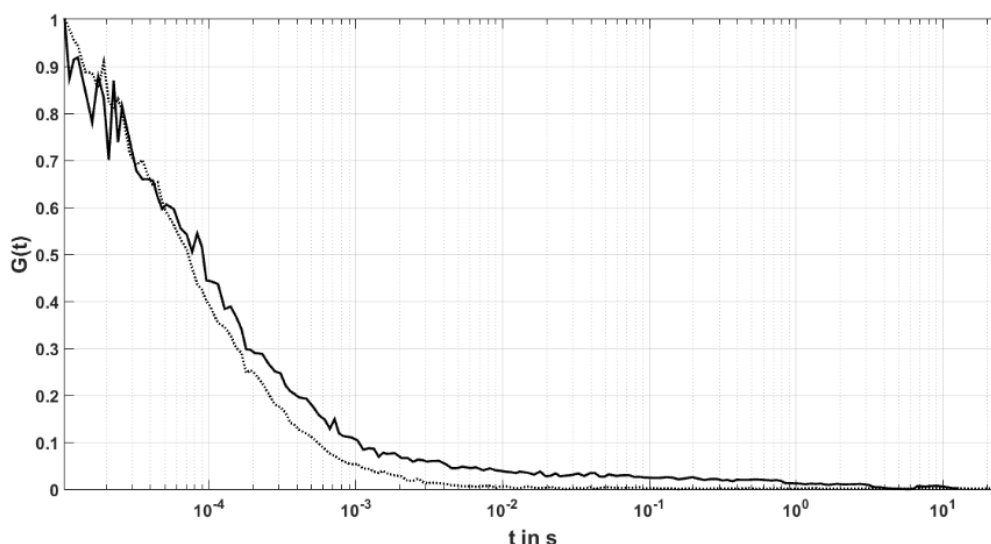


**Figure 24: Exemplary autocorrelation curves for (±)-TCB-2-Atto532 on SH-SY5Y cells.** Incubation of SH-SY5Y cells with 10 nM (±)-TCB-2-Atto532 for 30 min and subsequent FSC measurement on their surface (black line). The grey dotted line represents 10 nM (±)-TCB-2-Atto532 measured in solution next to cells.

## Results

**Table 17: FCS data for (±)-TCB-2-Atto532 on SH-SY5Y cells.** Diffusion time constants ( $T_{diff}$ ), their respective fractions and diffusion coefficients ( $D_{diff}$ ) for (±)-TCB-2-Atto532 on the surface of SH-SY5Y cells presented as mean  $\pm$  SD.

	$T_{diff1}$ [ms]	$T_{diff2}$ [ms]	$T_{diff3}$ [ms]	fraction $T_{diff1}$ [%]	fraction $T_{diff2}$ [%]	fraction $T_{diff3}$ [%]	$D_{diff1}$ [ $\mu\text{m}^2/\text{s}$ ]	$D_{diff2}$ [ $\mu\text{m}^2/\text{s}$ ]	$D_{diff3}$ [ $\mu\text{m}^2/\text{s}$ ]
10 nM	0.052*	14.55		89.0	11.0		192.31	0.69	
(±)-TCB-2- Atto532	$\pm$ 0.000	$\pm$ 12.2	n.a.	$\pm$ 2.8	$\pm$ 2.8	n.a.	$\pm$ 3.70	$\pm$ 0.58	n.a.

\* determined by measuring 10 nM (±)-TCB-2-Atto532 in solution next to cells

n.a. = not applicable

(±)-TCB-2-Atto532 displayed no notable selective binding to the 5-HT<sub>2A</sub> receptors on SH-SY5Y cells. With 11.0%, the amount was in the range of the measured non-specific binding for (±)-SAH268-Atto532 on C6 cells with 10.8%. (±)-TCB-2-Atto532 is not suitable for further 5-HT<sub>2A</sub> receptors binding studies. The introduction of the aminohexyl linker was necessary to construct a ligand with binding affinity to 5-HT<sub>2A</sub> receptors.

## Results

### 5.3 Selectivity of the 5-HT<sub>2A</sub> receptor binding for (±)-SAH268-Atto532

The binding of (±)-SAH268-Atto532 to 5-HT<sub>2A</sub> receptors was investigated on SH-SY5Y cells through displacement experiments using FCS measurements with different subtype-specific 5-HT ligands. The closely related 5-HT<sub>1A</sub>, 5-HT<sub>2C</sub> and 5-HT<sub>7</sub> receptors were chosen due to their high sequence homology compared to 5-HT<sub>2A</sub> receptors in regions associated with ligand binding<sup>35</sup>. To conduct the displacement experiments, an excess of (±)-TCB-2 (10 μM, 5-HT<sub>2A</sub> receptor agonist), WAY-100635 (5 μM, 5-HT<sub>1A</sub> receptor antagonist), SB-242084 (5 μM, 5-HT<sub>2C</sub> receptor antagonist), and SB-269970 (5 μM, 5-HT<sub>7</sub> receptor antagonist) was used. The binding of (±)-SAH268-Atto532 was measured before and after the addition of the compound of interest after 30 min incubation at room temperature. Each data set includes three independent experiments using the same cell before and after displacement. Binding of (±)-SAH268-Atto532 after displacement with the aforementioned compounds was normalized to the binding values before displacement (Figure 25, panel A). Only (±)-TCB-2 was able to significantly displace (±)-SAH268-Atto532 from the receptor-binding site. A 1,000-fold excess of (±)-TCB-2 significantly reduced the 5-HT<sub>2A</sub> receptor binding of (±)-SAH268-Atto532 to  $25.4 \pm 2.7\%$ , whereas WAY-100635 non-significantly increased it to  $103.5 \pm 24.4\%$ . SB-242084 with a decrease to  $93.9 \pm 3.1\%$  and SB-269970 with an increase to  $118.4 \pm 13.5\%$  showed no significant difference in (±)-SAH268-Atto532 receptor binding (Figure 25, panel B).

Results

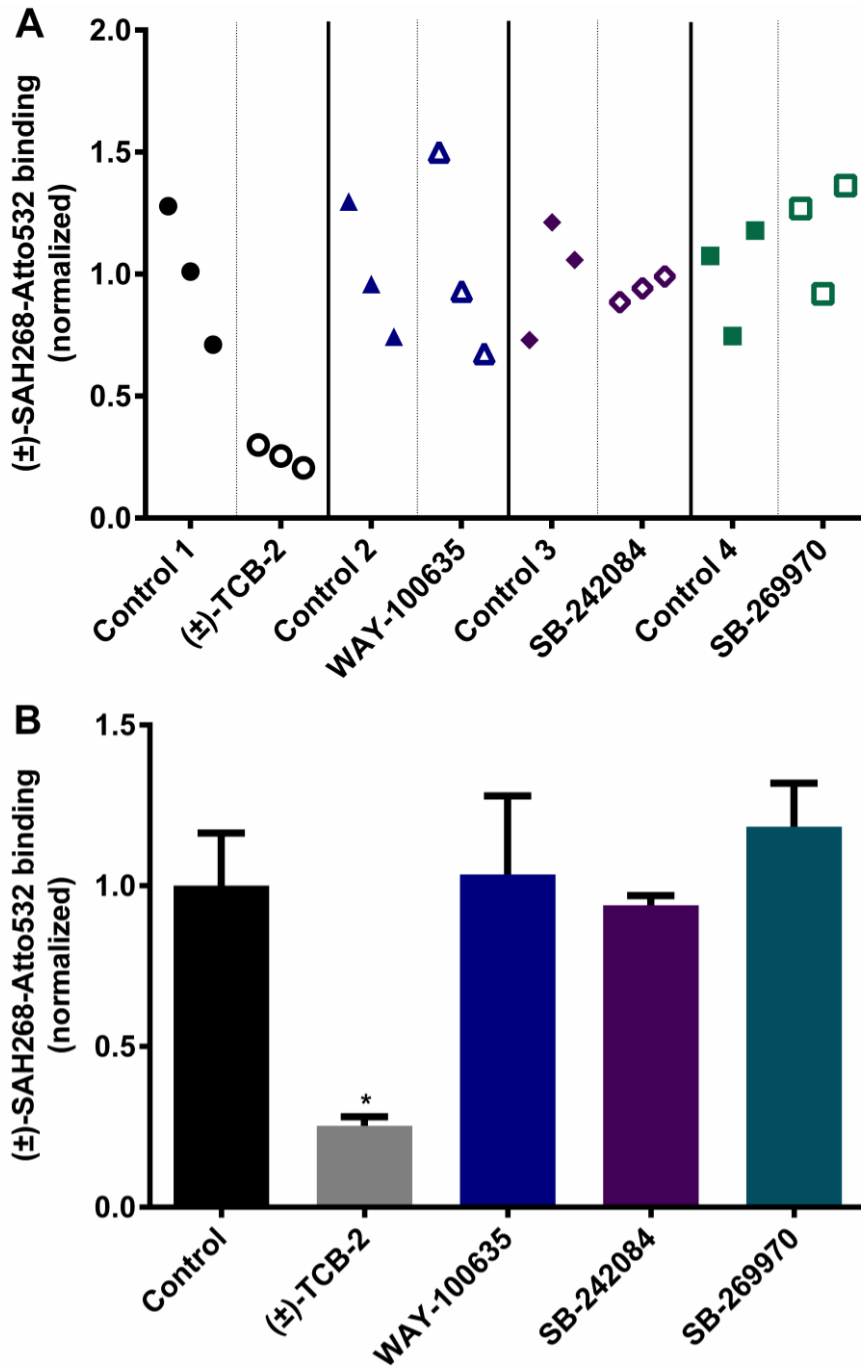


**Figure 25: Displacement experiments for (±)-SAH268-Atto532.** Displacement of 10 nM (±)-SAH268-Atto532 on SH-SY5Y cells using selective ligands for different 5-HT-receptors. Data are presented as single experiments with the same cell before (full dot) and after displacement (empty dot) in panel A and as mean + SEM for 3 independent experiments with  $n \geq 13$  for each column, with only one exemplary control column in panel B. The same cell was measured before and after displacement and normalized to their respective controls. Concentrations for the chosen ligands were 10  $\mu$ M for (±)-TCB-2 (5-HT<sub>2A</sub> receptor agonist) and 5  $\mu$ M each for WAY-100635 (5-HT<sub>1A</sub> receptor antagonist), SB-242084 (5-HT<sub>2C</sub> receptor antagonist) and SB-269970 (5-HT<sub>7</sub> receptor antagonist). Marked value \*  $p \leq 0.05$  is significantly different from its corresponding control, determined by Student's unpaired t-test.

## Results

Displacement experiments using selective ligands for 5-HT<sub>1A</sub>, 5-HT<sub>2C</sub> and 5-HT<sub>7</sub> receptors lead to the conclusion that the observed (±)-SAH268-Atto532 binding is mainly attributed to 5-HT<sub>2A</sub> receptors. It is proven for SH-SY5Y cells in several settings that they endogenously express 5-HT<sub>1A</sub> receptors<sup>75,76</sup>. Since it is not evident if SH-SY5Y cells express 5-HT<sub>2C</sub> and 5-HT<sub>7</sub> receptors, those two receptors were investigated further. To make sure the receptors of interest are expressed, three stably transfected cell lines originating from HEK293 cells were created. Availability of 5-HT<sub>2C</sub> and 5-HT<sub>7</sub> receptors was demonstrated by conducting second messenger assays for the respective cell line, which were negatable by selective antagonists (Figure S 29). HEK293-HiBiT-5HT2a, HEK293-Aequorin-HiBiT-5HT2c, and HEK293-GloSensor-HiBiT-5HT7 cells were investigated for (±)-SAH268-Atto532 binding to the respective receptor. After 30 min incubation at room temperature with 10 nM (±)-SAH268-Atto532, only cells transfected with human 5-HT<sub>2A</sub> receptors displayed binding with  $2.76 \pm 0.15$  nM. After treatment with a 1,000-fold excess of (±)-TCB-2, the binding of (±)-SAH268-Atto532 was significantly reduced by  $78.3 \pm 3.7\%$  to  $0.63 \pm 0.10$  nM. The measured binding of (±)-SAH268-Atto532 for the cells expressing the human 5-HT<sub>2C</sub> receptor with  $0.60 \pm 0.05$  nM and the human 5-HT<sub>7</sub> receptor with  $0.79 \pm 0.06$  nM were not significantly different from the cells expressing the 5-HT<sub>2A</sub> receptor after displacement with (±)-TCB-2 (Figure 26). Thus, (±)-SAH268-Atto532 is a selective 5-HT<sub>2A</sub> receptor ligand.

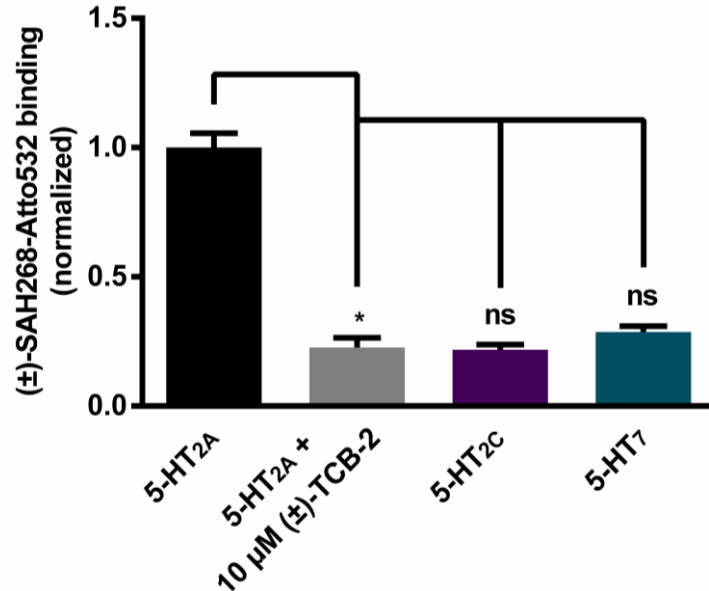


**Figure 26: 5-HT-receptor selectivity for (±)-SAH268-Atto532.** 5-HT receptor binding and displacement of 10 nM (±)-SAH268-Atto532 on HEK293-HiBiT-5HT2a, HEK293-Aequorin-HiBiT-5HT2c, and HEK293-GloSensor-HiBiT-5HT7 cells. Data are presented as mean + SEM for 3 independent experiments with  $n \geq 18$  for each data point. For displacement experiments on HEK293-HiBiT-5HT2a cells, the same cell was measured before and after displacement with a 1,000-fold excess of (±)-TCB-2. Measured binding was normalized to HEK293-HiBiT-5HT2a cells before displacement. Marked value \*  $p \leq 0.05$  is significantly different from its corresponding control, determined by Student's unpaired t-test (ns = not significant).

## Results

### 5.4 ( $\pm$ )-SAH268-Atto532 saturation experiments on SH-SY5Y cells

After demonstrating selectivity for 5-HT<sub>2A</sub> receptors, the binding affinity ( $K_D$ ) of ( $\pm$ )-SAH268-Atto532 and total receptor density ( $B_{max}$ ) of 5-HT<sub>2A</sub> receptors on SH-SY5Y cells were investigated. Saturation experiments with FCS were carried out by using different concentrations of ( $\pm$ )-SAH268-Atto532 ranging from 5 to 200 nM. SH-SY5Y cells were incubated for 30 min at room temperature. Afterwards, the total concentration of ( $\pm$ )-SAH268-Atto532 was plotted against the determined concentration of bound ( $\pm$ )-SAH268-Atto532. From the saturation curve, fitted by a nonlinear fit for one site-specific binding with Hill slope, a  $B_{max}$  value of  $23.95 \pm 5.91$  nM and a  $K_D$  value of  $81.03 \pm 24.99$  nM were obtained (Figure 27).

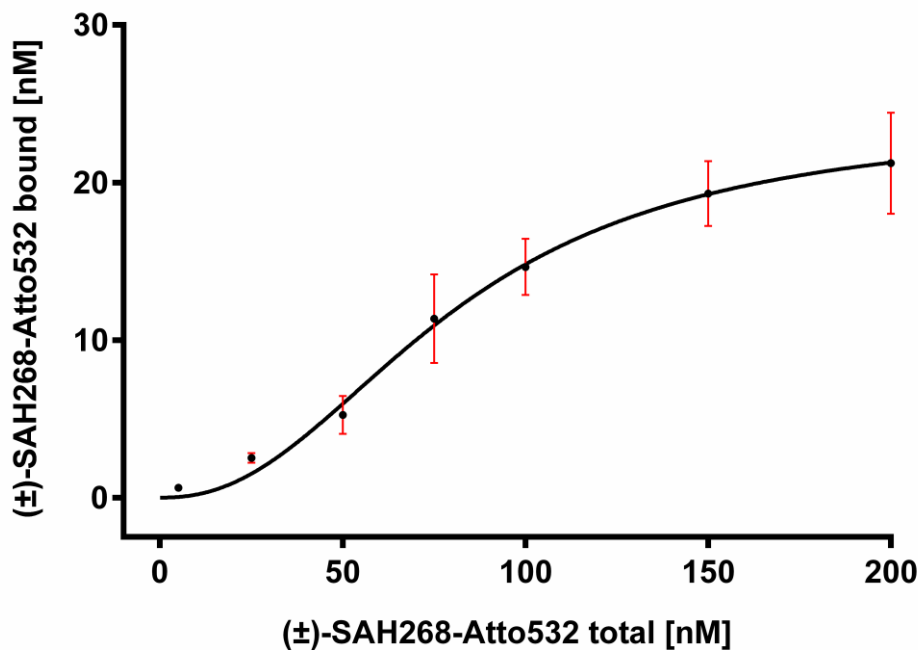


**Figure 27: FCS saturation experiments for ( $\pm$ )-SAH268-Atto532 on SH-SY5Y cells.** SH-SY5Y cells were incubated with 5, 25, 50, 75, 100, 150 and 200 nM ( $\pm$ )-SAH268-Atto532 for 30 min and measured afterwards. Data are presented as mean  $\pm$  SEM for 3 independent experiments with  $n \geq 19$  for each data point.

## Results

### 5.5 Lateral mobility of 5-HT<sub>2A</sub> receptor-(±)-SAH268-Atto532 complexes on SH-SY5Y cells

Further characterization of (±)-SAH268-Atto532 and 5-HT<sub>2A</sub> receptors was undertaken by applying the ligand in single-particle tracking (SPT) measurements. After incubating SH-SY5Y cells with 2 nM (±)-SAH268-Atto532 for 30 min at room temperature, pictures were taken and recorded particles were tracked using the u-track package and analyzed by variational Bayes single-particle tracking (vbSPT) (Figure 28)<sup>69,70</sup>.

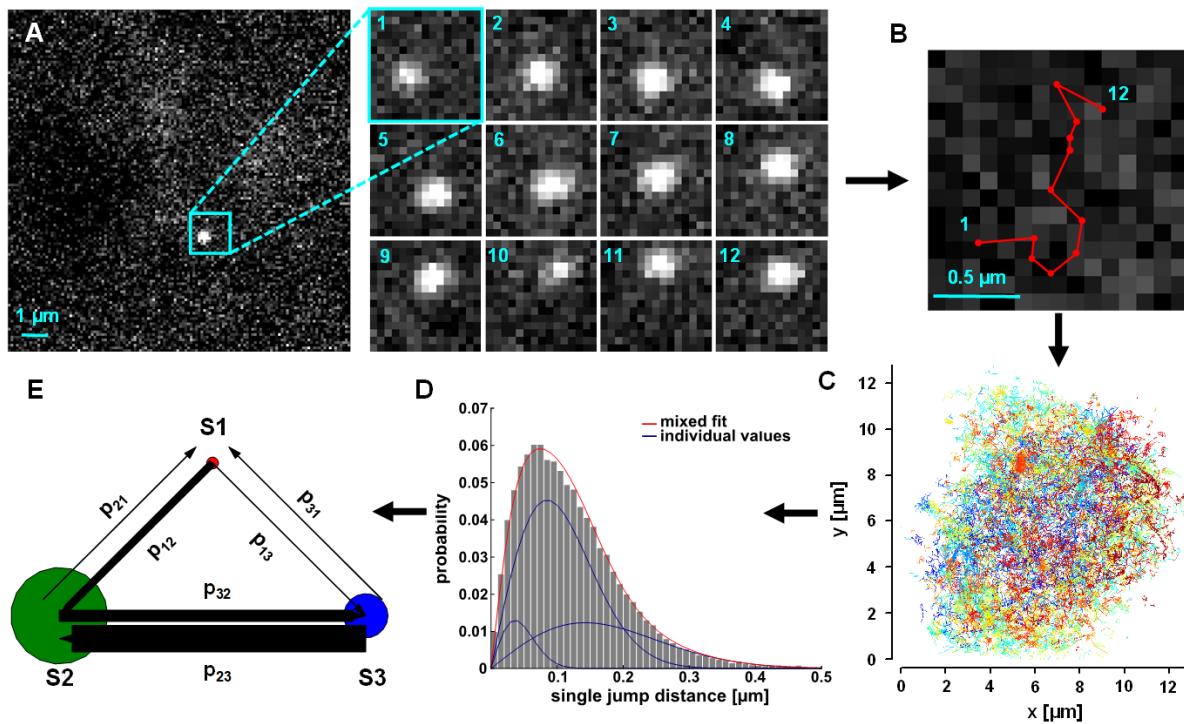


**Figure 28: Single-particle tracking and further analysis of (±)-SAH268-Atto532 receptor-ligand complexes on SH-SY5Y cells.** (A) Example of a single ligand-receptor complex on the surface of a single SH-SY5Y cell over the course of 600 ms (1-12). Individual frames and emerging trajectory of SPT recording acquired at 20 fps. (B) The trajectory of the particle recorded in A (C) Overlay of all recorded trajectories for (±)-SAH268-Atto532-receptor complexes. (D) Distribution of single jumping distances for the trajectories in C. Mixed fit for all diffusion coefficients and individually fitted diffusion coefficients are shown. (E) Trajectories analyzed by vbSPT. Each diffusive state (S1-S3) is represented by a circle. Circle area and arrow thickness are proportional to occupancy and intratrack transition probability.  $n \geq 18$  (overall 7350 trajectories).

## Results

Three distinct diffusive states S1-S3, their diffusion coefficients ( $D_{\text{SPT}}$ ), occupancy, and intratrack transition probability were identified (Table 18). The diffusive states account for almost immobile (diffusive state S1), slow diffusing (diffusive state S2) and fast diffusing (diffusive state S3) receptor-ligand complexes. Switches between diffusive states occurred mostly in sequential order from S1 to S3 and backward. Switches between  $S1 \rightleftharpoons S2$  and  $S1 \rightleftharpoons S3$  are relatively rare, while the transition from  $S3 \rightarrow S2$  clearly dominates (Figure 28).

Comparing diffusion coefficients acquired by SPT ( $D_{\text{SPT}}$ ) and FCS ( $D_{\text{FCS}}$ ) it can be concluded, that  $D_{3\text{SPT}}$  ( $0.2031 \pm 0.0017 \mu\text{m}^2/\text{s}$ ) and  $D_{3\text{FCS}}$  ( $0.18 \pm 0.07 \mu\text{m}^2/\text{s}$ ) represent the same population of receptor-ligand complexes (compare Table 15 and Table 18).

Taken together, FCS and SPT measurements enable the characterization of four distinct diffusive states of 5-HT<sub>2A</sub> receptor-ligand complexes, possibly representing different functionalities.

**Table 18: SPT data for ( $\pm$ )-SAH268-Atto532 receptor-ligand complexes on SH-SY5Y cells.**

Diffusion coefficients ( $D_{\text{SPT}}$ ), occupancy and intratrack transition probabilities of three different diffusive states S1, S2, and S3 of ( $\pm$ )-SAH268-Atto532-receptor-complexes acquired by single-particle tracking on SH-SY5Y cells and subsequent analysis with vbSPT. Data are presented as mean  $\pm$  SD for 3 independent experiments with  $n \geq 18$  (overall 7350 trajectories).

Diffusive state	$D_{\text{SPT}} [\mu\text{m}^2/\text{s}]$	Occupancy [%]	Transition probability to [%]		
			S1	S2	S3
S1	$0.0130 \pm 0.0002$	7.7	-	9.1	1.1
S2	$0.0718 \pm 0.0004$	63.3	1.3	-	14.3
S3	$0.2031 \pm 0.0017$	29.0	0.5	32.9	-

### 5.6 5-HT<sub>2A</sub> receptor agonistic profile of (±)-SAH268-Atto532

Lastly, the activity profile of (±)-SAH268-Atto532 was characterized. The G<sub>q</sub> coupled 5-HT<sub>2A</sub> receptor leads to increased cytosolic Ca<sup>2+</sup> levels after agonistic stimulation<sup>77</sup>. Therefore, HEK293 cells were transfected with a blue fluorescent calcium indicator (B-GECO1) alone and together with the human 5-HT<sub>2A</sub> receptor. The blue fluorescence does not interfere with the fluorescence of the Atto532 tag. Increasing cytosolic Ca<sup>2+</sup> levels, as seen after 5-HT<sub>2A</sub> receptor stimulation, result in elevated fluorescence signals from B-GECO1.

B-GECO1 consists of the blue fluorescent protein (BFP) coupled to calmodulin (CaM) and the calmodulin-binding region of chicken myosin light chain kinase (M13). In the presence of Ca<sup>2+</sup>, M13 interacts with Ca<sup>2+</sup>-loaded CaM, resulting in a reorganization of the CaM-BFP binding. Subsequently, hydrophilic interactions of CaM and the chromophore of BFP result in increased fluorescence of BFP at 446 nm after excitation at 378 nm (Figure 29)<sup>61</sup>.

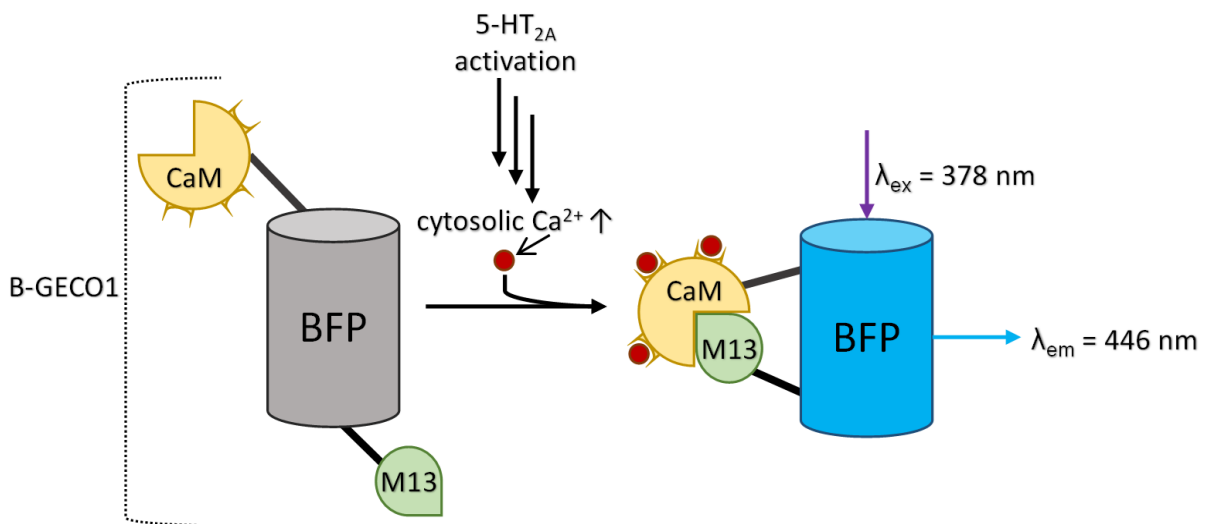


**Figure 29: Principle of cytosolic Ca<sup>2+</sup> detection using B-GECO1.** Fluorescence emission of B-GECO1 is measured at λ<sub>em</sub> = 446 nm after structural reorganization induced by Ca<sup>2+</sup> binding and excitation at λ<sub>ex</sub> = 378 nm.

## Results

HEK293 cells stably transfected with either B-GECO1 alone (HEK293-B-GECO1) or together with the human 5-HT<sub>2A</sub> receptor (HEK293-B-GECO1-5HT2a) were created. Using the B-GECO1 detection system, the following results were obtained. Ionomycin in a concentration of 1.4  $\mu$ M, was able to induce increased cytosolic Ca<sup>2+</sup> levels in both cell lines. It is a positive control for both cells lines by acting as a Ca<sup>2+</sup> ionophore. Additionally, 10  $\mu$ M ( $\pm$ )-TCB-2, as well as 5  $\mu$ M ( $\pm$ )-SAH268-Atto532 only induced an increase in cytosolic calcium in HEK293-B-GECO1-5HT2a cells (Figure 30). Thereby, the 5-HT<sub>2A</sub> receptor specific increase after ( $\pm$ )-TCB-2 or ( $\pm$ )-SAH268-Atto532 administration in contrast to Ionomycin is demonstrated.

Overall, ( $\pm$ )-SAH268-Atto532 can be described as a selective 5-HT<sub>2A</sub> receptor agonist with a binding affinity in the nanomolar range.

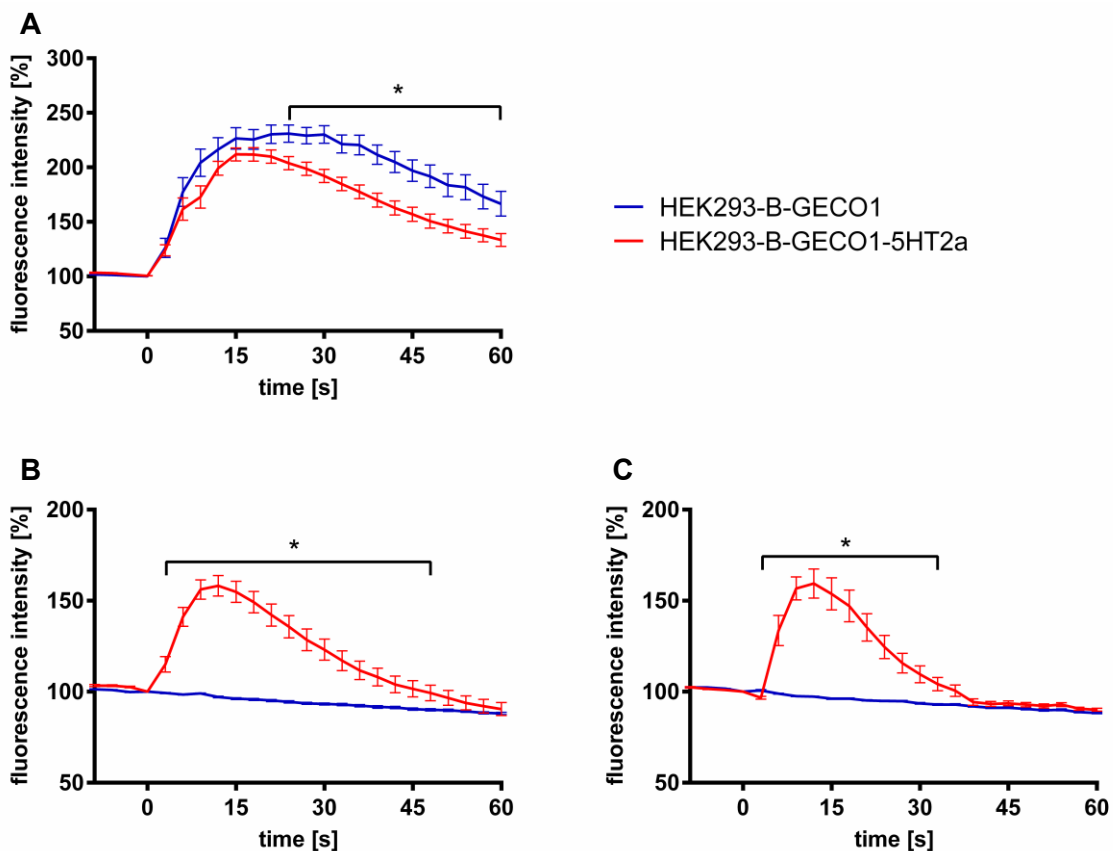


**Figure 30: Calcium measurements for ( $\pm$ )-SAH-268-Atto532.** HEK293-B-GECO1 and HEK293-B-GECO1-5HT2a cells were investigated for their fluorescence intensity following the treatment with ionomycin, ( $\pm$ )-TCB-2 and ( $\pm$ )-SAH268-Atto532. Nine seconds after starting the measurement the cells were treated with 1.4  $\mu$ M ionomycin (A) (positive control for both cell lines), 10  $\mu$ M ( $\pm$ )-TCB-2 (B) (positive control for HEK293-B-GECO1-5HT2a cells) or 5  $\mu$ M ( $\pm$ )-SAH268-Atto532 (C). Results of at least 3 independent experiments are shown as mean  $\pm$  SEM with  $n \geq 10$ . Marked values for HEK293-B-GECO1-5HT2a cells with  $p \leq 0.05$  are significantly different from HEK293-B-GECO1 cells, determined by Student's unpaired t-test.

### 5.7 Characterization of STW3-VI<sup>®</sup> via HPLC

This work aims to investigate the influence of STW3-VI<sup>®</sup> and two of its active ingredients hyperforin and hyperoside on 5-HT<sub>2A</sub> receptors. Therefore, STW3-VI<sup>®</sup> was analyzed via HPLC method 7 (Table 7) and its main components were identified using reference substances by comparing retention times and absorption spectra. Three different classes of natural substances were identified. Rutin, hyperoside, isoquercetin, quercetin, quercitrin and biapigenin represent the class of flavonoids. Hyperforin is a prenylated phloroglucin derivative and pseudohypericin and hypericin are naphthodiantrones. For the detection of the different chemical structures mentioned, two different detection wavelengths were necessary. All flavonoids and hyperforin were detected at  $\lambda=210$  nm, whereas the naphthodiantrones were detected at  $\lambda=590$  nm (Figure 31). Detection at 590 nm is inserted into the chromatogram for 210 nm starting from 60 minutes, as there were no peaks recorded at 590 nm until then. Concentrations for hyperforin and hyperoside were determined to be 36.8  $\mu$ M for hyperforin and 53.3  $\mu$ M for hyperoside (calculations in supplemental material). STW3-VI<sup>®</sup> was used for preincubations for the following experiments in the concentrations of 0.02, 0.002 and 0.0002 mg/ml. Hyperforin and hyperoside were used in concentrations of 1.0, 0.1 and 0.01  $\mu$ M.



## Results

### 5.8 Influence of STW3-VI<sup>®</sup>, hyperforin, and hyperoside on the ligand binding and diffusion of 5-HT<sub>2A</sub> receptors on the surface of SH-SY5Y cells

SH-SY5Y cells were preincubated for 6 days with 1.0, 0.1 and 0.01  $\mu$ M hyperforin and hyperoside or 0.02, 0.002 and 0.0002 mg/ml STW3-VI<sup>®</sup> and measured for the total receptor binding of ( $\pm$ )-SAH268-Atto532 and distribution of 5-HT<sub>2A</sub> receptor-ligand complexes into the diffusion time constants  $T_{diff2}$  and  $T_{diff3}$ , using the FCS setup described in 4.5.

The diffusion time constants  $T_{diff2}$  and  $T_{diff3}$  together with their calculated diffusion coefficient  $D_{diff2}$  and  $D_{diff3}$  are displayed in Table 19. They are shown for each preincubation in comparison to their respective control measurements. The fast diffusing receptor-ligand complexes, belonging to  $T_{diff2}$  and  $D_{diff2}$  respectively, were not influenced by any of the preincubations. In contrast,  $T_{diff3}$  representing the slow diffusing receptor-ligand complexes was increased from approx. 50 ms over all control measurements to more than 100 ms for all concentrations of STW3-VI<sup>®</sup>, 1.0  $\mu$ M Hyperforin and 0.1  $\mu$ M Hyperoside. An increase even beyond 200 ms was observed for 0.02 mg/ml STW3-VI<sup>®</sup>.

Total binding consists of the two fractions of  $f_{T_{diff2}}$  and  $f_{T_{diff3}}$ . Acquired total binding data was normalized to control cells preincubated with the highest ethanol concentration used in the measurements for each independent experiment and preincubation individually. Furthermore, the distribution of ( $\pm$ )-SAH268-Atto532 receptor-ligand complexes into the two diffusion time constants was investigated. Therefore, the determined fractions  $f_{T_{diff2}}$  and  $f_{T_{diff3}}$  after preincubation were compared to their respective fraction measured for control cells with the highest ethanol concentration used (Figure 32).

The highest concentration of 0.02 mg/ml STW3-VI<sup>®</sup> significantly increased the normalized total binding of ( $\pm$ )-SAH268-Atto532 to 5-HT<sub>2A</sub> receptors to  $1.27 \pm 0.08$ . For the concentrations of 0.002 and 0.0002 mg/ml STW3-VI<sup>®</sup>, the normalized total binding with  $0.99 \pm 0.03$  and  $1.08 \pm 0.04$  respectively was not significantly influenced. Hyperforin in the concentrations of 1.0, 0.1 and 0.01  $\mu$ M non-significantly altered the total binding to  $1.09 \pm 0.04$ ,  $0.99 \pm 0.04$  and  $0.94 \pm 0.03$ . Similar results were obtained for hyperoside, where 1.0, 0.1 and 0.01  $\mu$ M non-significantly changed the total binding to  $1.06 \pm 0.05$ ,  $1.03 \pm 0.03$  and  $0.93 \pm 0.04$  (Figure 32).

## Results

**Table 19: FCS data for (±)-SAH268-Atto532 receptor-ligand complexes on SH-SY5Y cells after preincubation with STW3-VI®, hyperforin, and hyperoside**

Experimental condition		T <sub>diff2</sub> [ms]	T <sub>diff3</sub> [ms]	D <sub>diff2</sub> [μm <sup>2</sup> /s]	D <sub>diff3</sub> [μm <sup>2</sup> /s]
0.02 mg/ml STW3-VI®	Control	1.50 ± 0.99	37.89 ± 23.36	6.68 ± 4.44	0.264 ± 0.163
	Preincubated	1.24 ± 1.00	203.83 ± 271.80	8.05 ± 6.51	0.049 ± 0.065
0.002 mg/ml STW3-VI®	Control	1.90 ± 1.88	53.51 ± 54.48	5.25 ± 5.17	0.187 ± 0.190
	Preincubated	1.59 ± 1.19	117.39 ± 140.26	6.31 ± 4.73	0.085 ± 0.102
0.0002 mg/ml STW3-VI®	Control	1.63 ± 1.91	55.84 ± 43.21	6.15 ± 5.66	0.179 ± 0.139
	Preincubated	2.22 ± 2.75	141.16 ± 190.06	4.50 ± 5.58	0.071 ± 0.095
1.0 μM Hyperforin	Control	1.55 ± 1.14	50.01 ± 35.01	6.46 ± 4.78	0.200 ± 0.140
	Preincubated	1.36 ± 0.67	117.57 ± 186.69	7.33 ± 3.62	0.085 ± 0.135
0.1 μM Hyperforin	Control	1.56 ± 1.52	44.84 ± 22.95	6.40 ± 6.22	0.223 ± 0.114
	Preincubated	1.79 ± 1.67	82.94 ± 74.44	5.58 ± 5.19	0.121 ± 0.108
0.01 μM Hyperforin	Control	2.10 ± 2.01	57.04 ± 57.04	4.76 ± 4.56	0.175 ± 0.175
	Preincubated	1.75 ± 1.56	67.73 ± 119.68	5.71 ± 5.09	0.148 ± 0.261
1.0 μM Hyperoside	Control	1.55 ± 1.30	51.21 ± 39.98	6.47 ± 5.45	0.195 ± 0.152
	Preincubated	1.71 ± 1.45	66.41 ± 52.03	6.11 ± 5.29	0.151 ± 0.118
0.1 μM Hyperoside	Control	1.61 ± 1.48	49.00 ± 34.75	6.23 ± 5.72	0.204 ± 0.145
	Preincubated	1.79 ± 1.76	100.81 ± 125.81	5.59 ± 5.50	0.099 ± 0.124
0.01 μM Hyperoside	Control	2.10 ± 2.01	57.04 ± 57.04	4.76 ± 4.56	0.175 ± 0.175
	Preincubated	1.72 ± 1.98	42.23 ± 46.41	5.81 ± 6.67	0.237 ± 0.260

## Results

Regarding the distribution of  $f_{T_{diff2}}$  and  $f_{T_{diff3}}$ , 1.0  $\mu\text{M}$  hyperforin and hyperoside, 0.1  $\mu\text{M}$  hyperoside and also 0.02 and 0.002 mg/ml STW3-VI<sup>®</sup> demonstrated significant differences. The lowest concentration of 0.0002 mg/ml STW3-VI<sup>®</sup> with  $f_{T_{diff2}} = 0.38 \pm 0.02$  /  $f_{T_{diff3}} = 0.69 \pm 0.04$  had no significant effect compared to control cells with  $f_{T_{diff2}} = 0.33 \pm 0.03$  /  $f_{T_{diff3}} = 0.67 \pm 0.03$ . The higher concentrations of STW3-VI<sup>®</sup> significantly and dose-dependently shifted the distribution by reducing  $f_{T_{diff3}}$  and elevating  $f_{T_{diff2}}$ . A distribution of  $f_{T_{diff2}} = 0.44 \pm 0.02$  /  $f_{T_{diff3}} = 0.54 \pm 0.02$  for 0.002 mg/ml STW3-VI<sup>®</sup> and  $f_{T_{diff2}} = 0.89 \pm 0.08$  /  $f_{T_{diff3}} = 0.38 \pm 0.04$  for 0.02 mg/ml STW3-VI<sup>®</sup> were determined (Figure 32).

Hyperforin in concentrations of 0.01  $\mu\text{M}$  with  $f_{T_{diff2}} = 0.29 \pm 0.03$  /  $f_{T_{diff3}} = 0.64 \pm 0.03$  and 0.1  $\mu\text{M}$  with  $f_{T_{diff2}} = 0.45 \pm 0.04$  /  $f_{T_{diff3}} = 0.54 \pm 0.04$  had no significant effect on the distribution of the bound fractions. The concentration of 1.0  $\mu\text{M}$  hyperforin displayed a significantly different distribution of  $f_{T_{diff2}} = 0.61 \pm 0.05$  /  $f_{T_{diff3}} = 0.48 \pm 0.04$ . The observed effects for hyperforin are comparable to STW3-VI<sup>®</sup> but in general less pronounced (Figure 32).

Hyperoside in a concentration of 0.01  $\mu\text{M}$  did not significantly affect the distribution of the bound fractions with  $f_{T_{diff2}} = 0.22 \pm 0.04$  /  $f_{T_{diff3}} = 0.71 \pm 0.05$ . Higher hyperoside concentrations of 0.1  $\mu\text{M}$  with  $f_{T_{diff2}} = 0.52 \pm 0.03$  /  $f_{T_{diff3}} = 0.51 \pm 0.03$  and 1.0  $\mu\text{M}$  with  $f_{T_{diff2}} = 0.53 \pm 0.04$  /  $f_{T_{diff3}} = 0.54 \pm 0.03$  significantly altered the ratio of the bound fractions. As seen for STW3-VI<sup>®</sup> and hyperforin, hyperoside significantly increased  $f_{T_{diff2}}$  and lowered  $f_{T_{diff3}}$ . But the shift from a predominating fraction  $f_{T_{diff2}}$  under control conditions to a predominating fraction  $f_{T_{diff3}}$  after preincubation was not observed (Figure 32).

The observed effects on the distribution of  $f_{T_{diff2}}$  and  $f_{T_{diff3}}$  after preincubation with STW3-VI<sup>®</sup>, hyperforin, and hyperoside were dose-dependent in any case. Remarkably, 0.1  $\mu\text{M}$  hyperoside already exhibited the maximum effect also observed for 1.0  $\mu\text{M}$ . Furthermore, the increased total binding observed for 0.02 mg/ml STW3-VI<sup>®</sup> resulted exclusively from an increase of fast diffusing receptor-ligand complexes in  $f_{T_{diff2}}$ .

The resulting influences of altered total binding and diffusion of 5-HT<sub>2A</sub> receptors after preincubation were investigated further. Receptor density, receptor internalization and receptor signaling activity after preincubation with STW3-VI<sup>®</sup>, hyperforin, and hyperoside were examined.

## Results

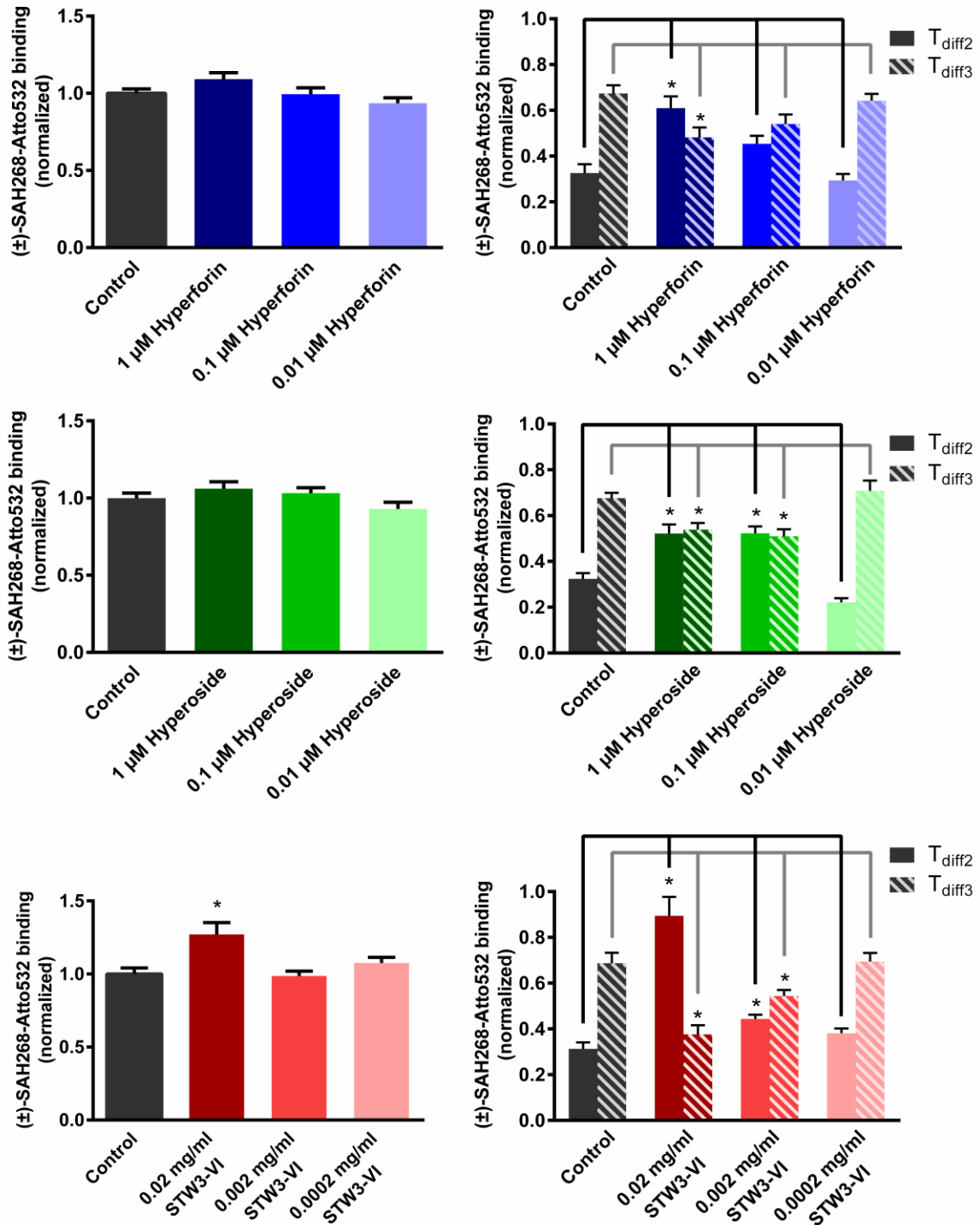


**Figure 32: Influence of STW3-VI<sup>®</sup>, hyperforin and hyperoside on the 5-HT<sub>2A</sub> receptor binding of (±)-SAH268-Atto532.** Total binding (left) and distribution of lateral mobilities of fast ( $T_{diff2}$ ) and slow ( $T_{diff3}$ ) diffusing receptor-ligand complexes. Results of at least 3 independent experiments with  $n \geq 20$  are shown as mean + SEM. Marked values \* with  $p \leq 0.05$  are significantly different from their respective controls, determined by Student's unpaired t-test.

## Results

### 5.9 Influence of STW3-VI<sup>®</sup>, hyperforin, and hyperoside on the receptor density and internalization of HiBiT-tagged 5-HT<sub>2A</sub> receptors on the surface of HEK293 cells

At first, the receptor density and receptor internalization of 5-HT<sub>2A</sub> receptors were investigated using the Nano-Glo<sup>®</sup> HiBiT Extracellular Detection System. In this detection system the NanoLuc<sup>®</sup> Binary Technology (NanoBiT<sup>®</sup>) is employed. It uses a divided NanoLuc<sup>®</sup> luciferase, with the small subunit consisting of 11 amino acids (HiBiT) coupled to the N-terminus of the protein of interest. The much bigger subunit of the luciferase consisting of 160 amino acids (LargeBiT, LgBiT) is added before assay start. Together the HiBiT and LgBiT form an active NanoLuc<sup>®</sup> luciferase, which converts added furimazine to furimamide to generate chemiluminescence, measured in relative light units (RLU) (Figure 33). The amount of emitted chemiluminescence is directly proportional to the total receptor density.

HEK293 cells were stably transfected with N-terminally HiBiT-tagged human 5-HT<sub>2A</sub> receptor. The receptor density was measured under non-stimulating conditions and after stimulation with 1.0 μM (±)-TCB-2 for 15 min according to the manufacturers manual. The difference between the receptor densities under non-stimulating conditions and after stimulation accounts for receptors undergoing internalization. Thereby, receptor internalization was determined indirectly by comparing receptor densities under non-stimulating and stimulating conditions.

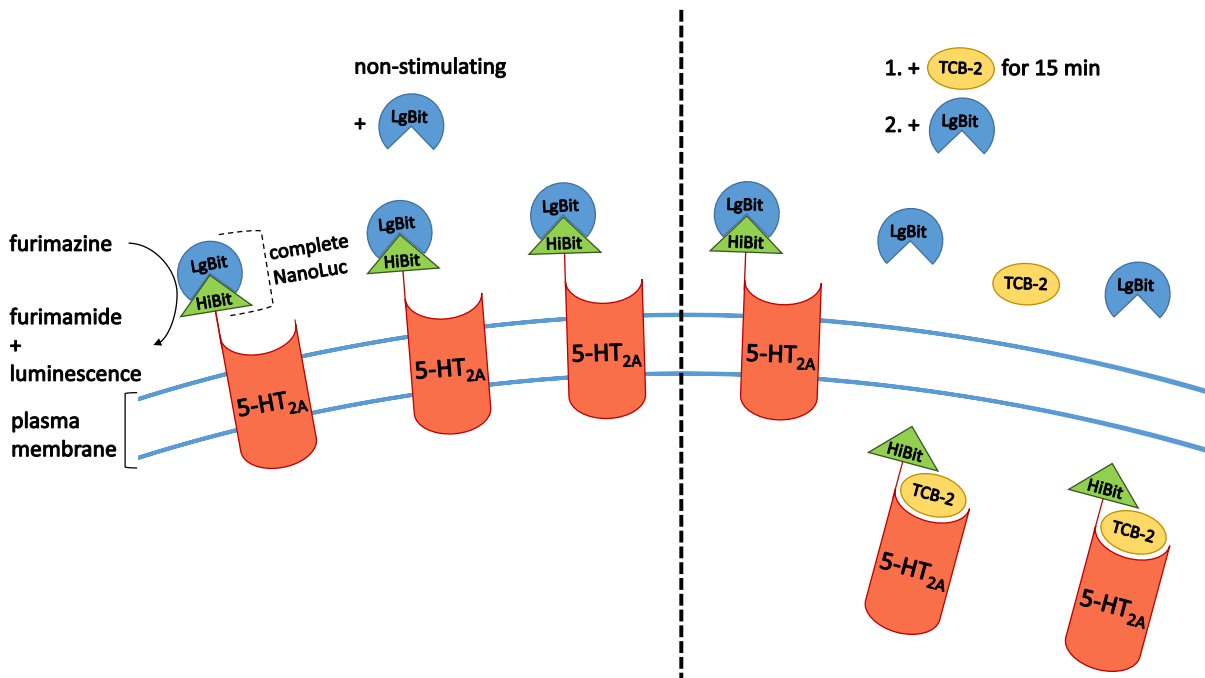


**Figure 33: Illustration of HiBiT-tagged 5-HT<sub>2A</sub> receptor detection in the plasma membrane of HEK293 cells.** Receptor density is determined using the Nano-Glo<sup>®</sup> HiBiT Extracellular Detection System under non-stimulating conditions and after stimulation with 1.0 μM (±)-TCB-2.

## Results

RLU values for HEK293-HiBiT-5HT<sub>2A</sub> cells preincubated for at least 6 days with 1.0  $\mu$ M hyperforin, 1.0  $\mu$ M hyperoside or 0.02, 0.002 and 0.0002 mg/ml STW3-VI<sup>®</sup> were all normalized to cells without preincubation and stimulation.

Under non-stimulating conditions STW3-VI<sup>®</sup> dose-dependently decreased the 5-HT<sub>2A</sub> receptor density with higher concentrations. The lowest concentration of 0.0002 mg/ml STW3-VI<sup>®</sup> displayed no significant effect with a receptor density of  $0.98 \pm 0.01$ . In contrast, 0.002 and 0.02 mg/ml STW3-VI<sup>®</sup> significantly reduced the receptor density to  $0.93 \pm 0.02$  and  $0.88 \pm 0.02$  respectively. Hyperforin and hyperoside in the highest concentration of 1.0  $\mu$ M did not significantly alter receptor density and displayed values of  $1.01 \pm 0.02$  for hyperforin and  $0.98 \pm 0.03$  for hyperoside (Figure 34). Therefore, no further experiments with lower concentrations of hyperforin and hyperoside were undertaken.

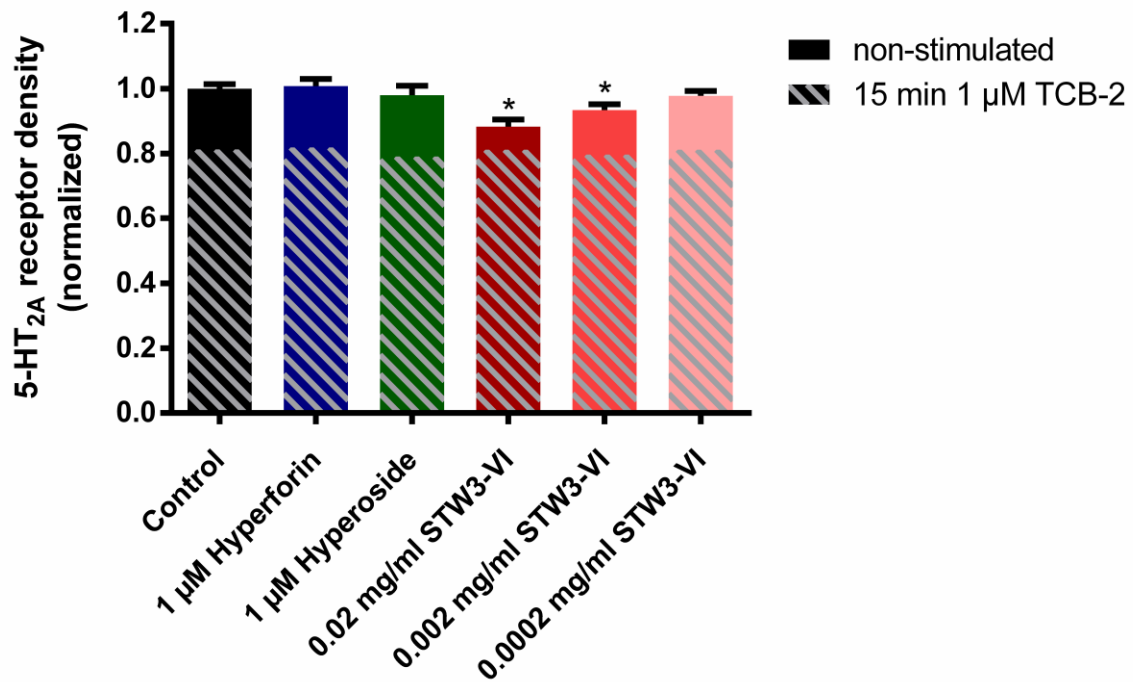


**Figure 34: Influence of STW3-VI<sup>®</sup>, hyperforin and hyperoside on the receptor density of HiBiT-tagged 5-HT<sub>2A</sub> receptors on the surface of HEK293 cells.** Amount of HiBiT-tagged 5-HT<sub>2A</sub> receptors is proportional to measured luminescence signal. Normalized receptor density is displayed for cells after different preincubations for six days without stimulation (plain) and after stimulation with 1.0  $\mu$ M ( $\pm$ )-TCB-2 for 15 min (striped). Results of at least 3 independent experiments with  $n \geq 12$  are shown as mean + SEM. Marked values with  $p \leq 0.05$  are significantly different from control data, determined by Student's unpaired t-test.

## Results

Receptor density under stimulating conditions was determined by treating HEK293-HiBiT-5HT<sub>2A</sub> cells with 1.0  $\mu$ M ( $\pm$ )-TCB-2 for 15 min before starting the assay. The measured receptor density after stimulation is displayed using striped bars (Figure 34). The difference in receptor density under non-stimulating and stimulating conditions expressed as percentages accounts for the ( $\pm$ )-TCB-2 induced receptor internalization (Figure 35).

In comparison to stimulated control cells with a 5-HT<sub>2A</sub> receptor internalization of  $18.8 \pm 1.8\%$ , STW3-VI<sup>®</sup> dose-dependently reduced receptor internalization. While 0.0002 and 0.002 mg/ml STW3-VI<sup>®</sup> in general reduced the receptor internalization to  $16.9 \pm 1.5\%$  and  $14.5 \pm 2.0\%$ , their effect was not statistically significant. On the other hand, 0.02 mg/ml STW3-VI<sup>®</sup> significantly inhibited receptor internalization, with  $8.1 \pm 1.5\%$  internalized receptors remaining. As seen for total 5-HT<sub>2A</sub> receptor density, 1.0  $\mu$ M hyperforin with  $18.6 \pm 2.2\%$  and 1.0  $\mu$ M hyperoside with  $20.6 \pm 2.2\%$  had no significant influence on 5-HT<sub>2A</sub> receptor internalization (Figure 35).

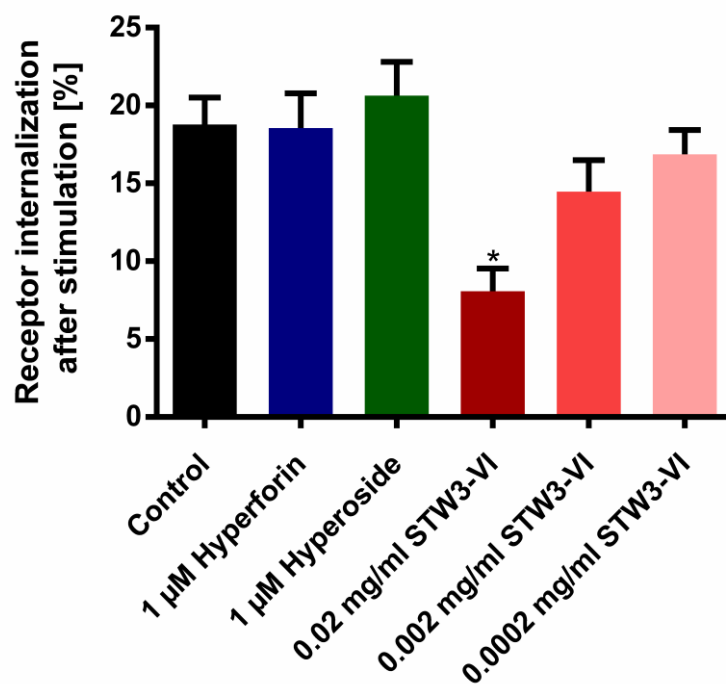


**Figure 35: Influence of STW3-VI<sup>®</sup>, hyperforin and hyperoside on the internalization of HiBiT-tagged 5-HT<sub>2A</sub> receptors on the surface of HEK293 cells.** Percentages represent the difference between non-stimulated cells and cells after treatment with 1.0  $\mu$ M ( $\pm$ )-TCB-2 for 15 min within the same preincubation. Results of at least 3 independent experiments with  $n \geq 12$  are shown as mean + SEM. Marked values with  $p \leq 0.05$  are significantly different from their respective controls, determined by Student's unpaired t-test (ns = not significant).

### 5.10 Influence of STW3-VI<sup>®</sup>, hyperforin, and hyperoside on the 5-HT<sub>2A</sub> receptor-mediated intracellular Ca<sup>2+</sup> levels in HEK293 cells

Investigating the influences of hyperforin and hyperoside on intracellular Ca<sup>2+</sup> levels after preincubation would be feasible with the B-GECO1 system described in 5.6. Unfortunately, the photophysical interference of the naphthodianthrones with B-GECO1 ruled out this possibility. The excitation light of  $\lambda_{\text{ex}} = 378$  nm for B-GECO1 also excited the naphthodianthrones contained in STW3-VI<sup>®</sup>, leading to wrong, elevated levels of emitted fluorescence. Therefore, a luciferase-based system was employed. The employed system had no need for excitation leading to the emission of fluorescence and therefore no interference with the naphthodianthrones or STW3-VI<sup>®</sup> in general was observed.

Using the calcium-dependent luciferase aequorin, the intracellular Ca<sup>2+</sup> levels in HEK293 cells, stably transfected with the human 5-HT<sub>2A</sub> receptor and apoaequorin, were determined. Aequorin consists of an apoprotein (apoaequorin) and a bound luciferin (coelenterazine). It exhibits three binding sites for Ca<sup>2+</sup> ions. After binding Ca<sup>2+</sup>, aequorin is subjected to conformational changes resulting in oxygenase-activity. Aequorin then converts coelenterazine to an unstable dioxethanone via oxidation (Figure 36, reaction A). The unstable dioxethanone is turned into the excited coelenteramide anion by decarboxylation (Figure 36, reaction B). As it returns to its non-excited state, the excited coelenteramide emits blue light of  $\lambda = 470$  nm (Figure 36, reaction C). To regenerate active aequorin, the bound Ca<sup>2+</sup> ions have to be removed in the presence of molecular oxygen and the coelenteramide needs to be exchanged with fresh coelenterazine (Figure 36, reaction D)<sup>62</sup>. The emitted luminescence, measured in RLU, is directly proportional to the intracellular Ca<sup>2+</sup> levels.

Results

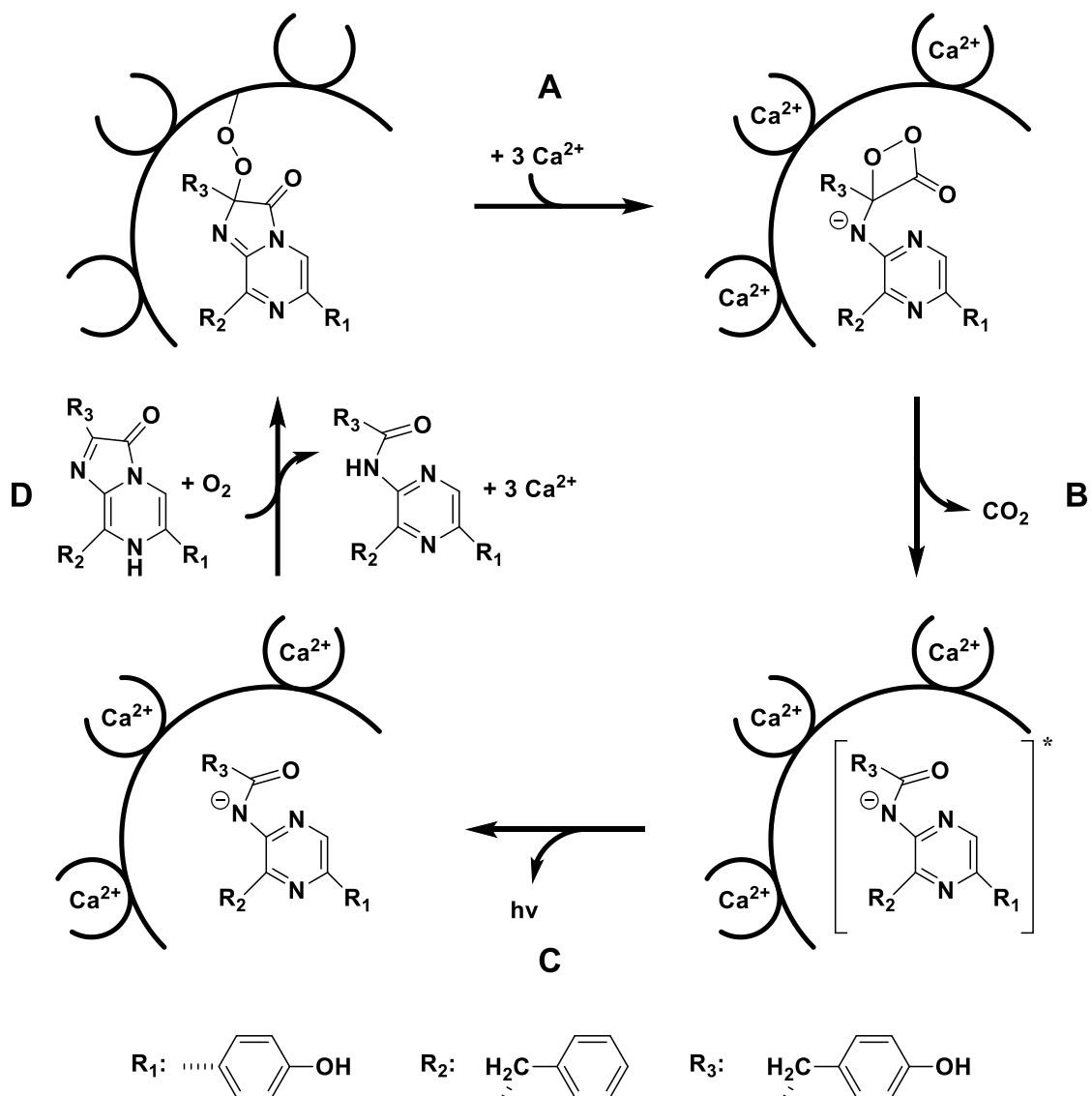


**Figure 36: Schematic representation of intracellular  $\text{Ca}^{2+}$  level detection by chemiluminescence using aequorin.** Apoaequorin and its substrate coelenterazine form the active aequorin. After binding three  $\text{Ca}^{2+}$  ions coelenterazine is converted to an unstable dioxethanone anion (A). Decarboxylation of the dioxethanone yields the excited coelenteramide anion (B). By returning to its non-excited state coelenteramide emits blue light of  $\lambda = 470 \text{ nm}$  (C). Regeneration of aequorin is achieved through removing  $\text{Ca}^{2+}$  ions in the presence of molecular oxygen and exchanging coelenteramide by coelenterazine (D).

Modified drawing according to: Aequorin mechanism.svg. (2008, April 4). Retrieved October 15, 2020, from [https://commons.wikimedia.org/wiki/File:Aequorin\\_mechanism.svg](https://commons.wikimedia.org/wiki/File:Aequorin_mechanism.svg)

## Results

RLU values were measured over the course of 50 s. After measuring background luminescence for 10 s, 10  $\mu\text{M}$  ( $\pm$ )-TCB-2 was added to the cells and the measurement was continued for an additional 40 s. AUC values were determined using the trapezoidal rule (see 4.11) for each preincubation and normalized to control cells. After 6 days preincubation with 0.0002 mg/ml STW3-VI<sup>®</sup>, the normalized intracellular  $\text{Ca}^{2+}$  levels with  $0.99 \pm 0.05$  were not significantly altered. By increasing the STW3-VI<sup>®</sup> concentration to 0.002 and 0.02 mg/ml the intracellular  $\text{Ca}^{2+}$  levels were significantly reduced in comparison to control cells with  $0.59 \pm 0.04$  and  $0.69 \pm 0.04$  respectively. Remarkably, 0.002 mg/ml STW3-VI<sup>®</sup> exhibited the maximum effect and increasing the STW3-VI<sup>®</sup> concentration to 0.02 mg/ml did not further reduce the intracellular  $\text{Ca}^{2+}$  levels. The reduction was even lower for 0.002 mg/ml STW3-VI<sup>®</sup> but without statistically significant difference compared to 0.02 mg/ml STW3-VI<sup>®</sup>. Hyperforin and hyperoside in a concentration of 1.0  $\mu\text{M}$  had no significant influence on the intracellular  $\text{Ca}^{2+}$  levels with values of  $1.05 \pm 0.04$  and  $1.03 \pm 0.04$  respectively (Figure 37). Therefore, no further experiments with lower concentrations of hyperforin and hyperoside were undertaken.

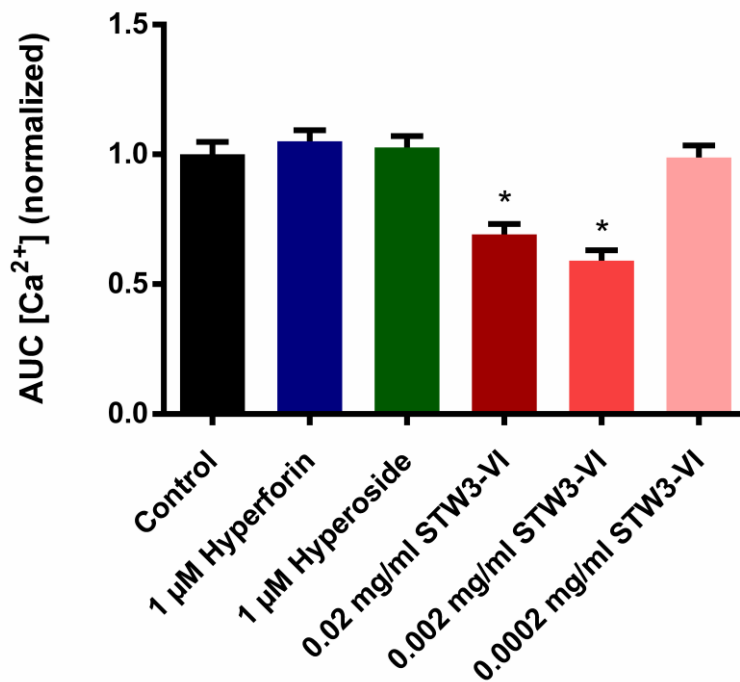


**Figure 37: Influence of STW3-VI<sup>®</sup>, hyperforin and hyperoside on the intracellular  $\text{Ca}^{2+}$  levels in HEK293 cells after stimulation with ( $\pm$ )-TCB-2.** RLU values are recorded every 2 s for 50 s and area under the curve (AUC) is determined via trapezoidal rule (see 4.11). Stimulation was carried out with 10  $\mu\text{M}$  ( $\pm$ )-TCB-2. Results of at least 3 independent experiments with  $n \geq 27$  are shown as mean + SEM. Marked values with  $p \leq 0.05$  are significantly different from control, determined by Student's unpaired t-test.

## Results

The 5-HT<sub>2A</sub> receptor specificity of the observed effect for STW3-VI<sup>®</sup> was investigated. Therefore, cells were preincubated for at least 6 days with 1.0 µM hyperforin, 1.0 µM hyperoside or 0.02 mg/ml STW3-VI<sup>®</sup>. The stimulation was carried out with 500 nM of the Ca<sup>2+</sup> ionophore ionomycin or 10 µM of the P<sub>2</sub>Y purinoceptor 1 (P<sub>2</sub>RY<sub>1</sub>) agonist ATP. Ionomycin induces a non-specific increase in intracellular Ca<sup>2+</sup> levels and was used for excluding a direct effect on the aequorin system. ATP was used to exclude non-specific influences of STW3-VI<sup>®</sup> on the signaling cascade of G<sub>q</sub> coupled GPCR. The intracellular Ca<sup>2+</sup> levels after stimulation with 500 nM ionomycin were not significantly affected for all preincubations with 1.06 ± 0.12 for 1.0 µM hyperforin, 0.96 ± 0.08 for 1.0 µM hyperoside and 0.92 ± 0.07 for 0.02 mg/ml STW3-VI<sup>®</sup> respectively. Additionally, the stimulation with 10 µM ATP did not lead to significantly altered intracellular Ca<sup>2+</sup> levels for all preincubations with the values being 1.04 ± 0.06 for 1.0 µM hyperforin, 1.12 ± 0.06 for 1.0 µM hyperoside and 0.94 ± 0.07 for 0.02 mg/ml STW3-VI<sup>®</sup> respectively (Figure 38). Therefore, STW3-VI<sup>®</sup> selectively influences the downstream signaling of 5-HT<sub>2A</sub> receptors.

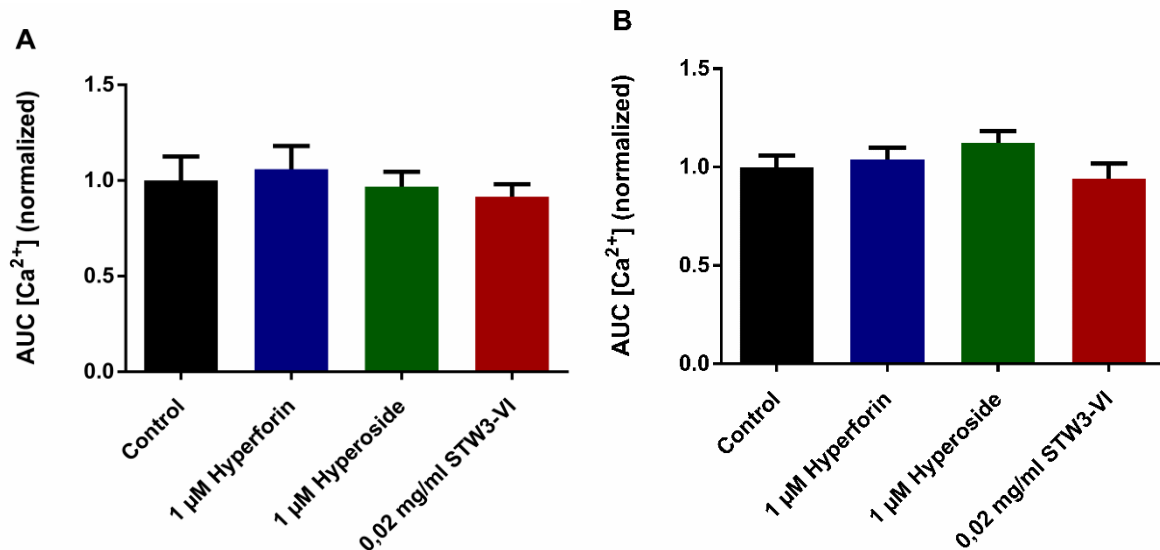


**Figure 38: Influence of STW3-VI<sup>®</sup>, hyperforin and hyperoside on the intracellular Ca<sup>2+</sup> levels in HEK293 cells after stimulation with ionomycin and ATP.** RLU values are recorded every 2 s for 50 s and area under the curve (AUC) is determined via trapezoidal rule (see 4.11). Stimulation was carried out with 500 nM ionomycin (A) or 10 µM ATP (B). Data are shown as mean + SEM for 3 independent experiments with n ≥ 7.

## 6. Discussion

5-HT<sub>2A</sub> receptors are involved in the development and treatment of depressive disorders. Inhibition of 5-HT<sub>2A</sub> receptor signaling, as it is seen after the treatment with many TCA, or receptor downregulation observed after the treatment with SSRI, both suggest that decreasing 5-HT<sub>2A</sub> receptor activity is beneficial in the treatment of depressive disorders<sup>37,43,78</sup>. Controversially, the same is also observed for 5-HT<sub>2A</sub> receptor activation. Hallucinogenic substances such as psilocybin or LSD led to antidepressant effects without a delayed onset in recent pilot trials<sup>49</sup>. Furthermore, desensitization of 5-HT<sub>1A</sub> receptors, which is known to be highly relevant in the regulation of mood, is observed after 5-HT<sub>2A</sub> receptor activation<sup>44</sup>. The complex processes behind 5-HT<sub>2A</sub> receptors need to be elucidated further. Additionally, the mode of action of St. John's wort extract STW3-VI<sup>®</sup> involving 5-HT<sub>2A</sub> receptors is still not fully known. For assessing those questions, a tool for the investigation of 5-HT<sub>2A</sub> receptors in living cells is necessary. Fluorescent ligands are well-suited for investigating receptor dynamics and interactions in single-molecule techniques as FCS and SPT<sup>51,52,54</sup>. Fluorescent ligands were constructed for many other serotonin receptor subtypes (e.g. 1A, 2B, 2C, 3, 4, 6), with a ligand for 5-HT<sub>2A</sub> receptors still missing<sup>55-60</sup>. Therefore, the aim of the first part of this work was to fill this gap and synthesize a fluorescent 5-HT<sub>2A</sub> receptor ligand.

The synthetic approach was started from (±)-TCB-2 due to its high affinity for 5-HT<sub>2A</sub> receptors and the ability to easily couple commercially available NHS-activated fluorophores to its primary amine group<sup>79</sup>. Furthermore, (±)-TCB-2 is characterized by a phenethylamine structure with two aromatic methoxy substituents, a hydrophobic bromide substituent and an aliphatic, protonable amine. All of these characteristics were proven to be important for 5-HT<sub>2A</sub> binding in computational studies with molecular docking operations<sup>71,72</sup>. (±)-TCB-2, (±)-SAH268 and all constructed ligands were employed in further measurements as their racemic mixtures. As described by McLean et al., (R)-TCB-2 displays a roughly 100-fold increased receptor affinity and 10-fold increased second messenger generation for human 5-HT<sub>2A</sub> receptors in comparison to (S)-TCB-2<sup>79</sup>. Consequently, it can be assumed that, all molecules derived from (±)-TCB-2 display similar eudysmic ratios. Nevertheless, the synthesis of (±)-SAH268-Atto532 yielded a fluorescent ligand with nanomolar binding affinity to 5-HT<sub>2A</sub> receptors. A chiral separation in its corresponding enantiomer and diastereomer was not deemed necessary, as its racemic mixture was well suited for all subsequent measurements.

Apart from (±)-SAH268-Atto532, several other ligands were created within the synthetic approach. Those ligands displayed remarkable characteristics which underline the difficulties in the synthesis of fluorescent ligands. For example, by coupling (±)-TCB-2 directly to the rhodamine-based dyes Alexa-Fluor532-NHS and Atto532-NHS, as well as the cyanine-based fluorophore Alexa-Fluor647-NHS, three ligands without detectable selective 5-HT<sub>2A</sub> receptor

## Discussion

binding were obtained. The autocorrelation curves acquired by FCS measurements in the plasma membrane for ( $\pm$ )-TCB-2-Atto532 and ( $\pm$ )-TCB-2-Alexa647 were nearly identical to those recorded in solution. In contrast, ( $\pm$ )-TCB-2-Alexa532 displayed high amounts of non-specific binding. This is remarkable, as previous experiments with ligands consisting of Alexa-Fluor532 did not show elevated non-specific binding<sup>80–82</sup>. Nevertheless, since Atto532 and Alexa-Fluor647 directly coupled to ( $\pm$ )-TCB-2 yielded ligands with no notable non-selective binding, it can be concluded that Alexa-Fluor532 is responsible for the high amounts of non-selective binding of ( $\pm$ )-TCB-2-Alexa532. By comparing different ligands constructed with Alexa-Fluor532, it is evident that predicting the suitability of a certain fluorophore is not possible. Coupling the same fluorophore to different ligands can lead to fundamentally different results. Therefore, the synthesis of fluorescent ligands is often conducted on a trial and error basis. The importance of the protonable amine moiety for 5-HT<sub>2A</sub> receptor interaction was already shown in molecular modeling studies<sup>71,72</sup>. The fluorescent ligands created by direct coupling to ( $\pm$ )-TCB-2 confirm those results. When compared to other fluorescent serotonin receptor ligands, it can be concluded that a protonable phenethylamine moiety is also important for 5-HT<sub>2B</sub> and 5-HT<sub>2C</sub> interaction<sup>56,57</sup>. The chemical structures of fluorescent ligands for the serotonin receptors 1A, 3, 4 and 6 are substantially different<sup>55,58–60</sup>. Therefore, this characteristic cannot be generalized for all serotonin receptor subspecies.

To retain the protonability of the aliphatic amine moiety a BOC-protected aminohexyl linker was introduced using 6-(BOC-amino)hexyl bromide in a direct alkylation reaction. The BOC-protection was necessary to prevent the bromocarbon moiety from reacting with the newly introduced amine. By following a protocol employing CsOH as a base, a reaction was conducted almost exclusively leading to the secondary amine ( $\pm$ )-SAH267<sup>83</sup>. A reaction without CsOH would result in mixture of secondary and tertiary amines as well as quaternary ammonium cations<sup>84</sup>. Acid-catalyzed cleavage of the BOC-amine moiety with 85% aqueous H<sub>3</sub>PO<sub>4</sub> led to ( $\pm$ )-SAH268<sup>85</sup>. ( $\pm$ )-SAH268 is characterized by a protonable secondary amine in its phenethylamine moiety and a terminal primary amine for coupling to NHS-activated fluorophores. In addition to retaining protonability, introducing an aminohexyl linker leads to more distance between the fluorophore and the phenethylamine moiety of the ligands responsible for receptor binding, possibly preventing negative influences of the fluorophore. Conversely, too much flexibility resulting from increased linker lengths could lead to a refolding of the fluorophore. Thereby, the fluorophore is prone to interaction with components of the plasma membrane, which could inhibit the binding to the receptor of interest. The influence of different linker lengths for a variety of fluorophores on binding affinity and efficacy was already studied for fluorescent adenosine A1 receptor ligands. There was no general rule deductible concerning the optimal linker length, as it was different for each fluorophore investigated<sup>86</sup>. Using Alexa-Fluor532-NHS, Alexa-Fluor647-NHS and Atto532-NHS, allowed us to investigate

## Discussion

fluorophores with different distances from the succinimidylester to the fluorophore already present in their chemical structure. For Alexa-Fluor532-NHS, the fluorophore is in direct proximity of the succinimidylester, whereas Atto532-NHS displays a distance of four carbons and Alexa-Fluor647-NHS a distance of five carbons.

As already observed for their ( $\pm$ )-TCB-2 counterparts, ( $\pm$ )-SAH268-Alexa532 exhibited a high amount of non-specific binding and ( $\pm$ )-SAH268-Alexa647 as well as ( $\pm$ )-SAH268-Atto532 displayed nearly no binding to the plasma membrane of C6 cells. This again demonstrates that Alexa-Fluor532-NHS is responsible for the elevated amounts of non-specific binding of the respective ligands. Unfortunately, the introduction of an aminohexyl linker did not lead to a functioning fluorescent ligand for 5-HT<sub>2A</sub> receptors. Since C6 cells are originally isolated from *Rattus norvegicus*, they express murine 5-HT<sub>2A</sub> receptors. Murine and human receptors display differences in affinity for ligands or even signaling after ligand binding<sup>79,87,88</sup>. For the 5-HT<sub>2A</sub> receptors, those differences originate from three varying amino acids in their transmembrane region, which are associated with ligand binding. The different amino acids are threonine and alanine at position 82, isoleucine and valine at position 150 and alanine and serine at position 242. General consensus is that the alanine/serine-242 exchange is mainly responsible for the species-related differences in ligand binding<sup>73,74</sup>. The serine at this position of human monoamine receptors was found to be responsible for the formation of hydrogen bonds. Those bonds are formed with the oxygens present in the catecholamine moiety of dopamine and epinephrine<sup>74,89</sup>. The importance of serine at position 242 for receptor-ligand interaction was also investigated for tryptamine- and phenethylamine based hallucinogenic substances binding to the 5-HT<sub>2A</sub> receptor<sup>90</sup>. Consequently, the human neuroblastoma cell line SH-SY5Y originally isolated from bone marrow tissue, was used to investigate whether ( $\pm$ )-SAH268-Alexa647, ( $\pm$ )-TCB-2-Atto532 and ( $\pm$ )-SAH268-Atto532 display binding affinity to human 5-HT<sub>2A</sub> receptors. Both ( $\pm$ )-TCB-2-Atto532 and ( $\pm$ )-SAH268-Alexa647 displayed nearly no binding affinity, as their autocorrelation curves for a measurement in the plasma membrane were nearly identical to a measurement in the solution above the cells. In contrast, FCS binding measurements for ( $\pm$ )-SAH268-Atto532 revealed two distinct diffusion time constants for receptor-ligand complexes, of which 75.2% were displaceable by a 1000-fold excess of ( $\pm$ )-TCB-2. Observing two distinct diffusion time constants, one in the single digit and one in the two- to three-digit millisecond range is very common for FCS experiments investigating fluorescent ligands for GPCR, since the ligand-occupied receptors are in different diffusive states<sup>51</sup>. The specific binding, diffusion time constants for the two receptor-ligand complexes and the respective calculated diffusion coefficients of ( $\pm$ )-SAH268-Atto532 are in general well comparable to other fluorescent GPCR ligands, such as BEA-X-BY630, Alexa532-NA or XAC-BY630<sup>82,91,92</sup>. The adenosine A3 receptor agonist BEA-X-BY630 for example displays diffusion time constants for receptor-ligand complexes of  $T_{diff2} = 5.9 \pm 0.7$  ms and  $T_{diff3} = 131 \pm 15$  ms

## Discussion

compared to  $T_{diff2} = 1.27 \pm 0.19$  ms and  $T_{diff3} = 55.40 \pm 22.96$  ms for ( $\pm$ )-SAH268-Atto532<sup>91</sup>. The amount of roughly 75% specifically bound fluorescent ligand is also observed for BEA-X-BY630 and Alexa532-NA<sup>82,91</sup>.

Taken together, a fluorescent 5-HT<sub>2A</sub> receptor ligand was ultimately synthesized with ( $\pm$ )-SAH268-Atto532. The protonability of the phenethylamine moiety was retained and an aminohexyl linker was introduced to ( $\pm$ )-TCB-2. Even though ( $\pm$ )-SAH268-Alexa647 shares this properties, binding to the 5-HT<sub>2A</sub> receptor could not be observed. This proves once again that a prediction of the functionality of fluorescent ligands is very challenging. The flexibility resulting from the higher total distance between phenethylamine moiety and fluorophore could allow for a refolding of the Alexa-Fluor647 fluorophore. Thereby, the interactions of the phenethylamine moiety within the 5-HT<sub>2A</sub> receptor binding pocket could be hindered. The recently published cryoelectron microscopy and X-ray crystal structures of the 5-HT<sub>2A</sub> receptor in its active state with bound hallucinogenic ligands show that the ligand binds at a position deep within the binding pocket of the receptor<sup>93</sup>. A refolding of the fluorophore permitting the phenethylamine from entering the binding pocket can therefore be considered a probable cause for the missing 5-HT<sub>2A</sub> receptor binding of ( $\pm$ )-SAH268-Alexa647.

The selectivity of ( $\pm$ )-SAH268-Atto532 binding was demonstrated using two different approaches. In a first experiment, SH-SY5Y cells were incubated with ( $\pm$ )-SAH268-Atto532 and the binding was recorded using FCS. After that, selective ligands for different 5-HT receptors (1A, 2A, 2C and 7) were added and binding was measured again. Only ( $\pm$ )-TCB-2 was able to significantly reduce the receptor binding after incubation, demonstrating that the detected binding using SH-SY5Y cells is attributed to 5-HT<sub>2A</sub> receptors. Unfortunately, this does not rule out the possibility of 5-HT<sub>1A</sub>, 5-HT<sub>2C</sub> or 5-HT<sub>7</sub> receptors not being endogenously expressed in SH-SY5Y cells. Since it is proven in different experiments in recent literature for SH-SY5Y cells to endogenously express 5-HT<sub>1A</sub> receptors but no proof exists for 5-HT<sub>2C</sub> and 5-HT<sub>7</sub> receptors, further experiments regarding 5-HT<sub>2C</sub> and 5-HT<sub>7</sub> receptors were conducted<sup>75,76</sup>. Therefore, HEK293 cells were stably transfected with the human 5-HT<sub>2A</sub>, 5-HT<sub>2C</sub>, and 5-HT<sub>7</sub> receptors and investigated for binding of ( $\pm$ )-SAH268-Atto532 by FCS. Only cells transfected with the 5-HT<sub>2A</sub> receptor displayed binding of ( $\pm$ )-SAH268-Atto532 comparable to SH-SY5Y cells. This binding was also displaceable by a 1,000-fold excess of ( $\pm$ )-TCB-2. For cells stably transfected with the 5-HT<sub>2C</sub> or 5-HT<sub>7</sub> receptor, nearly no binding of ( $\pm$ )-SAH268-Atto532 was detected. The detected levels were very similar to the levels of non-specific binding measured with SH-SY5Y cells and HEK293 cells stably expressing 5-HT<sub>2A</sub> receptors. The functionality and availability of 5-HT<sub>2C</sub> and 5-HT<sub>7</sub> receptors were demonstrated in second messenger accumulation experiments ruling out the possibility of non-functional receptors or problems during transfection and selection of the cells. Second messenger

## Discussion

generation was negated by selective antagonists for the respective cell line (please refer to Figure S 29 and following descriptions).

The class of serotonin receptors with 13 members and high conservation in amino acid sequence turns the development of a selective ligand for a distinct receptor into a demanding endeavor. When focusing on the 5-HT<sub>2A</sub> receptor, proving the selective binding of a ligand compared to the 5-HT<sub>2C</sub> receptor is the most challenging part due to their high homology levels in regions associated with ligand binding<sup>35</sup>. Radioligand and computational studies using non-labeled ligands for 5-HT<sub>2A</sub> and 5-HT<sub>2C</sub> receptors underline this issue. The commonly used agonist 2,5-Dimethoxy-4-iodoamphetamine (DOI) has only a 10-fold selectivity for 5-HT<sub>2A</sub> receptors over 5-HT<sub>2C</sub> receptors<sup>94,95</sup>. Di Giovanni et al. even questioned the selectivity of (±)-TCB-2 for 5-HT<sub>2A</sub> receptors in a recent work. This presumption was founded on a lack of pharmacological data for other receptor subtypes and inconsistencies in behavioral studies<sup>96</sup>. To be precise, the 5-HT<sub>2A</sub> receptor antagonist MDL 11,939 was not able to reverse (±)-TCB-2 induced reduction in the feeding behavior in mice. This characteristic is commonly associated with 5-HT<sub>2A</sub> receptor activation<sup>97</sup>. Furthermore, (±)-TCB-2 induced flat body posture, hindlimb abduction, piloerection and decreased number of rearings in mice, previously only seen for the 5-HT<sub>1A</sub> receptor agonist 8-OH-DPAT<sup>98</sup>. All of these findings regarding (±)-TCB-2 need to be considered carefully. Nevertheless, transferring experimental results between animal models and cell models and even human studies proves to be difficult in many cases. For example, the selectivity of (±)-TCB-2 for 5-HT<sub>2A</sub> receptors could be masked in animal models due to the many interactions that are known for 5-HT<sub>2A</sub> receptors. They are known to form functional heterodimers with a variety of receptors, such as the 5-HT<sub>1A</sub>, 5-HT<sub>2C</sub> and dopamine D2 receptor, possibly explaining the observed 5-HT<sub>1A</sub> receptor effects in mouse models<sup>99-101</sup>. Accordingly, experimental results from cellular experiments also cannot be easily transferred into animal models or even human studies. Overall, in contrast to the in-vivo findings for (±)-TCB-2, (±)-SAH268-Atto532 is proven to be selective for 5-HT<sub>2A</sub> receptors compared to 5-HT<sub>1A</sub>, 5-HT<sub>2C</sub> and 5-HT<sub>7</sub> receptors in in-vitro cell-based binding studies demonstrated by two different experiments outlined above. However, the findings for (±)-SAH268-Atto532 do not rule out the possibility of (±)-TCB-2 being a non-selective agonist for 5-HT<sub>2A</sub> receptors.

Altogether, predicting the functionality of fluorescent ligands based on their structure proves to be difficult<sup>80,102</sup>. It depends on the characteristics of the starting molecule, the utilized fluorescent dye, and even the cellular system employed. Nonetheless, after exploring several different routes, a promising fluorescent 5-HT<sub>2A</sub> receptor-ligand, (±)-SAH268-Atto532, was created.

Binding affinity represented by the dissociation constant  $K_D$  of (±)-SAH268-Atto532 to the human 5-HT<sub>2A</sub> receptor and the total receptor concentration  $B_{max}$  for 5-HT<sub>2A</sub> receptors was

## Discussion

determined in saturation experiments using different concentrations of ( $\pm$ )-SAH268-Atto532 on SH-SY5Y cells. A total receptor concentration  $B_{\max} = 23.95 \pm 5.91$  nM was determined. Since  $B_{\max}$  values are typically expressed as fmol/mg protein in tissue samples, a comparison to  $B_{\max}$  expressed as nM in a defined observation volume is very complicated. By using a biomathematical modeling approach, a  $B_{\max}$  value of 21.50 nM for the 5-HT<sub>6</sub> receptor in the human striatum and 3.70 nM for the 5-HT<sub>2C</sub> receptor in the rabbit frontal cortex were calculated<sup>103</sup>. The determined  $B_{\max}$  value for 5-HT<sub>2A</sub> receptors on SH-SY5Y cells is comparable to  $B_{\max}$  values for other serotonin receptors in tissue samples. The identified  $K_D$  of  $81.03 \pm 24.99$  nM is approx. 100 times weaker in comparison to ( $\pm$ )-TCB-2 with  $K_D = 0.75 \pm 0.09$  nM<sup>79</sup>. As already mentioned, the eudysmic ratio of ( $\pm$ )-TCB-2 is approx. 100 to 1 when comparing the binding affinity to the human 5-HT<sub>2A</sub> receptor for the eutomer (R)-TCB-2 with the distomer (S)-TCB-2<sup>79</sup>. A similar eudysmic ratio is expected for ( $\pm$ )-SAH268-Atto532. For obtaining a fluorescent 5-HT<sub>2A</sub> receptor ligand with the highest binding affinity, a racemic separation followed by an identification of the eutomer would be necessary. Nevertheless, the determined  $K_D$  of ( $\pm$ )-SAH268-Atto532 is highly sufficient to employ it in receptor binding studies using FCS and SPT. Therefore, a racemic separation was not deemed necessary. Even though the linker keeps the dye moiety at a distance, the drastic changes in structure by introducing an aminohexyl linker and a huge fluorophore afterwards result in significantly reduced binding affinity. When compared to the endogenous ligand serotonin with a  $K_D = 16.22 \pm 0.06$  nM the difference is only 5-fold<sup>94</sup>. Moreover, the determined  $K_D$  value is similar to other fluorescent GPCR ligands used in molecular drug research. For example, fluorescent ligands for the kappa opioid receptor with binding affinities ranging from 5 to 20 nM were identified<sup>104</sup>. Additionally, CA200645 a fluorescent xanthine amine congener analogue and antagonist for adenosin A3 receptors displays a binding affinity of  $K_D = 6.17 \pm 0.09$  nM and was recently employed as a tool to screen a library of competing adenosine A1 and A3 receptors<sup>105</sup>. With a nanomolar binding affinity and the photophysical properties of Atto532, ( $\pm$ )-SAH268-Atto532 is a useful tool to investigate receptor-ligand interaction on the molecular level using FCS, SPT, fluorescence recovery after photobleaching (FRAP), Förster resonance energy transfer (FRET) or receptor internalization studies<sup>102</sup>.

Further characterization of 5-HT<sub>2A</sub> receptors using ( $\pm$ )-SAH268-Atto532 was achieved by undertaking SPT experiments on SH-SY5Y cells. SPT studies additionally allow the detection of nearly immobile receptor-ligand complexes or ones with pronounced hindered mobility. Additionally, the diffusion coefficients belonging to those diffusive states, the proportional occupation and transition probability between those states as well as confinement of receptor-ligand complexes can be elucidated using SPT. In contrast to SPT where the whole surface of a cell observed, FCS records fluorescence fluctuation in a distinct focal volume of approx.  $0.125 \mu\text{m}^2$ . Immobile receptor-ligand complexes or receptor-ligand complexes with hindered

## Discussion

lateral diffusion do not leave or enter the focus during the time of observation and are not registered<sup>106</sup>. By comparing the slowest diffusion time constant and the corresponding diffusion coefficient obtained by FCS  $D_{3\text{FCS}} = 0.18 \pm 0.07 \mu\text{m}^2/\text{s}$  with the fastest diffusing fraction in SPT experiments  $D_{3\text{SPT}} = 0.2031 \pm 0.0017 \mu\text{m}^2/\text{s}$  for ( $\pm$ )-SAH268-Atto532 receptor-ligand complexes, it is evident that they are very similar and probably represent the same population of receptor-ligand complexes. Additionally, two fractions of receptor-ligand complexes were detected by SPT, one with hindered lateral mobility  $D_{2\text{SPT}} = 0.0718 \pm 0.0004 \mu\text{m}^2/\text{s}$  and one nearly immobile fraction  $D_{1\text{SPT}} = 0.0130 \pm 0.0002$ . Analyzing the recorded trajectories using the variational Bayes single-particle tracking (vbSPT) together with the Track-Mate plugin featured in the Fiji software, revealed different fractions for the distinct diffusive states S1 nearly immobile, S2 hindered diffusing and S3 fast diffusing. State S2 is the preferred state of 5-HT<sub>2A</sub> receptor-ligand complexes in SPT experiments. The probability of one receptor-ligand complex to change its diffusion behavior in a single track is called intratrack transition probability. The probability to change from fast diffusing state S3 to hindered diffusing state S2 in one track,  $p_{32}$  is most prominent. GPCR alone, without ligand occupation, display similar characteristics, as seen for SNAP-tagged  $\alpha$ 2- and  $\beta$ 2-adrenergic receptors in CHO cells as well as  $\beta$ 2-adrenergic receptors in HEK293 cells<sup>107,108</sup>. Combining the results obtained by FCS and SPT, ( $\pm$ )-SAH268-Atto532 allows the observation of four distinct receptor-ligand complexes in total, each of which could be representing different functionalities of 5-HT<sub>2A</sub> receptors. The hypothesis that receptor activity is correlated with their lateral mobility is supported by FCS and SPT data regarding second messenger generation of  $\beta$ 2-adrenergic receptors in C6 cells and the activity of GABA<sub>A</sub> receptors in hippocampal neurons after changes in their mobility were observed<sup>109–111</sup>. Additionally, a comparison of diffusion coefficients acquired by single molecule detection for a variety of receptors, e.g. 5-HT<sub>2A</sub>,  $\beta$ 2-adrenergic or metabotropic glutamate receptor 3 with and without ligand occupation is provided in recent literature<sup>112</sup>. Thereby, ( $\pm$ )-SAH268-Atto532 is a valuable tool to investigate mobility and activity of 5-HT<sub>2A</sub> receptors.

Lastly, the functional activity of ( $\pm$ )-SAH268-Atto532 was characterized. 5-HT<sub>2A</sub> receptors are G<sub>q</sub> coupled receptors and lead to an activation of beta-type phospholipase C (PLC). PLC facilitates the formation of inositol 1,4,5-trisphosphate (IP<sub>3</sub>) and diacylglycerol (DAG) by hydrolyzing phosphatidylinositol 4,5-bisphosphate (PIP<sub>2</sub>). IP<sub>3</sub> in turn binds to IP<sub>3</sub> receptors at the endoplasmatic reticulum. IP<sub>3</sub> receptors are specialized calcium channels and release stored Ca<sup>2+</sup> into the cytoplasm after activation<sup>77,113</sup>. In such a signaling cascade, there are many steps during which the activity of a ligand can be registered. Measuring intracellular Ca<sup>2+</sup> levels after stimulation of G<sub>q</sub> coupled GPCR with calcium-dependent fluorescent dyes (e.g. Fura-2 or Fluo4) is a very common approach. Intracellular Ca<sup>2+</sup> determination with Fura-2 uses a ratiometric measurement method. More precisely, the ratio of the emitted fluorescent light

## Discussion

measured at  $\lambda_{em} = 510$  after being excited at  $\lambda_{ex1} = 340$  nm and  $\lambda_{ex2} = 380$  nm is directly proportional to the  $Ca^{2+}$  concentration<sup>114</sup>. This detection method has many advantages, e.g. rapid detection speed or being unaffected by varying dye concentrations. Nevertheless, it is not suitable to be used in conjunction with Atto532 ( $\lambda_{ex} = 532$  nm /  $\lambda_{em} = 552$  nm) because the emission spectrum of Fura-2 overlaps with the excitation spectrum of Atto532. The fluorescence excitation and emission spectra of Atto532 and Fluo4 ( $\lambda_{ex} = 494$  nm /  $\lambda_{em} = 516$  nm) as well as the calcium-dependent proteinaceous reporter GCaMP6f, in which GFP ( $\lambda_{ex} = 489$  nm /  $\lambda_{em} = 509$  nm) produces fluorescent light, are overlapping likewise<sup>115</sup>. Furthermore, for Fura-2 and Fluo4 an additional incubation step has to be carried out where the dye is loaded into the cells of interest. B-GECO1 is a calcium-dependent proteinaceous reporter stably transfected into the host cell line, which emits blue fluorescence of  $\lambda_{em} = 446$  nm after being subjected to increased  $Ca^{2+}$  levels and excited at  $\lambda_{ex} = 378$  nm<sup>61</sup>. The fluorescence emission of B-GECO1 does not interfere with the excitation spectrum of Atto532 and since it is stably expressed in the cells of interest, there is no additional incubation step necessary. B-GECO1 was recently used to elucidate the calcium signaling of the intracellular parasitic organism *Toxoplasma gondii*<sup>116</sup>. With the closely related red fluorescent analogue R-GECO, carbachol-dependent signaling in HEK293 cells transfected with  $G_q$  coupled muscarinic acetylcholine receptors (mAChR1) was investigated<sup>117</sup>. After careful consideration, HEK293 cells were stably transfected with B-GECO1 and the human 5-HT<sub>2A</sub> receptor to investigate the agonistic activity of ( $\pm$ )-SAH268-Atto532. Another HEK293 cell line only stably transfected with B-GECO1 was created as a 5-HT<sub>2A</sub> receptor independent control for ( $\pm$ )-TCB-2, and ( $\pm$ )-SAH268-Atto532. Admission of ( $\pm$ )-TCB-2, as well as ( $\pm$ )-SAH268-Atto532, led to a similar and time-dependent increase in cytosolic  $Ca^{2+}$  levels only in the cell line expressing the human 5-HT<sub>2A</sub> receptor and B-GECO1. The cell line only expressing B-GECO1 showed no response. The calcium ionophore ionomycin was used as a non-specific positive control. It induced elevated cytosolic  $Ca^{2+}$  in both cell lines, demonstrating general functionality of B-GECO1 in both cell lines. Those results clearly indicate the agonistic profile of ( $\pm$ )-SAH268-Atto532 at 5-HT<sub>2A</sub> receptors.

After the synthesis and characterization of ( $\pm$ )-SAH268-Atto532 as a selective 5-HT<sub>2A</sub> receptor agonist was completed, the synthesized ligand was used to determine whether the St. John's wort extract STW3-VI<sup>®</sup> influences 5-HT<sub>2A</sub> receptors. St. John's wort extracts are the only phytopharmaceutical preparation included in the German S3-Leitlinie "Unipolare Depression" with a recommendation to treat patients with mild to moderate depressive disorders<sup>6</sup>. In terms of clinical efficacy for STW3-VI<sup>®</sup>, non-inferiority compared to sertraline and citalopram as well as the superiority compared to placebo was proven in double-blind, randomized, placebo-controlled clinical trials. The safety and tolerability for STW3-VI<sup>®</sup> treatment was either comparable to placebo or sertraline treatment or superior to citalopram treatment<sup>118-120</sup>. Data

## Discussion

from additional clinical studies regarding other St. John's wort extracts is summarized in a recent Cochrane review<sup>10</sup>. St. John's wort extracts are characterized as quantified herbal substances, since only a part of their mode of action can be attributed to distinct substances. The classes of natural substances contributing to their activity are the naphodianthrones, phloroglucin derivatives and flavonoids<sup>121</sup>. Accordingly, the European Pharmacopoeia monograph 1874 "St. John's wort dry extract, quantified" specifies the content of the active markers total hypericins, hyperforin and flavonoids, expressed as rutin<sup>122</sup>. In the case of herbal medicinal products, the active pharmaceutical ingredient (API) is the whole extract itself and not distinct substances being part of it. Based on available clinical data for St. John's wort extracts, a monograph of the Committee on Herbal Medicinal Products (HMPC) on *Hypericum Perforatum* L., Herba was created. STW3-VI<sup>®</sup> with a drug-extract-ratio (DER) of 3 – 6 : 1 and 80% ethanol (v/v) as the extracting agent is included within this monograph<sup>121</sup>. STW3-VI<sup>®</sup> exhibits a wide variety of effects, all contributing to its antidepressant action, such as anti-inflammatory, anti-oxidative and cytoprotective effects, regulation of neurotransmitter systems and influences on the regulation of gene expression<sup>123–126</sup>. The influence on the gene expression of FKBP5 was demonstrated for STW3-VI<sup>®</sup> and could at least be partially attributed to its active ingredients the phloroglucin derivative hyperforin and the flavonoid miquelianin<sup>124</sup>. Furthermore cytoprotective, anti-inflammatory and neurotrophic properties of STW3-VI<sup>®</sup> were observed using mouse hippocampal neurons<sup>125</sup>. Taken together with the already described inhibition of serotonin reuptake observed for hyperforin and the anti-oxidative properties known for flavonoids and phenolic acids contained in St. John's wort extracts in general, a multi-target effect in the treatment of depressive disorders is evident for STW3-VI<sup>®</sup><sup>27,127</sup>.

A HPLC-fingerprint analysis to characterize STW3-VI<sup>®</sup> was carried out according to a well-established analytical method for St. John's wort extracts<sup>128</sup>. Substances belonging to the classes of naphodianthrones, phloroglucin derivatives and flavonoids were identified by comparing retention times and absorption spectra of reference substances. In total, nine substances were detected, of which six were flavonoids, one was a phloroglucin derivative and two were naphodianthrones. Out of those nine substances, the phloroglucin derivative hyperforin and flavonoid hyperoside were quantified. Hyperoside was chosen because it is the principal compound for the substance class of flavonoids in STW3-VI<sup>®</sup>. Additionally, anti-oxidative effects for hyperoside in concentrations of 10  $\mu\text{M}$  and higher were recently demonstrated<sup>129</sup>. Hyperforin was selected due to the vast knowledge regarding its pharmacological effects, the ability to cross the blood-brain barrier and data concerning its pharmacokinetics<sup>130,131</sup>. The determined concentrations in a solutions of 1 mg/ml STW3-VI<sup>®</sup> were 36.8  $\mu\text{M}$  for hyperforin and 53.3  $\mu\text{M}$  for hyperoside. Hypericin, representing the substance class of naphodianthrones, was also considered as a test substance. Due to its high fluorescence it can be applied and FCS experiments by itself and would therefore strongly

## Discussion

interfere with the FCS experiments involving ( $\pm$ )-SAH268-Atto532<sup>132</sup>. In general, the interference could have been reduced by using different detection wavelengths and filters, but because of the restrictions from the fluorescent ligand and the setup of the FCS device using hypericin as a test substance was not feasible.

The influence of STW3-VI<sup>®</sup>, hyperforin and hyperoside on the 5-HT<sub>2A</sub> receptor was determined by employing ( $\pm$ )-SAH268-Atto532 in FCS studies using SH-SY5Y cells. FCS studies allow the measurement of fluorescence fluctuation within a tiny observation volume. By using the autocorrelation function, diffusion time constants and diffusion coefficients as well as binding characteristics of different receptor-ligand complexes can be determined in living cells in real-time<sup>110,133</sup>. Choosing the right concentration for natural substances and extracts is challenging. In general, concentrations in the low micromolar range for pure compounds and the corresponding concentration for the employed extract proved sufficient in preclinical practice<sup>134</sup>. Therefore, the six days preincubation of SH-SY5Y cells was carried out using 1.0, 0.1 and 0.01  $\mu$ M of hyperforin and hyperoside. Since concentrations of 36.8  $\mu$ M for hyperforin and 53.3  $\mu$ M for hyperoside, were determined for a solution of 1 mg/ml STW3-VI<sup>®</sup>, it was employed in the concentrations of 0.02, 0.002 and 0.0002 mg/ml. The preincubation period of six days takes the commonly observed delayed onset of antidepressant action in clinical practice into account. Only slow diffusing receptor ligand complexes with their diffusion time constant  $T_{diff3}$  and diffusion coefficient  $D_{diff3}$  were influenced after preincubation with hyperforin, hyperoside and STW3-VI<sup>®</sup>. In general their mobility was reduced, which can be seen by the increase of the diffusion time constant  $T_{diff3}$  and accordingly a reduced diffusion coefficient  $D_{diff3}$ . The effect was most pronounced for STW3-VI<sup>®</sup>, which increased  $T_{diff3}$  in its highest concentration of 0.02 mg/ml from approx. 50 ms to more than 200 ms. Furthermore, 0.002 and 0.0002 mg/ml STW3-VI<sup>®</sup> as well as 1.0  $\mu$ M hyperforin and 0.1  $\mu$ M hyperoside increased  $T_{diff3}$  beyond 100 ms. Fast diffusing receptor-ligand complexes with  $T_{diff2}$  and  $D_{diff2}$  were not affected by the preincubations. Since the standard deviation of the recorded diffusion time constants is often higher than the actual value, there was no statistical evaluation undertaken. For total 5-HT<sub>2A</sub> receptor binding, 0.02 mg/ml STW3-VI<sup>®</sup> significantly increased the normalized total 5-HT<sub>2A</sub> receptor binding of ( $\pm$ )-SAH268-Atto532 to  $1.27 \pm 0.08$ . Hyperforin and hyperoside both displayed a dose-dependent but statistically non-significant increase of normalized receptor binding to a maximum of  $1.09 \pm 0.04$  and  $1.06 \pm 0.05$  in an employed concentration of 1.0  $\mu$ M, respectively. The substances contained in STW3-VI<sup>®</sup> which are responsible for the increase in total 5-HT<sub>2A</sub> receptor binding are not known, since hyperforin and hyperoside showed no effect on the total receptor binding. When comparing the fractions  $f_{T_{diff2}}$  and  $f_{T_{diff3}}$  of 5-HT<sub>2A</sub> receptor-ligand complexes belonging to the diffusion time constants  $T_{diff2}$  and  $T_{diff3}$ , it is observed that all test substances in general increased the amounts of fast diffusing receptor-ligand complexes in  $f_{T_{diff2}}$  while decreasing the slow diffusing ones in  $f_{T_{diff3}}$ . STW3-VI<sup>®</sup> significantly and dose-

## Discussion

dependently increased the  $f_{T_{diff2}}/f_{T_{diff3}}$  ratio from 0.49 for control cells and 0.55 for 0.0002 mg/ml to 0.81 for 0.002 mg/ml and even further to 2.34 for 0.02 mg/ml. A similar dose-dependent effect was observed for hyperforin and hyperoside. Hyperforin displayed  $f_{T_{diff2}}/f_{T_{diff3}}$  ratios of 1.27 for 1.0  $\mu$ M, 0.83 for 0.1  $\mu$ M and 0.45 for 0.01  $\mu$ M respectively. The determined shift in  $f_{T_{diff2}}/f_{T_{diff3}}$  ratios after preincubation with hyperoside was determined with 0.98 for 1.0  $\mu$ M, 1.02 for 0.1  $\mu$ M and 0.31 for 0.01  $\mu$ M. The effect was similar but less pronounced when compared to hyperforin. Remarkably, the maximum effect for hyperoside was already observed at a concentration of 0.1  $\mu$ M, while 0.01  $\mu$ M was still not significantly different from control cells. As already seen for the normalized total 5-HT<sub>2A</sub> receptor binding of ( $\pm$ )-SAH268-Atto532, the shift in distribution of that binding into  $f_{T_{diff2}}$  and  $f_{T_{diff3}}$  after incubation with 0.02 mg/ml STW3-VI® cannot be explained by either hyperforin or hyperoside alone. In summary, STW3-VI®, hyperforin and hyperoside, influenced the diffusion and binding behavior of 5-HT<sub>2A</sub> receptor-ligand complexes. For GPCR, those two characteristics are directly linked to their activity<sup>135</sup>. In general GPCR interact with their respective G proteins in certain areas of the cellular membranes. For  $\beta$ 2-adrenergic receptor, which are often used as an exemplary GPCR, the interaction with the G proteins preferably takes place in areas of the cellular membrane where receptor and G protein are located together, e.g. lipid rafts, caveolae or clathrin-coated pits. Receptor-G protein interactions with a duration of 1-2 s were observed for  $\beta$ 2-adrenergic receptors, preferably in membrane hot spots at least partially defined by clathrin-coated pits and the cytoskeleton<sup>107</sup>. Activation of a GPCR by an agonist and subsequent association to the respective G protein result in a restriction of the receptor's mobility<sup>107,135</sup>. It could be concluded that by increasing the receptors mobility an association to the respective G protein becomes less likely, since its dwell time in membrane hot spots is reduced. Thereby, the overall signaling activity of the receptor is reduced. With this theory in mind, the highly increased mobility of 5-HT<sub>2A</sub> receptors after treatment with STW3-VI® is expected to result in reduced signaling activity of the receptor. The alteration of receptor mobility after treatment with hyperforin is less pronounced, but its influence on membrane fluidity could at least be partially responsible for the observed effects<sup>136</sup>. Alpha-hederin, one of the main active ingredients of *Hedera helix*, altered the diffusion behavior of  $\beta$ 2-adrenergic receptors in A549 cells in a similar manner. The increased mobility of  $\beta$ 2-adrenergic receptors resulted in a decreased receptor internalization after agonistic stimulation, possibly caused by inhibition of regulatory processes after stimulation<sup>82</sup>. In contrast to the proposed theory of reduced receptor signaling after increasing its mobility, a preincubation of A549 cells with alpha-hederin displayed increased  $\beta$ 2-adrenergic receptor signaling after stimulation<sup>137</sup>. Since different compounds, cells and receptors were investigated, it is not evident if the results are transferable to 5-HT<sub>2A</sub> receptors. Apart from binding and diffusing behavior of GPCR, their density in the cellular membrane and their trafficking are important for subsequent signaling activity. 5-HT<sub>2A</sub> receptors are known to

## Discussion

undergo internalization after treatment with agonists and antagonists such as doxepine<sup>77,138</sup>. Internalization is even observed with dopamine, which is likely due to its closely related chemical structure when compared to serotonin<sup>139</sup>. Influencing receptor desensitization and downregulation of 5-HT<sub>2A</sub> receptors seems to be of importance in the treatment of depressive disorders<sup>37</sup>. The importance of 5-HT<sub>2A</sub> receptor internalization with antagonist for the treatment of depressive disorders can only be estimated, since internalization was only observed for the anxiolytic drug doxepine and not for clinically used antidepressants. But since desensitization and downregulation of 5-HT<sub>2A</sub> receptors are considered beneficial in the treatment of depressive disorders, internalization after treatment with antagonists for the 5-HT<sub>2A</sub> receptor could further contribute to the antidepressant effect of 5-HT<sub>2A</sub> antagonist in addition to the antagonistic effect itself. Moreover, the antidepressant effects observed for LSD or psilocybin as strong 5-HT<sub>2A</sub> receptor agonists, could also at least be partially mediated by influencing 5-HT<sub>2A</sub> receptors internalization<sup>140</sup>. After preincubation with STW3-VI<sup>®</sup>, hyperforin and hyperoside, receptor density was measured using the Nano-Glo<sup>®</sup> HiBiT Extracellular Assay System. In this Assay system, a divided NanoLuc<sup>®</sup> luciferase is used to detect the amount of the tagged protein of interest in living cells. Therefore, the small subunit HiBiT, consisting of 11 amino acids, is coupled to the N-terminus of the protein of interest. The much bigger subunit LgBiT, consisting of 160 amino acids, is added before assay start. HiBiT and LgBiT form an active NanoLuc<sup>®</sup> luciferase when binding together with very high affinity. The completed, then functional, NanoLuc<sup>®</sup> luciferase converts the added substrate furimazine to furimamide to generate chemiluminescence. The described system only detects tagged receptors on the surface of the cell due to the LgBiT not being able to enter the cell. This characteristic resulted in the usage of the Nano-Glo<sup>®</sup> HiBiT Extracellular Assay System in a variety of experiments, during which only plasma membrane-associated proteins needed to be investigated (e.g. Receptor proximity analysis in the cellular membrane or entry of virus particles into cells)<sup>141–143</sup>. Due to the high accuracy of the luminescence measurement, it was used to determine the amount of HiBiT-tagged 5-HT<sub>2A</sub> receptors on the surface of stably transfected HEK293 cells. Additionally, the usage of a luminescence-based system allowed us to avoid the interference of the naphthodianthrones contained in STW3-VI<sup>®</sup> completely. The receptor density on the cell surface was measured under non-stimulating conditions and after treatment with the 5-HT<sub>2A</sub> receptor agonist (±)-TCB-2. The difference in receptor densities between non-stimulating conditions and after stimulation accounts for receptors undergoing internalization. Receptor internalization was thereby determined indirectly. Remarkably, STW3-VI<sup>®</sup> dose-dependently decreased the receptor density under non-stimulating conditions to  $0.88 \pm 0.02$  and  $0.93 \pm 0.02$  for 0.02 and 0.002 mg/ml STW3-VI<sup>®</sup>. Since the Nano-Glo<sup>®</sup> HiBiT Extracellular Assay System only detects receptors on the cell surface and not internalized receptors, a STW3-VI<sup>®</sup> forced 5-HT<sub>2A</sub> receptor internalization cannot be excluded. However, STW3-VI<sup>®</sup>

## Discussion

might also inhibit the expression of 5-HT<sub>2A</sub> receptors, especially since a decrease in FKBP5 and NET expression was described for STW3-VI<sup>®</sup> after dexamethasone-induced stress in SH-SY5Y cells<sup>124</sup>. In a concentration of 0.0002 mg/ml, STW3-VI<sup>®</sup> had no effect on normalized receptor density. Similarly, 1.0 μM hyperforin and 1.0 μM hyperoside were not able to significantly influence the normalized 5-HT<sub>2A</sub> receptor density. Therefore, no further experiments with lower concentrations of hyperforin and hyperoside were undertaken. Under (±)-TCB-2 stimulating conditions 0.02 mg/ml STW3-VI<sup>®</sup> significantly decreased 5-HT<sub>2A</sub> receptor internalization to 8.1 ± 1.5% when compared to control cells with 18.8 ± 1.8%. Although the receptor density after pre-incubation with STW3-VI<sup>®</sup> was decreased by 12% under non-stimulating conditions, there should still be enough receptors on the cell surface in an overexpressing system to allow internalization comparable to that observed in untreated control cells after stimulation. The dose-dependent reduction of 5-HT<sub>2A</sub> receptor internalization after stimulation is therefore considered to be clearly evident for STW3-VI<sup>®</sup>, even though the results for 0.002 mg/ml STW3-VI<sup>®</sup> were not significantly different from control cells. Hyperforin and hyperoside had no significant effect on 5-HT<sub>2A</sub> receptor internalization after stimulation. For GFP-tagged β1-adrenergic receptors, receptor internalization was observed after preincubation with 1.0 μM hyperforin and 1.0 μM hyperoside already under non-stimulating conditions. The internalization after stimulation was not clearly affected<sup>123</sup>. Until today, STW3-VI<sup>®</sup> was not investigated in receptor internalization studies. Overall, the observed amount of roughly 20% receptor internalization is rather low when compared to other GPCR (e.g. human bombesin receptor subtype 3 and human orexin type 2 receptor determined by flow cytometry)<sup>144</sup>. The observed differences could be attributed to the different receptors as well as the time span of agonist stimulation. HEK293 cells with HiBiT-tagged 5-HT<sub>2A</sub> receptors were only stimulated with (±)-TCB-2 for 15 min before the assay was started. Additionally, it is possible that not all transfected receptors were functional, or the cellular systems responsible for receptor internalization were not able to internalize the high amounts of overexpressed HiBiT-tagged 5-HT<sub>2A</sub> receptors during the measurement. Nevertheless, a statistical significant effect of STW3-VI<sup>®</sup> on 5-HT<sub>2A</sub> receptor internalization was observed. This highlights the previously mentioned high accuracy of the Nano-Glo<sup>®</sup> HiBiT Extracellular Assay System. The observed effects further contribute to the theory that blocking 5-HT<sub>2A</sub> receptors is one part of the mode of action of St. John's wort extract STW3-VI<sup>®</sup>. A lowered receptor density is expected to reduce the overall signaling activity after stimulating 5-HT<sub>2A</sub> receptors. The reduced internalization could be explained by an increased amount of receptors unable to induce downstream signaling. As already mentioned, the elevated amounts of highly mobile receptors registered in FCS experiments are one possible explanation. In case of 5-HT<sub>2A</sub> receptor density and internalization, hyperforin and hyperoside are not responsible for observed effects after

## Discussion

preincubation with STW3-VI<sup>®</sup>. The single compounds responsible, at least partially, are still not known.

After investigating 5-HT<sub>2A</sub> receptor ligand binding, diffusion, density and internalization, it remains to be seen, how the observed effects influence the signaling activity of 5-HT<sub>2A</sub> receptors. Therefore, the 5-HT<sub>2A</sub> receptor downstream signaling activity was determined. All former investigations only allowed speculations about the effects the preincubations show on 5-HT<sub>2A</sub> receptor activity. Results for receptor binding, mobility, density, and internalization all point into a direction where STW3-VI<sup>®</sup> lowers 5-HT<sub>2A</sub> receptor activity. This needs to be clarified by measuring the second messenger generation after stimulation with (±)-TCB-2. For the determination of the agonistic activity of (±)-SAH268-Atto532, the B-GECO1 system for the determination of intracellular Ca<sup>2+</sup> levels was employed. As already mentioned, the naphthodianthrones in STW3-VI<sup>®</sup> are possibly interfering with fluorescence detection. Therefore, a luminescence-based detection system for intracellular Ca<sup>2+</sup> levels was chosen. Luminescence-based detection systems are highly sensitive and remove the need for fluorescence excitation<sup>145</sup>. In this assay system, the protein apoaequorin binds its substrate coelenterazine and after being subjected to increased Ca<sup>2+</sup> concentrations converts it to coelenteramide. In the course of the conversion to coelenteramide chemiluminescence is generated<sup>146</sup>. Aequorin, which was isolated from the jellyfish *Aequorea Victoria*, is the name for apoaequorin together with the bound substrate coelenterazine. For the regeneration of aequorin in vitro, the bound Ca<sup>2+</sup> ions have to be removed in the presence of molecular oxygen and the coelenteramide needs to be exchanged with fresh coelenterazine. The exact mechanism for the regeneration in *Aequorea Victoria* is still not fully known<sup>62,147</sup>. Aequorin is often used as a GFP-fusion protein to generate a fluorescent read-out after bioluminescence resonance energy transfer (BRET). This mechanism has already been observed in the jellyfish *Aequorea victoria* itself. These advances with a chimeric GFP-aequorin-protein make increased Ca<sup>2+</sup> levels detectable by fluorescent read-out<sup>62,148</sup>. The fluorescent read out allows for more accurate detection of increasing Ca<sup>2+</sup> levels on the single cell level<sup>62</sup>. But for the outlined measurements a luminescence detection is suitable since no single cell detection is necessary and the protein of interest for expression in HEK293 is smaller, making it overall favorable. Additionally, aequorin was used in mammalian cells without being coupled to GFP over the years for the detection of intracellular Ca<sup>2+</sup> levels after administration of ATP, histamine, bradykinin and many others<sup>149,150</sup>. Therefore, the cells were stably transfected with apoaequorin and the human 5-HT<sub>2A</sub> receptor and preincubated with STW3-VI<sup>®</sup>, hyperforin and hyperoside. Baseline luminescence was determined before adding (±)-TCB-2. For the course of the measurement, the luminescence signals, representing the amounts of Ca<sup>2+</sup> in the cytoplasm, were recorded, the AUC was calculated and normalized to control cells. STW3-VI<sup>®</sup> significantly and dose-dependently reduced intracellular Ca<sup>2+</sup> levels after stimulation with

## Discussion

(±)-TCB-2. In comparison to control cells, 0.02 and 0.002 mg/ml STW3-VI<sup>®</sup> significantly decreased intracellular Ca<sup>2+</sup> levels after stimulation to  $0.69 \pm 0.04$  and  $0.59 \pm 0.04$  respectively. Neither the preincubation with 0.0002 mg/ml STW3-VI<sup>®</sup> nor 1.0 μM hyperforin or hyperoside displayed significant effects on intracellular Ca<sup>2+</sup> levels after stimulation with (±)-TCB-2. Notably, the effect observed for 0.02 mg/ml STW3-VI<sup>®</sup> is less pronounced in comparison to 0.002 mg/ml STW3-VI<sup>®</sup>. Since they do not differ significantly from one another, it can only be concluded that the maximum effect is already observed at 0.002 mg/ml STW3-VI<sup>®</sup> and further increasing the concentration is not beneficial. Even though an influence of hyperforin on GPCR-dependent Ca<sup>2+</sup> signaling was already shown for the formyl peptide receptor 1, 5-HT<sub>2A</sub> receptor induced signaling is not affected. Although the inhibitory effect of STW3-VI<sup>®</sup> cannot be compared to synthetic 5-HT<sub>2A</sub> receptor antagonist like ketanserin with inhibitory effects in the nanomolar range, it is still highly effective in a concentration of 0.002 mg/ml, reducing 5-HT<sub>2A</sub> receptor activity by roughly 40%<sup>151</sup>. Instead of being 5-HT<sub>2A</sub> selective, the observed effect could as well be mediated by direct interaction of STW3-VI<sup>®</sup> with aequorin or a general influence on the downstream signaling of G<sub>q</sub> coupled receptors. Therefore, the selectivity of STW3-VI<sup>®</sup> for the 5-HT<sub>2A</sub> receptor signaling was demonstrated by investigating intracellular Ca<sup>2+</sup> levels through different pathways with ionomycin as a calcium ionophore and ATP as a P<sub>2</sub>RY<sub>1</sub> agonist. No significant influence for STW3-VI<sup>®</sup> as well as hyperforin or hyperoside was detected. In conclusion, the decrease of intracellular Ca<sup>2+</sup> levels following agonistic stimulation by (±)-TCB-2 after preincubation with STW3-VI<sup>®</sup>, is considered selective for the 5-HT<sub>2A</sub> receptor.

### 7. Conclusion and Outlook

Starting from ( $\pm$ )-TCB-2 a selective, fluorescent 5-HT<sub>2A</sub> receptor agonist, namely ( $\pm$ )-SAH268-Atto532, was synthesized. ( $\pm$ )-SAH268-Atto532 was characterized for its binding affinity, selectivity for 5-HT<sub>2A</sub> receptors, agonistic profile and suitability for FCS studies in mammalian cells after preincubation with pure compounds and even complex mixtures such as herbal extracts. Overall, ( $\pm$ )-SAH268-Atto532 was well suited for the study of 5-HT<sub>2A</sub> receptors using fluorescence microscopy techniques. Investigating receptor crosstalk or dimerization together with other GPCR and their respective ligands is another possible usage. With this tool, studying the function of 5-HT<sub>2A</sub> receptors on the molecular level under a variety of conditions is achievable, possibly resulting in a better understanding of their involvement in the development and treatment depressive disorders and other diseases. For some of those investigations it might be necessary to employ a 5-HT<sub>2A</sub> receptor agonist with even higher affinity and efficacy. In this case, it is beneficial to conduct a chiral separation of the racemic mixture of ( $\pm$ )-SAH268-Atto532. In addition to ( $\pm$ )-SAH268-Atto532, two other tools were used for investigations. The determination of receptor density and internalization with the Nano-Glo<sup>®</sup> HiBiT Extracellular Assay System could be extended to any other GPCR of interest, e.g.  $\beta$ 1- and  $\beta$ 2-adrenergic receptors or the 5-HT receptors in general. Furthermore, the introduced HEK293 cell line stably expressing HiBiT-tagged 5-HT<sub>2A</sub> receptors is usable for a general investigation of 5-HT<sub>2A</sub> receptors. They are fairly easy to handle concerning their cell culture conditions and the introduced HiBiT tag is very small and does not interact with the activity of the 5-HT<sub>2A</sub> receptor. Another valuable tool for further research is the HEK293 cell line stably expressing aequorin and the human 5-HT<sub>2A</sub> receptor. In general, this cell line is employable for the investigation 5-HT<sub>2A</sub> receptor signaling in various settings, preferably in cases where interactions with fluorescent molecules are expected. In addition, the expression of the 5-HT<sub>2A</sub> receptor can be regulated by tetracyclines. This allows the investigation of 5-HT<sub>2A</sub> receptor at different expression levels in future experiments. Since the receptor density of 5-HT<sub>2A</sub> receptors is of great interest in the development and treatment of depressive disorders, the characteristics of this cell line could be highly desired from this point onward. All results concerning STW3-VI<sup>®</sup>, point towards an inhibition of 5-HT<sub>2A</sub> receptor activity being part of its antidepressant mode of action. For receptor binding and mobility this could at least be partially attributed to hyperforin and hyperoside. Unfortunately the degree of said effects and the decrease in receptor density, internalization and signaling activity cannot be attributed to hyperforin and hyperoside. The aim of this work was to investigate how St. John's wort extract STW3-VI<sup>®</sup> and/or its active ingredients hyperforin and hyperoside mediate parts of their antidepressant action via the 5-HT<sub>2A</sub> receptor. Even though this goal was reached, future investigation into which distinct substances out of STW3-VI<sup>®</sup> mediate the observed effects are necessary.

## 8. References

1. Otte, C. *et al.* Major depressive disorder. *Nat. Rev. Dis. Prim.* **2**, 1–21 (2016).
2. James, S. L. *et al.* Global, regional, and national incidence, prevalence, and years lived with disability for 354 Diseases and Injuries for 195 countries and territories, 1990-2017: A systematic analysis for the Global Burden of Disease Study 2017. *Lancet* **392**, 1789–1858 (2018).
3. Seedat, S. *et al.* Disorders in the WHO World Mental Health Surveys. *Arch. Gen. Psychiatry* **66**, 785–795 (2009).
4. Wang, P. S. *et al.* Use of mental health services for anxiety, mood, and substance disorders in 17 countries in the WHO world mental health surveys. *Lancet* **370**, 841–850 (2007).
5. Kessler, R. C. The Cost of Depression NIH Public Access. *Psychiatr. Clin. North Am.* **35**, 1–14 (2012).
6. DGPPN, BÄK, KBV, AWMF, AkdÄ, BpTK, BApK, DAGSHG, DEGAM, DGPM, DGPs, D. S3-Leitlinie / Nationale VersorgungsLeitlinie Unipolare Depression Langfassung. *Ärztliches Zent. für Qual. der Medizin* (2015) doi:10.6101/AZQ/000266.
7. Cipriani, A. *et al.* Comparative efficacy and acceptability of 12 new-generation antidepressants: a multiple-treatments meta-analysis. *Lancet* **373**, 746–758 (2009).
8. Linde, K. St. John's Wort - An overview. *Forsch. Komplementarmed.* **16**, 146–155 (2009).
9. Lakhan, S. E. & Vieira, K. F. Nutritional and herbal supplements for anxiety and anxiety-related disorders: systematic review. *Nutr. J.* **9**, 42 (2010).
10. Linde, K., Berner, M. M. & Kriston, L. St John's wort for major depression. *Cochrane Database Syst. Rev.* **5**, 144 (2008).
11. Zahner, C. *et al.* No Clinically Relevant Interactions of St. John's Wort Extract Ze 117 Low in Hyperforin With Cytochrome P450 Enzymes and P-glycoprotein. *Clin. Pharmacol. Ther.* **106**, 432–440 (2019).
12. Malhi, G. S. & Mann, J. J. Depression. *Lancet* **392**, 2299–2312 (2018).
13. Reiche, S. *et al.* Serotonergic hallucinogens in the treatment of anxiety and depression in patients suffering from a life-threatening disease: A systematic review. *Prog. Neuro-Psychopharmacology Biol. Psychiatry* **81**, 1–10 (2018).
14. Willner, P., Scheel-Krüger, J. & Belzung, C. The neurobiology of depression and antidepressant action. *Neurosci. Biobehav. Rev.* **37**, 2331–2371 (2013).
15. Stetler, C. & Miller, G. E. Depression and hypothalamic-pituitary-adrenal activation: A quantitative summary of four decades of research. *Psychosom. Med.* **73**, 114–126 (2011).

## References

16. Gjerstad, J. K., Lightman, S. L. & Spiga, F. Role of glucocorticoid negative feedback in the regulation of HPA axis pulsatility. *Stress* **21**, 403–416 (2018).
17. Leonard, B. E. Inflammation and depression: A causal or coincidental link to the pathophysiology? *Acta Neuropsychiatr.* **30**, 1–16 (2018).
18. Mittal, M., Siddiqui, M. R., Tran, K., Reddy, S. P. & Malik, A. B. Reactive oxygen species in inflammation and tissue injury. *Antioxidants Redox Signal.* **20**, 1126–1167 (2014).
19. Napoli, E. *et al.* Phytochemical profiles, phototoxic and antioxidant properties of eleven Hypericum species – A comparative study. *Phytochemistry* **152**, 162–173 (2018).
20. Egeland, M., Zunszain, P. A. & Pariante, C. M. Molecular mechanisms in the regulation of adult neurogenesis during stress. *Nat. Rev. Neurosci.* **16**, 189–200 (2015).
21. Butz, M., Wörgötter, F. & van Ooyen, A. Activity-dependent structural plasticity. *Brain Res. Rev.* **60**, 287–305 (2009).
22. Liu, W. *et al.* The Role of Neural Plasticity in Depression: From Hippocampus to Prefrontal Cortex. *Neural Plast.* **2017**, (2017).
23. Schröder, C. *et al.* Outpatient antidepressant drug use in children and adolescents in Germany between 2004 and 2011. *Pharmacoepidemiol. Drug Saf.* **26**, 170–179 (2017).
24. Dell'Osso, L., Carmassi, C., Mucci, F. & Marazziti, D. Depression, Serotonin and Tryptophan. *Curr. Pharm. Des.* **22**, 949–954 (2016).
25. Lochmann, D. & Richardson, T. Selective Serotonin Reuptake Inhibitors. in *Handbook of Experimental Pharmacology* 135–144 (2018). doi:10.1007/164\_2018\_172.
26. Shelton, R. C. Serotonin and Norepinephrine Reuptake Inhibitors. in *Handbook of Experimental Pharmacology* 145–180 (2018). doi:10.1007/164\_2018\_164.
27. Singer, A., Wonnemann, M. & Müller, W. E. Hyperforin, a major antidepressant constituent of St. John's Wort, inhibits serotonin uptake by elevating free intracellular Na<sup>+</sup>. *J. Pharmacol. Exp. Ther.* **290**, 1363–8 (1999).
28. Russo, E. *et al.* Hypericum perforatum: Pharmacokinetic, mechanism of action, tolerability, and clinical drug-drug interactions. *Phyther. Res.* **28**, 643–655 (2014).
29. Hamon, M. & Bourgoin, S. Pharmacological profile of antidepressants: a likely basis for their efficacy and side effects? *Eur. Neuropsychopharmacol.* **16**, (2006).
30. Owens, M. J., Knight, D. L. & Nemeroff, C. B. Second-generation SSRIs: Human monoamine transporter binding profile of escitalopram and R-fluoxetine. *Biol. Psychiatry* **50**, 345–350 (2001).
31. Sanchez, C., Reines, E. H. & Montgomery, S. A. A comparative review of escitalopram, paroxetine, and sertraline: Are they all alike? *Int. Clin. Psychopharmacol.* **29**, 185–196 (2014).

## References

32. Gillman, P. K. Tricyclic antidepressant pharmacology and therapeutic drug interactions updated. *Br. J. Pharmacol.* **151**, 737–748 (2007).
33. Finberg, J. P. M. & Rabey, J. M. Inhibitors of MAO-A and MAO-B in psychiatry and neurology. *Front. Pharmacol.* **7**, 1–15 (2016).
34. Thomas, S. J., Shin, M., McInnis, M. G. & Bostwick, J. R. Combination therapy with monoamine oxidase inhibitors and other antidepressants or stimulants: Strategies for the management of treatment-resistant depression. *Pharmacotherapy* **35**, 433–449 (2015).
35. Kroeze, W. K., Kristiansen, K. & Roth, B. L. Molecular biology of serotonin receptors - structure and function at the molecular level. *Curr. Top. Med. Chem.* **2**, 507–528 (2002).
36. Jacobson, K. A. New paradigms in GPCR drug discovery. *Biochem Pharmacol.* **98**, 541–555 (2016).
37. Fakhoury, M. Revisiting the Serotonin Hypothesis: Implications for Major Depressive Disorders. *Mol. Neurobiol.* **53**, 2778–2786 (2016).
38. Meadows, S. M. *et al.* Characterizing the differential roles of striatal 5-HT<sub>1A</sub> auto- and hetero-receptors in the reduction of L-DOPA-induced dyskinesia. *Exp. Neurol.* **292**, 168–178 (2017).
39. McDevitt, R. A. & Neumaier, J. F. Regulation of dorsal raphe nucleus function by serotonin autoreceptors: a behavioral perspective. *J. Chem. Neuroanat.* **41**, 234–46 (2011).
40. Jakobs, D. P. Einfluss der Johanniskrautinhaltstoffe Hyperforin, Hyperosid und Hypericin auf die laterale Mobilität und die Signaltransduktion von 5-HT<sub>1A</sub>-Rezeptoren. *ULB Bonn* (2014).
41. Teufel-Mayer, R. Effects of long-term administration of hypericum extracts on the affinity and density of the central serotonergic 5-HT<sub>1A</sub> and 5-HT<sub>2A</sub> receptors. *Pharmacopsychiatry* **30**, 113–116 (1997).
42. Aznar, S. & Hervig, M. E. S. The 5-HT<sub>2A</sub> serotonin receptor in executive function: Implications for neuropsychiatric and neurodegenerative diseases. *Neurosci. Biobehav. Rev.* **64**, 63–82 (2016).
43. Pehek, E. A., Nocjar, C., Roth, B. L., Byrd, T. A. & Mabrouk, O. S. Evidence for the preferential involvement of 5-HT<sub>2A</sub> serotonin receptors in stress- and drug-induced dopamine release in the rat medial prefrontal cortex. *Neuropsychopharmacology* **31**, 265–277 (2006).
44. Zhang, Y. *et al.* Desensitization of 5-HT<sub>1A</sub> Receptors by 5-HT<sub>2A</sub> Receptors in Neuroendocrine Neurons in Vivo. *J. Pharmacol. Exp. Ther.* **310**, 59–66 (2004).
45. Gray, J. A. & Roth, B. L. Molecular targets for treating cognitive dysfunction in schizophrenia. *Schizophr. Bull.* **33**, 1100–1119 (2007).
46. Murat, S. *et al.* 5-HT<sub>2A</sub> receptor-dependent phosphorylation of mGlu<sub>2</sub> receptor at Serine 843 promotes mGlu<sub>2</sub> receptor-operated Gi/o signaling. *Mol. Psychiatry* **1** (2018).

## References

47. Araújo, A. M., Carvalho, F., Bastos, M. de L., Guedes de Pinho, P. & Carvalho, M. The hallucinogenic world of tryptamines: an updated review. *Arch. Toxicol.* **89**, 1151–1173 (2015).
48. Lee, H.-M. & Roth, B. L. Hallucinogen actions on human brain revealed. *Proc. Natl. Acad. Sci.* **109**, 1820–1821 (2012).
49. Nichols, D. E. Dark Classics in Chemical Neuroscience: Lysergic Acid Diethylamide (LSD). *ACS Chem. Neurosci.* **9**, 2331–2343 (2018).
50. Elphick, G. F. *et al.* The human polyomavirus, JCV, uses serotonin receptors to infect cells. *Science (80-. )*. **306**, 1380–1383 (2004).
51. Briddon, S. J., Kilpatrick, L. E. & Hill, S. J. Studying GPCR Pharmacology in Membrane Microdomains: Fluorescence Correlation Spectroscopy Comes of Age. *Trends Pharmacol. Sci.* **39**, 158–174 (2018).
52. Barden, A. O. *et al.* Tracking individual membrane proteins and their biochemistry: The power of direct observation. *Neuropharmacology* **98**, 22–30 (2015).
53. Thorn, K. Genetically encoded fluorescent tags. *Mol. Biol. Cell* **28**, 848–857 (2017).
54. Stoddart, L. A., Kilpatrick, L. E., Briddon, S. J. & Hill, S. J. Probing the pharmacology of G protein-coupled receptors with fluorescent ligands. *Neuropharmacology* **98**, 48–57 (2015).
55. Alonso, D. *et al.* Development of fluorescent ligands for the human 5-HT<sub>1A</sub> receptor. *ACS Med. Chem. Lett.* **1**, 249–253 (2010).
56. Azuaje, J. *et al.* Development of Fluorescent Probes that Target Serotonin 5-HT<sub>2B</sub> Receptors. *Sci. Rep.* **7**, 1–16 (2017).
57. Cornelius, P. *et al.* Design, Synthesis, and Pharmacology of Fluorescently Labeled Analogs of Serotonin: Application to Screening of the 5-HT<sub>2C</sub> Receptor. *J. Biomol. Screen.* **14**, 360–370 (2009).
58. Jack, T. *et al.* Characterizing new fluorescent tools for studying 5-HT<sub>3</sub> receptor pharmacology. *Neuropharmacology* **90**, 63–73 (2015).
59. Berque-Bestel, I. *et al.* Synthesis and Characterization of the First Fluorescent Antagonists for Human 5-HT<sub>4</sub> Receptors. *J. Med. Chem.* **46**, 2606–2620 (2003).
60. Vázquez-Villa, H. *et al.* Development of molecular probes for the human 5-HT<sub>6</sub> receptor. *J. Med. Chem.* **53**, 7095–7106 (2010).
61. Zhao, Y. *et al.* An expanded palette of genetically encoded Ca<sup>2+</sup> indicators. *Science* **333**, 1888–91 (2011).
62. Kendall, J. M. & Badminton, M. N. *Aequorea victoria* bioluminescence moves into an exciting new era. *Trends Biotechnol.* **16**, 216–224 (1998).

## References

63. Rodriguez-Garcia, A. *et al.* GAP, an aequorin-based fluorescent indicator for imaging Ca<sup>2+</sup> in organelles. *Proc. Natl. Acad. Sci. U. S. A.* **111**, 2584–2589 (2014).
64. Zhang, Z. *et al.* Oligonucleotide-induced alternative splicing of serotonin 2C receptor reduces food intake. *EMBO Mol. Med.* **8**, 878–894 (2016).
65. Kroeze, W. K. *et al.* PRESTO-Tango as an open-source resource for interrogation of the druggable human GPCRome. *Nat. Struct. Mol. Biol.* **22**, 362–369 (2015).
66. Hsiao, E. C. *et al.* Constitutive G<sub>s</sub> activation using a single-construct tetracycline-inducible expression system in embryonic stem cells and mice. *Stem Cell Res. Ther.* **2**, 11 (2011).
67. Pronobis, M. I., Deutch, N. & Peifer, M. The Miraprep: A protocol that uses a Miniprep kit and provides Maxiprep yields. *PLoS One* **11**, 1–12 (2016).
68. Binkowski, B. F. *et al.* A luminescent biosensor with increased dynamic range for intracellular cAMP. *ACS Chem. Biol.* **6**, 1193–1197 (2011).
69. Jaqaman, K. *et al.* Robust single-particle tracking in live-cell time-lapse sequences. *Nat. Methods* **5**, 695–702 (2008).
70. Persson, F., Lindén, M., Unoson, C. & Elf, J. Extracting intracellular diffusive states and transition rates from single-molecule tracking data. *Nat. Methods* **10**, 265–269 (2013).
71. McLean, T. H. *et al.* C-(4,5,6-Trimethoxyindan-1-yl)methanamine: A Mescaline Analogue Designed Using a Homology Model of the 5-HT<sub>2A</sub> Receptor. *J. Med. Chem.* **49**, 7558–7558 (2006).
72. Isberg, V., Paine, J., Leth-Petersen, S., Kristensen, J. L. & Gloriam, D. E. Structure-activity relationships of constrained phenylethylamine ligands for the serotonin 5-HT<sub>2</sub> receptors. *PLoS One* **8**, 9–11 (2013).
73. Johnson, M. P., Baez, M., Kursar, J. D. & Nelson, D. L. Species differences in 5-HT<sub>2A</sub> receptors: cloned pig and rhesus monkey 5-HT<sub>2A</sub> receptors reveal conserved transmembrane homology to the human rather than rat sequence. *BBA - Biomembr.* **1236**, 201–206 (1995).
74. Kao, H. T. *et al.* Site-directed mutagenesis of a single residue changes the binding properties of the serotonin 5-HT<sub>2</sub> receptor from a human to a rat pharmacology. *FEBS Lett.* **307**, 324–328 (1992).
75. Levitt, E. S., Purington, L. C. & Traynor, J. R. Gi/o-coupled receptors compete for signaling to adenylyl cyclase in SH-SY5Y cells and reduce opioid-mediated cAMP overshoot. *Mol. Pharmacol.* **79**, 461–471 (2011).
76. Adeosun, S. O., Albert, P. R., Austin, M. C. & Iyo, A. H. 17 $\beta$ -estradiol-induced regulation of the novel 5-HT<sub>1A</sub>- related transcription factors NUDR and freud-1 in SH SY5Y cells. *Cell. Mol. Neurobiol.* **32**, 517–521 (2012).

## References

77. Bhattacharyya, S., Puri, S., Miledi, R. & Panicker, M. M. Internalization and recycling of 5-HT<sub>2A</sub> receptors activated by serotonin and protein kinase C-mediated mechanisms. *Proc. Natl. Acad. Sci.* **99**, 14470–14475 (2002).
78. Celada, P., Puig, M., Amargós-Bosch, M., Adell, A. & Artigas, F. The therapeutic role of 5-HT<sub>1A</sub> and 5-HT<sub>2A</sub> receptors in depression. *J. Psychiatry Neurosci.* **29**, 252–65 (2004).
79. McLean, T. H. *et al.* 1-Aminomethylbenzocycloalkanes: Conformationally restricted hallucinogenic phenethylamine analogues as functionally selective 5-HT<sub>2A</sub> receptor agonists. *J. Med. Chem.* **49**, 5794–5803 (2006).
80. Hegener, O., Jordan, R. & Haberlein, H. Dye-labeled benzodiazepines: development of small ligands for receptor binding studies using fluorescence correlation spectroscopy. *J. Med. Chem.* **47**, 3600–3605 (2004).
81. Caballero-George, C. *et al.* Fluorescence correlation spectroscopy in drug discovery: study of Alexa532-endothelin 1 binding to the endothelin ETA receptor to describe the pharmacological profile of natural products. *ScientificWorldJournal.* **2012**, 524169 (2012).
82. Hegener, O. *et al.* Dynamics of  $\beta$  2 -Adrenergic Receptor–Ligand Complexes on Living Cells †. *Biochemistry* **43**, 6190–6199 (2004).
83. Salvatore, R. N., Nagle, A. S. & Kyung, W. J. Cesium effect: High chemoselectivity in direct N-alkylation of amines. *J. Org. Chem.* **67**, 674–683 (2002).
84. Trost, B. M. & Schreiber, S. L. *Comprehensive Organic Synthesis I.* (Elsevier Science Ltd., 1991).
85. Li, B. *et al.* Aqueous phosphoric acid as a mild reagent for deprotection of tert-butyl carbamates, esters, and ethers. *J. Org. Chem.* **71**, 9045–9050 (2006).
86. Baker, J. G. *et al.* Influence of fluorophore and linker composition on the pharmacology of fluorescent adenosine A<sub>1</sub> receptor ligands: Themed section: Imaging in pharmacology research paper. *Br. J. Pharmacol.* **159**, 772–786 (2010).
87. Canal, C. E. *et al.* Molecular Pharmacology and Ligand Docking Studies Reveal a Single Amino Acid Difference between Mouse and Human Serotonin 5-HT<sub>2A</sub> Receptors That Impacts Behavioral Translation of Novel 4-Phenyl-2-dimethylaminotetralin Ligands. *J. Pharmacol. Exp. Ther.* **347**, 705–716 (2013).
88. Hancock, A. A. The challenge of drug discovery of a GPCR target: Analysis of preclinical pharmacology of histamine H<sub>3</sub> antagonists/inverse agonists. *Biochem. Pharmacol.* **71**, 1103–1113 (2006).
89. Strader, C. D., Sigal, I. S. & Dixon, R. A. F. Structural basis of  $\beta$ -adrenergic receptor function. *FASEB J.* **3**, 1825–1832 (1989).

## References

90. Braden, M. R. & Nichols, D. E. Assessment of the roles of serines 5.43(239) and 5.46(242) for binding and potency of agonist ligands at the human serotonin 5-HT<sub>2A</sub> receptor. *Mol. Pharmacol.* **72**, 1200–1209 (2007).
91. Cordeaux, Y., Briddon, S. J., Alexander, S. P. H., Kellam, B. & Hill, S. J. Agonist-occupied A<sub>3</sub> adenosine receptors exist within heterogeneous complexes in membrane microdomains of individual living cells. *FASEB J.* **22**, 850–860 (2007).
92. Briddon, S. J. *et al.* Quantitative analysis of the formation and diffusion of A<sub>1</sub>-adenosine receptor-antagonist complexes in single living cells. *Proc. Natl. Acad. Sci. U. S. A.* **101**, 4673–4678 (2004).
93. Kim, K. *et al.* Structure of a Hallucinogen-Activated Gq-Coupled 5-HT<sub>2A</sub> Serotonin Receptor. *Cell* **182**, 1574-1588.e19 (2020).
94. Knight, A. R. *et al.* Pharmacological characterisation of the agonist radioligand binding site of 5-HT<sub>2A</sub>, 5-HT<sub>2B</sub> and 5-HT<sub>2C</sub> receptors. *N-S Arch Pharmacol* **370**, 114–123 (2004).
95. Córdova-Sintjago, T., Sakhuja, R., Kondabolu, K., Canal, C. E. & Booth, R. G. Molecular Determinants for Ligand Binding at Serotonin 5-HT<sub>2A</sub> and 5-HT<sub>2C</sub> GPCRs: Experimental Affinity Results Analyzed by Molecular Modeling and Ligand Docking Studies. *Int J Quantum Chem.* **112**, 3807–3814 (2013).
96. Di Giovanni, G. & De Deurwaerdère, P. TCB-2 [(7R)-3-bromo-2,5-dimethoxy-bicyclo[4.2.0]octa-1,3,5-trien-7-yl]methanamine]: A hallucinogenic drug, a selective 5-HT<sub>2A</sub> receptor pharmacological tool, or none of the above? *Neuropharmacology* **142**, 20–29 (2018).
97. Fox, M. A., French, H. T., Laporte, J. L., Blackler, A. R. & Murphy, D. L. The serotonin 5-HT<sub>2A</sub> receptor agonist TCB-2: A behavioral and neurophysiological analysis. *Psychopharmacology (Berl)*. **212**, 13–23 (2010).
98. Haberzettl, R., Fink, H. & Bert, B. Role of 5-HT<sub>1A</sub>- and 5-HT<sub>2A</sub> receptors for the murine model of the serotonin syndrome. *J. Pharmacol. Toxicol. Methods* **70**, 129–133 (2014).
99. Szlachta, M. *et al.* Repeated Clozapine Increases the Level of Serotonin 5-HT<sub>1A</sub>R Heterodimerization with 5-HT<sub>2A</sub> or Dopamine D<sub>2</sub> Receptors in the Mouse Cortex. *Front. Mol. Neurosci.* **11**, 1–14 (2018).
100. Fongang, B., Cunningham, K. A., Rowicka, M. & Kudlicki, A. Coevolution of Residues Provides Evidence of a Functional Heterodimer of 5-HT<sub>2A</sub>R and 5-HT<sub>2C</sub>R Involving Both Intracellular and Extracellular Domains. *Neuroscience* **412**, 48–59 (2019).
101. Łukasiewicz, S., Faron-Górecka, A., Kędracka-Krok, S. & Dziedzicka-Wasylewska, M. Effect of clozapine on the dimerization of serotonin 5-HT<sub>2A</sub> receptor and its genetic variant 5-HT<sub>2A</sub>H425Y with dopamine D<sub>2</sub> receptor. *Eur. J. Pharmacol.* **659**, 114–123 (2011).
102. Bosch, P. J. *et al.* Evaluation of fluorophores to label SNAP-Tag fused proteins for multicolor single-molecule tracking microscopy in live cells. *Biophys. J.* **107**, 803–814 (2014).

## References

103. Guo, Q., Brady, M. & Gunn, R. N. A Biomathematical Modeling Approach to Central Nervous System Radioligand Discovery and Development. *J. Nucl. Med.* **50**, 1715–1723 (2009).
104. Houghten, R. A., Dooley, C. T. & Appel, J. R. De novo identification of highly active fluorescent kappa opioid ligands from a rhodamine labeled tetrapeptide positional scanning library. *Bioorg. Med. Chem. Lett.* **14**, 1947–1951 (2004).
105. Stoddart, L. A. *et al.* Fragment Screening at Adenosine-A3 Receptors in Living Cells Using a Fluorescence-Based Binding Assay. *Chem. Biol.* **19**, 1105–1115 (2012).
106. Harwardt, M. L. I. E., Dietz, M. S., Heilemann, M. & Wohland, T. SPT and Imaging FCS Provide Complementary Information on the Dynamics of Plasma Membrane Molecules. *Biophys. J.* **114**, 2432–2443 (2018).
107. Sungkaworn, T. *et al.* Single-molecule imaging reveals receptor–G protein interactions at cell surface hot spots. *Nature* **550**, 543–547 (2017).
108. Schwenzer, N., Bussmann, H., Franken, S. & Häberlein, H. Live-cell single-molecule analysis of  $\beta$  2 -adrenergic receptor diffusion dynamics and confinement. *bioRxiv* **3**, 406488 (2018).
109. Prenner, L., Sieben, A., Zeller, K., Weiser, D. & Häberlein, H. Reduction of high-affinity  $\beta$ 2-adrenergic receptor binding by hyperforin and hyperoside on rat C6 glioblastoma cells measured by fluorescence correlation spectroscopy. *Biochemistry* **46**, 5106–5113 (2007).
110. Meissner, O. & Häberlein, H. Lateral mobility and specific binding to GABAA receptors on hippocampal neurons monitored by fluorescence correlation spectroscopy. *Biochemistry* **42**, 1667–1672 (2003).
111. Meissner, O. & Häberlein, H. Influence of Xanthohumol on the Binding Behavior of GABA A Receptors and their Lateral Mobility at Hippocampal Neurons. *Planta Med.* **72**, 656–658 (2006).
112. Yanagawa, M. *et al.* Single-molecule diffusion-based estimation of ligand effects on G protein–coupled receptors. *Sci. Signal.* **11**, eaao1917 (2018).
113. Kramer, H. K., Poblete, J. C. & Azmitia, E. C. Activation of protein kinase C (PKC) by 3,4-methylenedioxymethamphetamine (MDMA) occurs through the stimulation of serotonin receptors and transporter. *Neuropsychopharmacology* **17**, 117–129 (1997).
114. Grynkiewicz, G., Poenie, M. & Tsien, R. Y. A new generation of  $\text{Ca}^{2+}$  indicators with greatly improved fluorescence properties. *J. Biol. Chem.* **260**, 3440–50 (1985).
115. Chen, T. *et al.* Ultrasensitive fluorescent proteins for imaging neuronal activity. *Nature* **499**, 295–300 (2013).
116. Vella, S. A., Calixto, A., Asady, B., Li, Z.-H. & Moreno, S. N. J. Genetic Indicators for Calcium Signaling Studies in *Toxoplasma gondii*. in *Physiology & behavior* (ed. Tonkin, C. J.) vol. 2071 187–207 (Springer US, 2020).

## References

117. Tewson, P. *et al.* Simultaneous detection of CA 2+ and diacylglycerol signaling in living cells. *PLoS One* **7**, 1–6 (2012).
118. Uebelhack, R., Gruenwald, J., Graubaum, H.-J. & Busch, R. Efficacy and tolerability of Hypericum extract STW 3-VI in patients with moderate depression: A double-blind, randomized, placebo-controlled clinical trial. *Adv. Ther.* **21**, 265–275 (2004).
119. Gastpar, M., Singer, A. & Zeller, K. Efficacy and Tolerability of Hypericum Extract STW3 in Long-term Treatment with a Once-daily Dosage in Comparison with Sertraline. *Pharmacopsychiatry* **38**, 78–86 (2005).
120. Gastpar, M., Singer, A. & Zeller, K. Comparative Efficacy and Safety of a Once-Daily Dosage of Hypericum Extract STW3-VI and Citalopram in Patients with Moderate Depression: A Double-Blind, Randomised, Multicentre, Placebo-Controlled Study. *Pharmacopsychiatry* **39**, 66–75 (2006).
121. Committee on Herbal Medicinal Products & (HMPC). Community Herbal Monograph on Hypericum Perforatum L., Herba (Well-established medicinal use). *EMA/HMPC/101304/2008* (2009).
122. Council of Europe. Monograph 1874 'St. John's wort dry extract, quantified'. *Ph. Eur.* 10th Edition (2019).
123. Jakobs, D. *et al.* Downregulation of  $\beta$ 1-adrenergic receptors in rat C6 glioblastoma cells by hyperforin and hyperoside from St John's wort. *J. Pharm. Pharmacol.* **65**, 907–915 (2013).
124. Verjee, S., Weston, A., Kolb, C., Kalbhenn-Aziz, H. & Butterweck, V. Hyperforin and Miquelianin from St Johns Wort Attenuate Gene Expression in Neuronal Cells after Dexamethasone-Induced Stress. *Planta Med.* **84**, 696–703 (2018).
125. Bonaterra, G. A. *et al.* Neurotrophic, cytoprotective, and anti-inflammatory effects of St. John's wort extract on differentiated mouse hippocampal HT-22 neurons. *Front. Pharmacol.* **8**, 1–13 (2018).
126. Grundmann, O., Lv, Y., Kelber, O. & Butterweck, V. Mechanism of St. John's wort extract (STW3-VI) during chronic restraint stress is mediated by the interrelationship of the immune, oxidative defense, and neuroendocrine system. *Neuropharmacology* **58**, 767–773 (2010).
127. Orčić, D. Z., Mimica-Dukić, N. M., Francišković, M. M., Petrović, S. S. & Jovin, E. T. Antioxidant activity relationship of phenolic compounds in Hypericum perforatum L. *Chem. Cent. J.* **5**, 1–8 (2011).
128. Hölzl, J., Ostrowski, E. Johanniskraut (Hypericum perforatum L.) HPLC-Analyse der wichtigsten Inhaltsstoffe und deren Variabilität in einer Population. *Dtsch. Apotheker Zeitung* **23**, 1227–1230 (1987).

## References

129. Qi, X.-C., Li, B., Wu, W.-L., Liu, H.-C. & Jiang, Y.-P. Protective effect of hyperoside against hydrogen peroxide-induced dysfunction and oxidative stress in osteoblastic MC3T3-E1 cells. *Artif. Cells, Nanomedicine, Biotechnol.* **48**, 377–383 (2020).
130. Wurglics, M. & Schubert-Zsilavecz, M. Hypericum Perforatum: A 'Modern' Herbal Antidepressant. *Clin. Pharmacokinet.* **45**, 449–468 (2006).
131. Butterweck, V. Mechanism of action of St John's wort in depression: What is known? *CNS Drugs* **17**, 539–562 (2003).
132. Liu, J. *et al.* Study of interaction of hypericin and its pharmaceutical preparation by fluorescence techniques. *J. Biomed. Opt.* **14**, 014003 (2009).
133. Vukojević, V. *et al.* Study of molecular events in cells by fluorescence correlation spectroscopy. *Cell. Mol. Life Sci.* **62**, 535–550 (2005).
134. Butterweck, V. & Nahrstedt, A. What Is the Best Strategy for Preclinical Testing of Botanicals? A Critical Perspective. *Planta Med.* **78**, 747–754 (2012).
135. Veya, L., Piguet, J. & Vogel, H. Single molecule imaging deciphers the relation between mobility and signaling of a prototypical G protein-coupled receptor in living cells. *J. Biol. Chem.* **290**, 27723–27735 (2015).
136. Eckert, G. P. *et al.* Hyperforin modifies neuronal membrane properties in vivo. *Neurosci. Lett.* **367**, 139–143 (2004).
137. Sieben, A. *et al.* Alpha-hederin, but not hederacoside C and hederagenin from *Hedera helix*, affects the binding behavior, dynamics, and regulation of beta 2-adrenergic receptors. *Biochemistry* **48**, 3477–82 (2009).
138. Bhatnagar, A. *et al.* The Dynamin-dependent, Arrestin-independent Internalization of 5-Hydroxytryptamine 2A (5-HT<sub>2A</sub>) Serotonin Receptors Reveals Differential Sorting of Arrestins and 5-HT<sub>2A</sub> Receptors during Endocytosis. *J. Biol. Chem.* **276**, 8269–8277 (2001).
139. Bhattacharyya, S., Raote, I., Bhattacharya, A., Miledi, R. & Panicker, M. M. Activation, internalization, and recycling of the serotonin 2A receptor by dopamine. *Proc. Natl. Acad. Sci. U. S. A.* **103**, 15248–15253 (2006).
140. Karaki, S. *et al.* Quantitative phosphoproteomics unravels biased phosphorylation of serotonin 2A Receptor at Ser280 by hallucinogenic versus nonhallucinogenic agonists. *Mol. Cell. Proteomics* **13**, 1273–1285 (2014).
141. Sasaki, M. *et al.* Development of a rapid and quantitative method for the analysis of viral entry and release using a NanoLuc luciferase complementation assay. *Virus Res.* **243**, 69–74 (2018).

## References

142. Oh-Hashi, K., Furuta, E., Fujimura, K. & Hirata, Y. Application of a novel HiBiT peptide tag for monitoring ATF4 protein expression in Neuro2a cells. *Biochem. Biophys. Reports* **12**, 40–45 (2017).
143. Hoare, B. L., Kocan, M., Bruell, S., Scott, D. J. & Bathgate, R. A. D. Using the novel HiBiT tag to label cell surface relaxin receptors for BRET proximity analysis. *Pharmacol. Res. Perspect.* **7**, 1–13 (2019).
144. Kumagai, H. *et al.* Quantitative measurement of GPCR endocytosis via pulse-chase covalent labeling. *PLoS One* **10**, 1–13 (2015).
145. Fan, F. & Wood, K. V. Bioluminescent Assays for High-Throughput Screening. *Assay Drug Dev. Technol.* **5**, 127–136 (2007).
146. Shimomura, O., Johnson, F. H. & Saiga, Y. Extraction, Purification and Properties of Aequorin, a Bioluminescent Protein from the Luminous Hydromedusan, Aequorea. *J. Cell. Comp. Physiol.* **59**, 223–239 (1962).
147. Shimomura, O. & Johnson, F. H. Regeneration of the photoprotein aequorin. *Nature* **256**, 236–238 (1975).
148. Webb, S. E., Karplus, E. & Miller, A. L. Retrospective on the development of aequorin and aequorin-based imaging to visualize changes in intracellular free [Ca<sup>2+</sup>]. *Mol. Reprod. Dev.* **82**, 563–586 (2015).
149. Bonora, M. *et al.* Subcellular calcium measurements in mammalian cells using jellyfish photoprotein aequorin-based probes. *Nat. Protoc.* **8**, 2105–2118 (2013).
150. Cobbold, P. H., Cuthbertson, K. S., Goyns, M. H. & Rice, V. Aequorin measurements of free calcium in single mammalian cells. *J. Cell Sci.* **Vol. 61**, 123–136 (1983).
151. Van Nueten, J. M. *et al.* Vascular effects of ketanserin (R 41 468), a novel antagonist of 5-HT<sub>2</sub> serotonergic receptors. *J. Pharmacol. Exp. Ther.* **218**, 217–30 (1981).

9. Supplemental Material

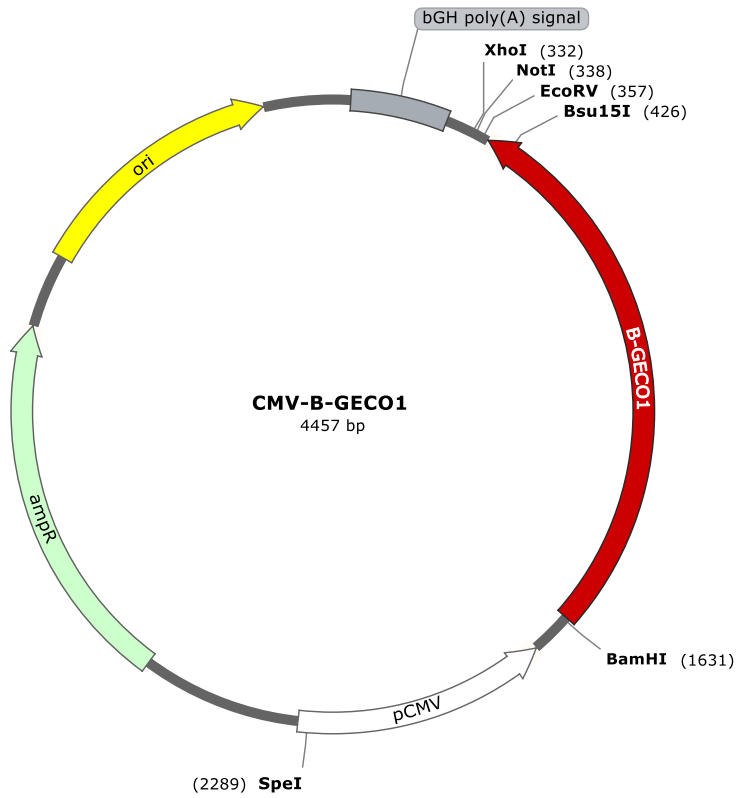


Figure S 1: Plasmid card of CMV-B-GECO1

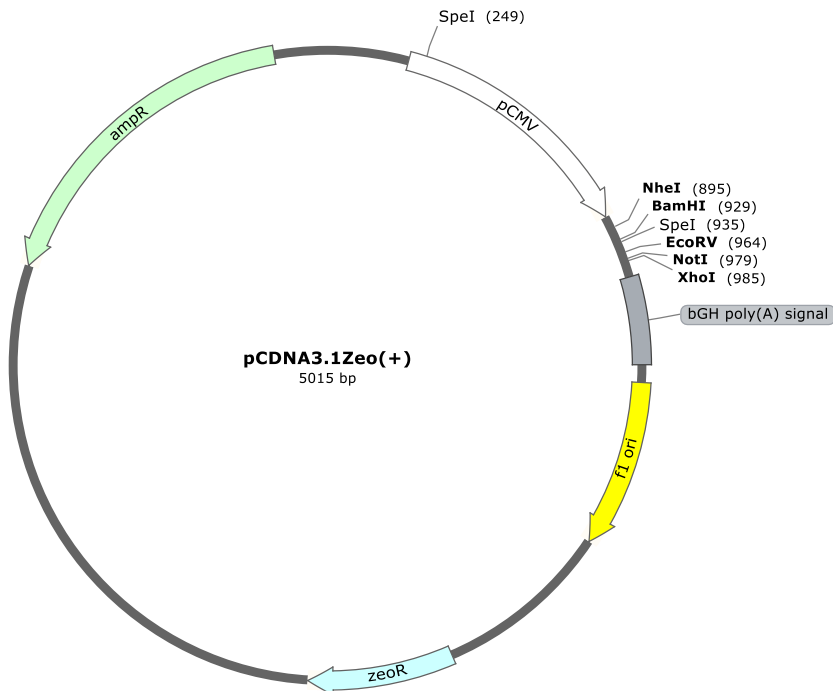
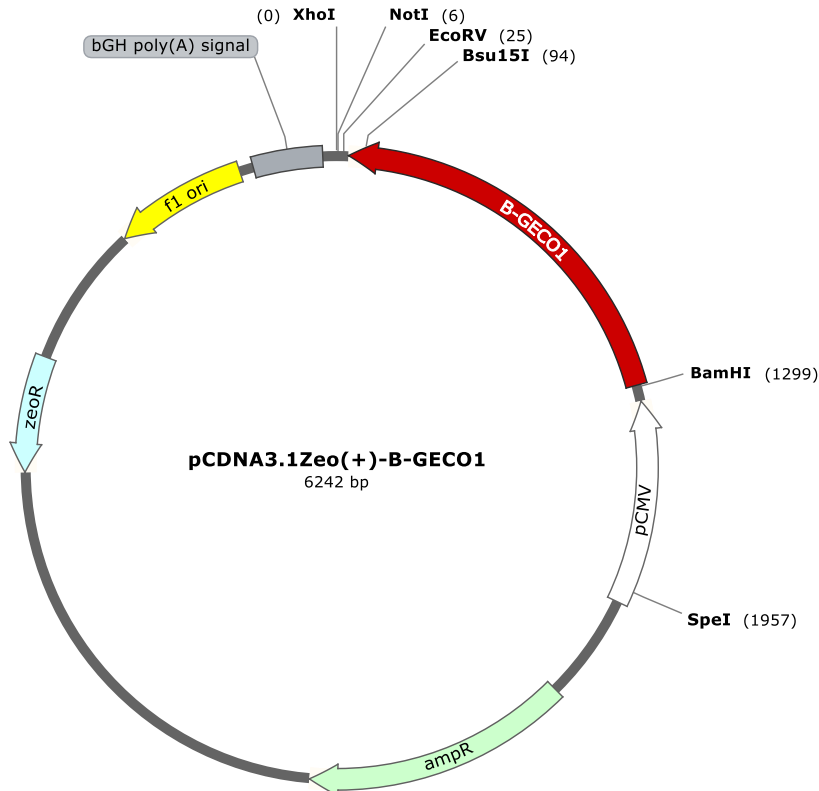
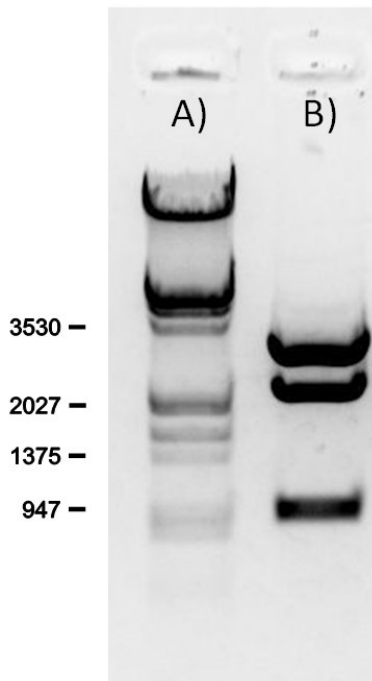


Figure S 2: Plasmid card of pCDNA3.1Zeo(+)



**Figure S 3: Plasmid card of pCDNA3.1Zeo(+)-B-GECO1**



**Figure S 4: Enzymatic digestion of pCDNA3.1Zeo(+)-B-GECO1.** A) Lambda DNA/EcoRI+HindIII Marker 3 (Thermo Fisher Scientific) B) pCDNA3.1Zeo(+)-B-GECO1 digested by Sall, expected band sizes 3133, 2188, 887 and 34 (not visible) bp. Restriction enzyme was obtained from Thermo Fisher Scientific.

Supplemental Material

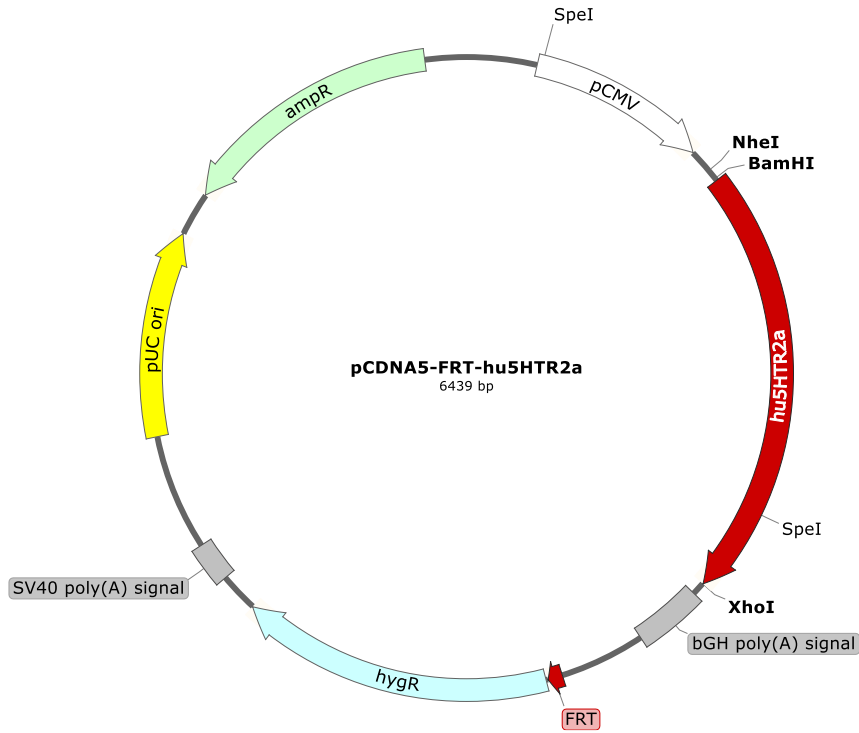


Figure S 5: Plasmid card of pCDNA5-FRT-hu5HTR2a

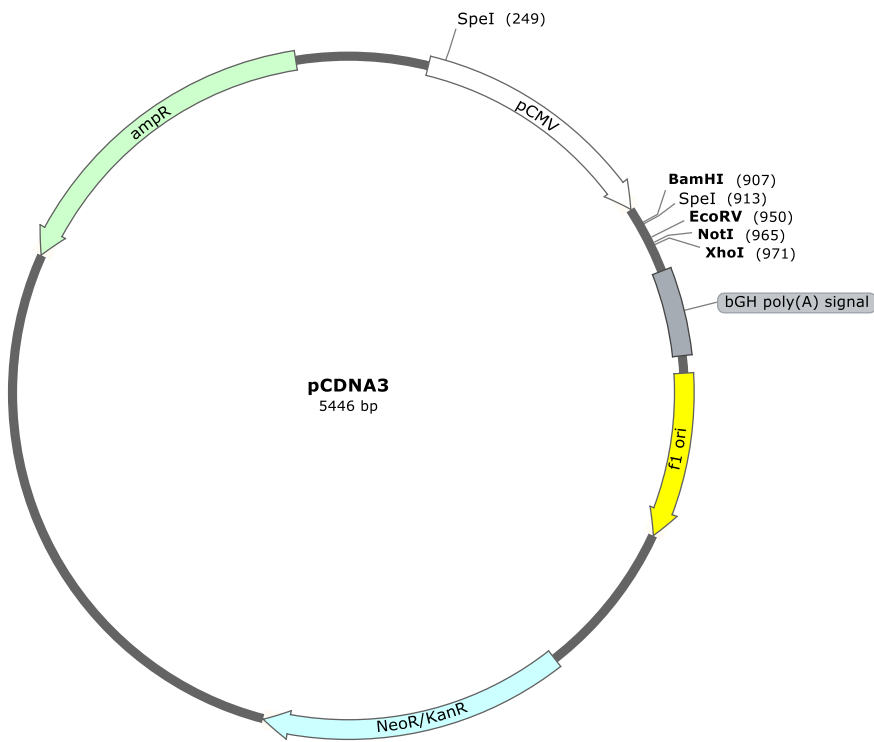


Figure S 6: Plasmid card of pCDNA3

Supplemental Material

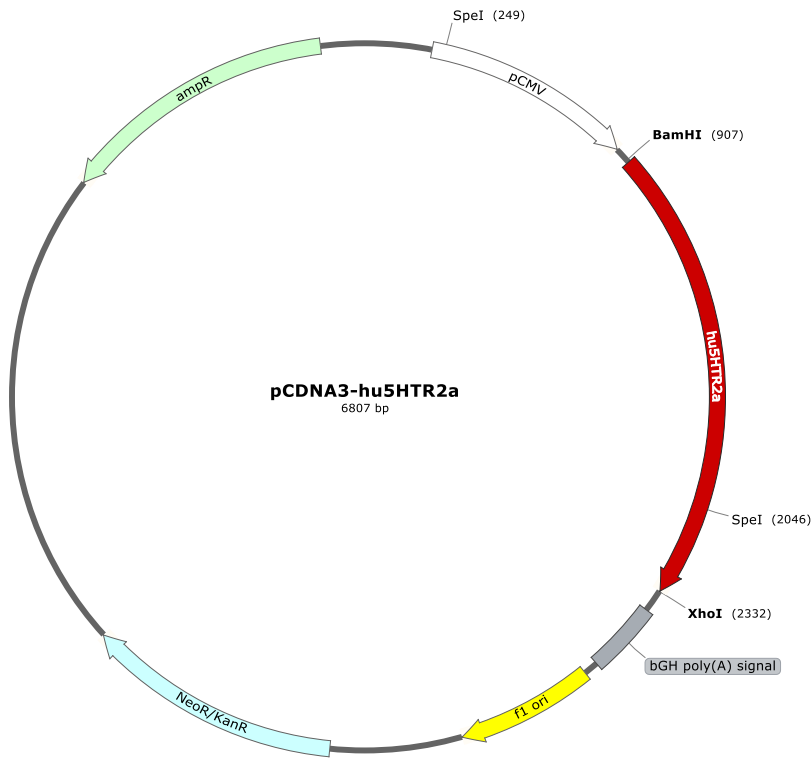


Figure S 7: Plasmid card of pCDNA3-hu5HTR2a

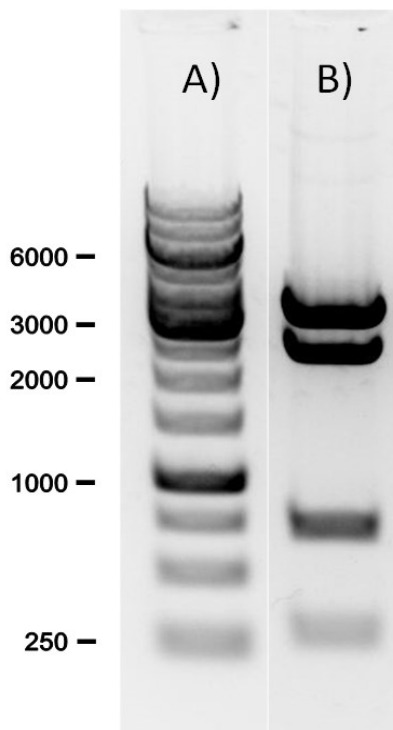


Figure S 8: Enzymatic digestion of pCDNA3-hu5HTR2a. A) GeneRuler 1 kb DNA ladder (Thermo Fisher Scientific) B) pCDNA3-hu5HTR2a digested by NcoI, expected band sizes 3345, 2424, 735 and 305 bp. Restriction enzyme was obtained from Thermo Fisher Scientific.

Supplemental Material

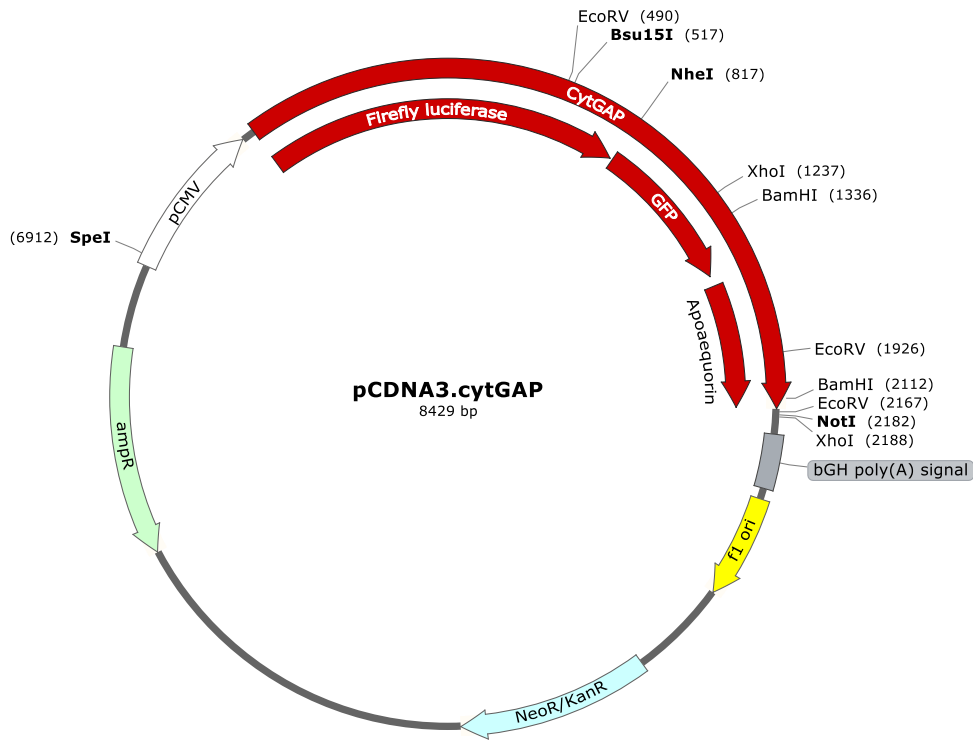


Figure S 9: Plasmid card of pCDNA3.cytGAP

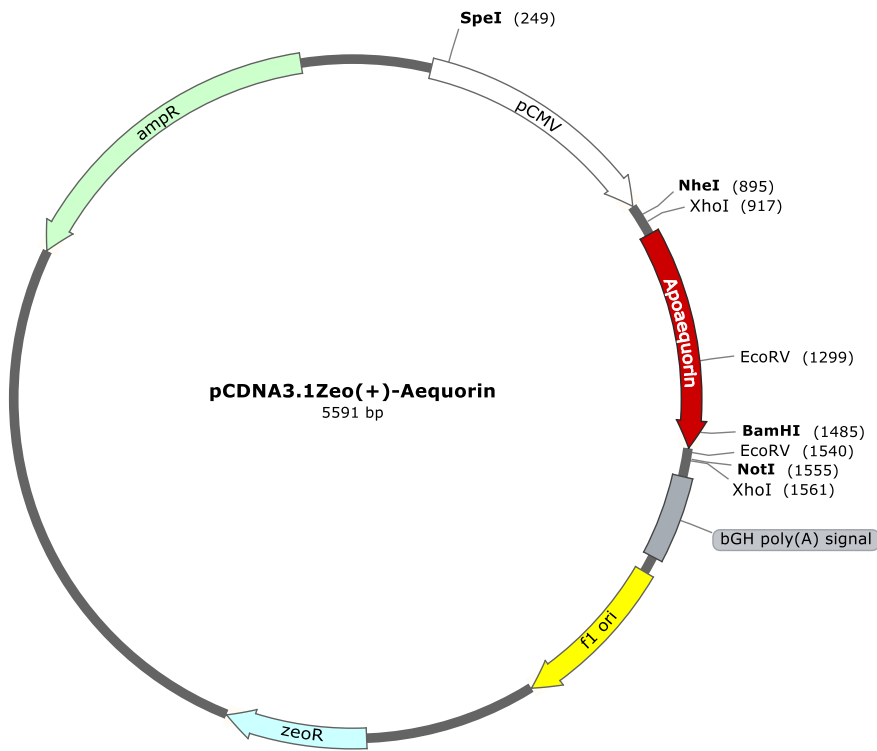
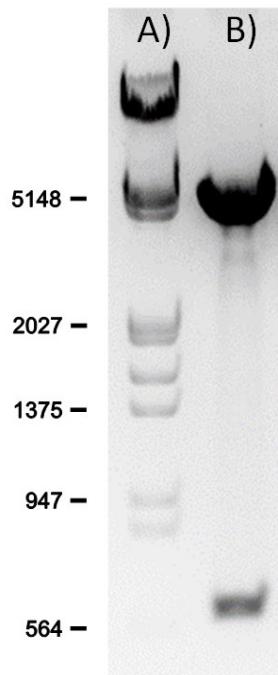
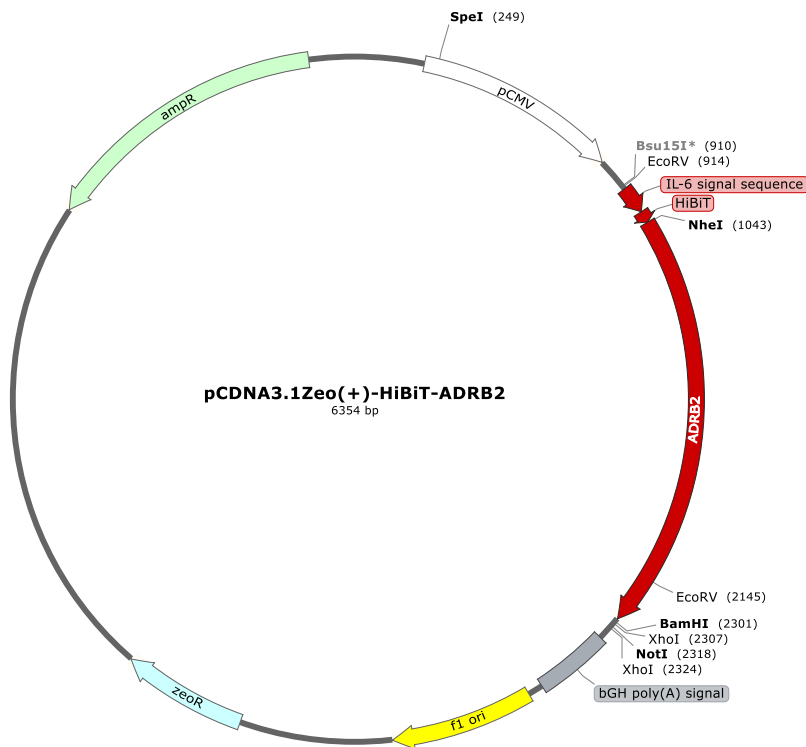


Figure S 10: Plasmid card of pCDNA3.1Zeo(+)-Aequorin

Supplemental Material



**Figure S 11: Enzymatic digestion of pCDNA3.1Zeo(+)-Aequorin.** A) Lambda DNA/EcoRI+HindIII Marker 3 (Thermo Fisher Scientific) B) pCDNA3.1Zeo(+)-Aequorin digested by EcoRI, expected band sizes 4996 and 595 bp. Restriction enzyme was obtained from Thermo Fisher Scientific.



**Figure S 12: Plasmid card of pCDNA3.1Zeo(+)-HiBiT-ADRB2**

Supplemental Material

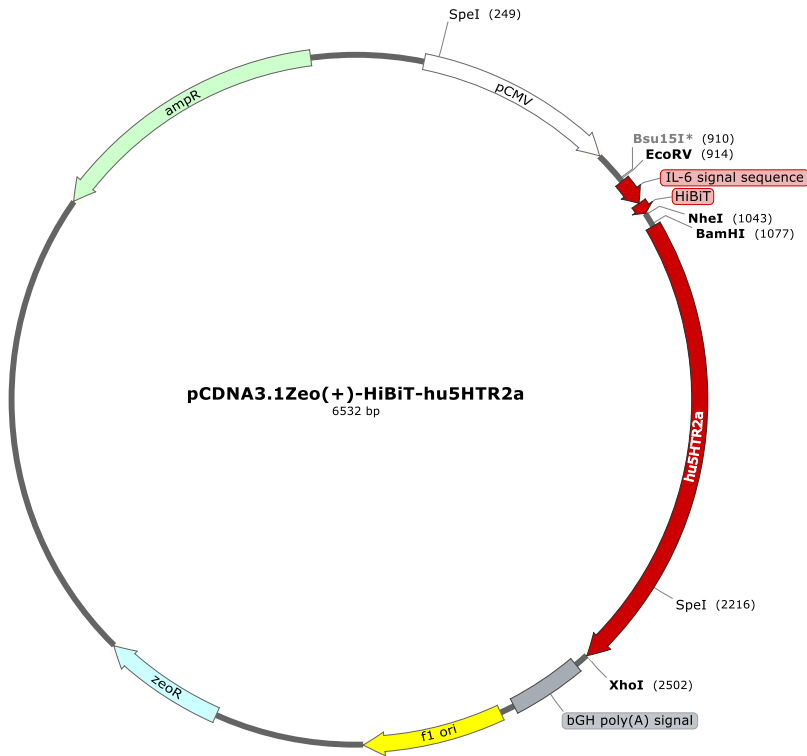


Figure S 13: Plasmid card of pCDNA3.1Zeo(+)-HiBiT-hu5HTR2a

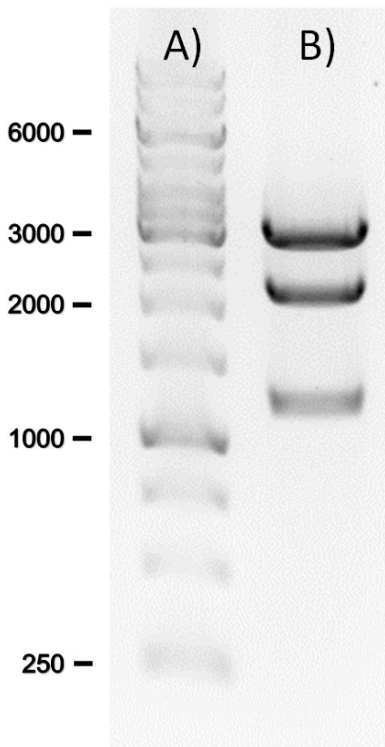


Figure S 14: Enzymatic digestion of pCDNA3.1Zeo(+)-HiBiT-hu5HTR2a. A) GeneRuler 1 kb DNA ladder (Thermo Fisher Scientific) B) pCDNA3.1Zeo(+)-HiBiT-hu5HTR2a digested by Sall, expected band sizes 3118, 2188, 1292 and 34 (not visible) bp. Restriction enzyme was obtained from Thermo Fisher Scientific.

Supplemental Material

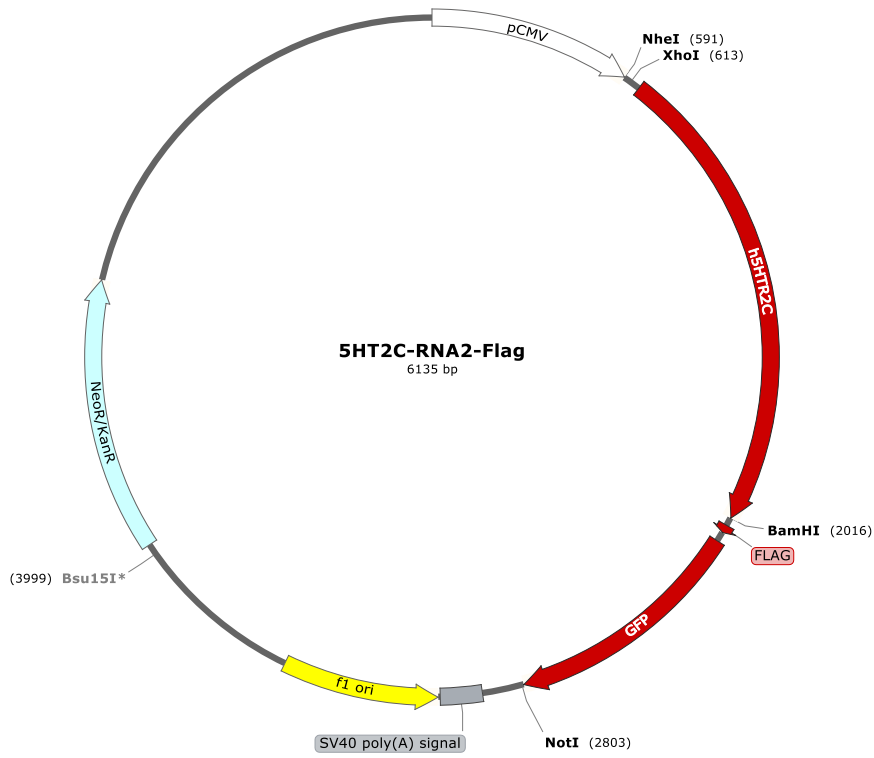


Figure S 15: Plasmid card of 5HT2C-RNA2-Flag

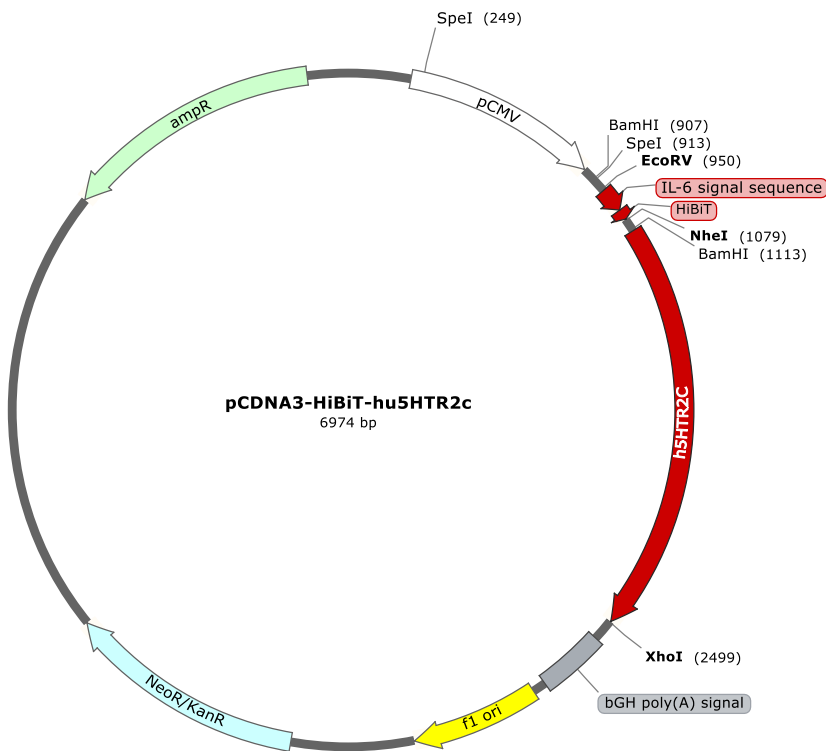
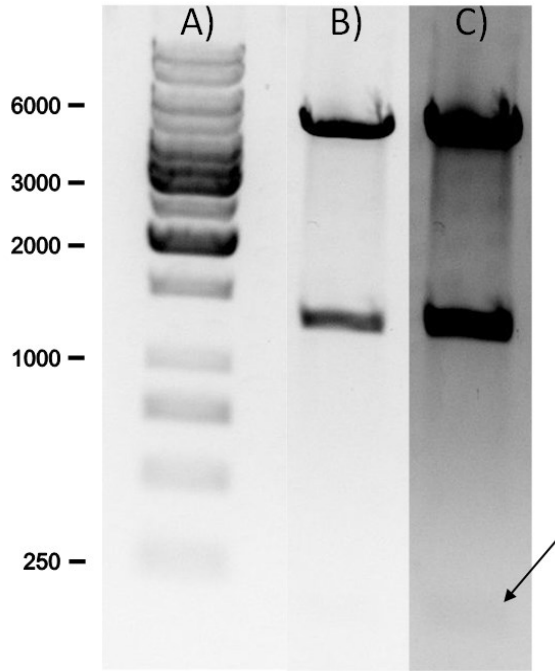
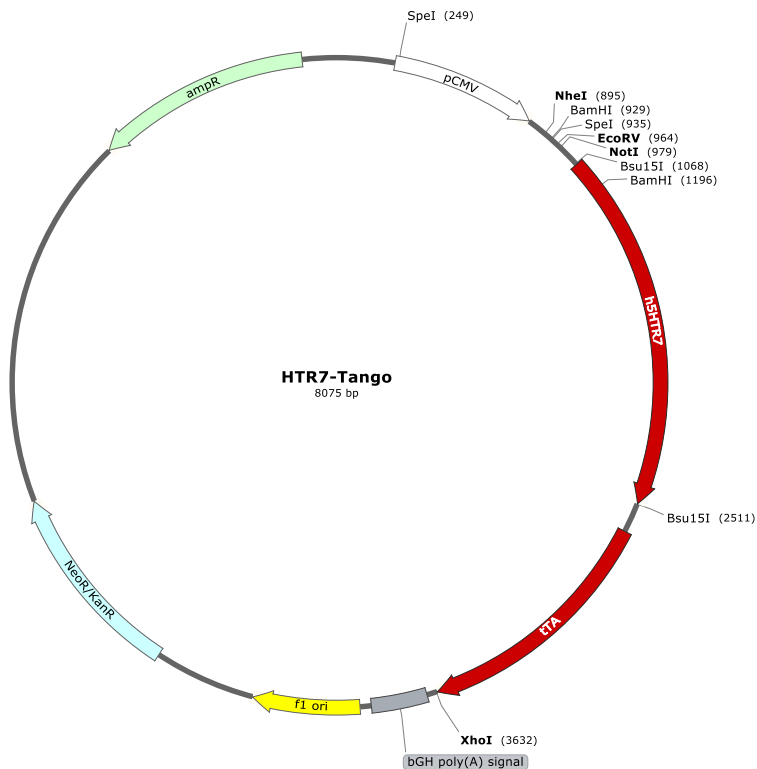


Figure S 16: Plasmid card of pCDNA3-HiBiT-hu5HTR2c



**Figure S 17: Enzymatic digestion of pCDNA3-HiBiT-hu5HTR2c.** A) GeneRuler 1 kb DNA ladder (Thermo Fisher Scientific) B) + C) pCDNA3-HiBiT-hu5HTR2chu5HTR2a digested by *SacI* with different illumination times, expected band sizes 5239, 1442, 206 (arrow) and 87 (not visible) bp. Restriction enzyme was obtained from Thermo Fisher Scientific.



**Figure S 18: Plasmid card of HTR7-Tango**

Supplemental Material

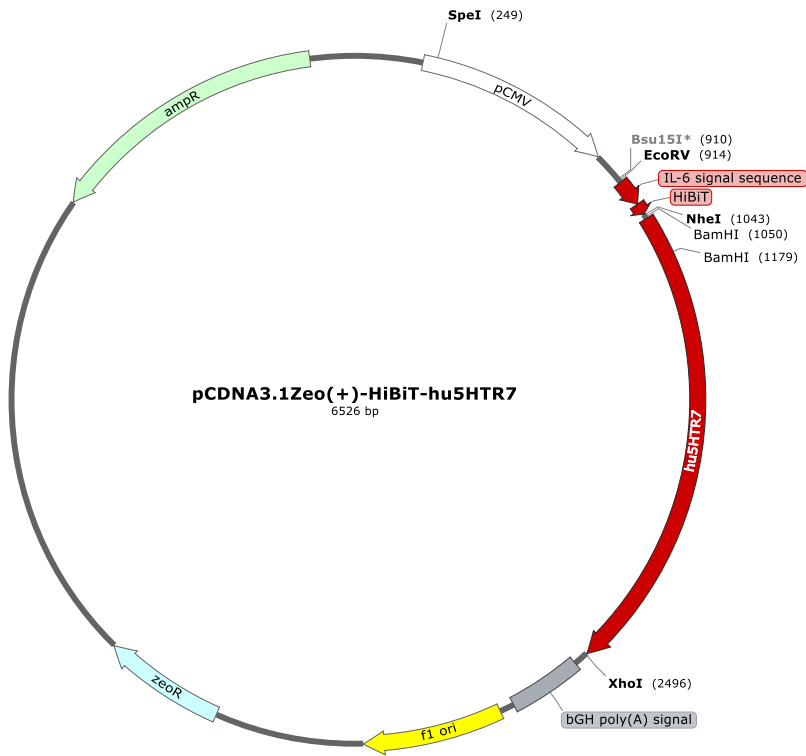


Figure S 19: Plasmid card of pCDNA3.1Zeo(+)-HiBiT-hu5HTR7

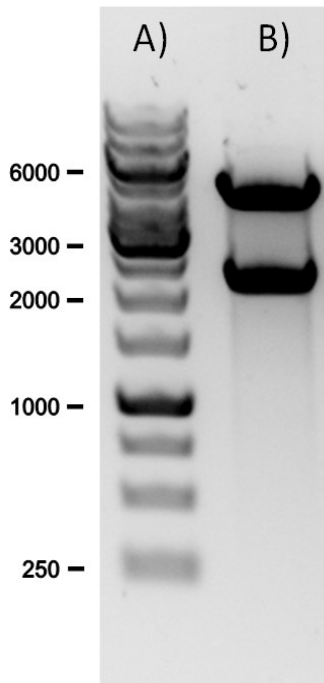
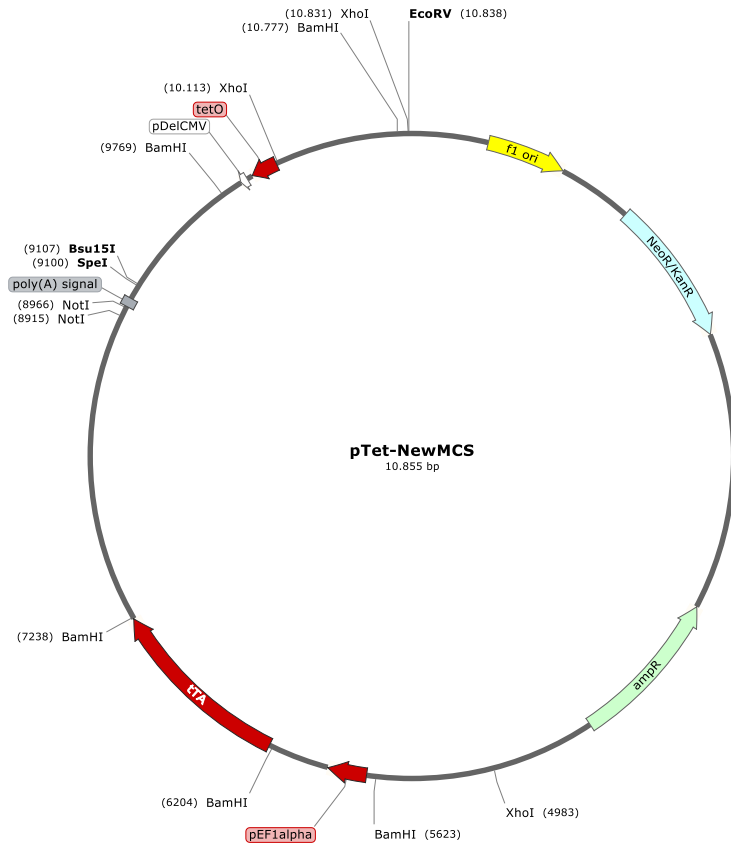
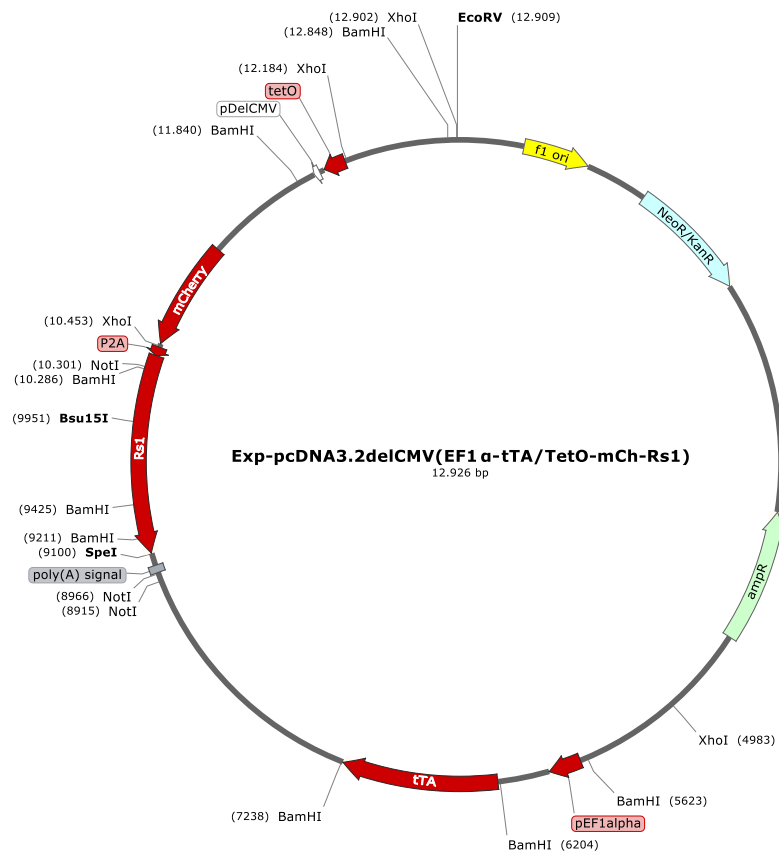


Figure S 20: Enzymatic digestion of pCDNA3.1Zeo(+)-HiBiT-hu5HTR7. A) GeneRuler 1 kb DNA ladder (Thermo Fisher Scientific) B) pCDNA3.1Zeo(+)-HiBiT-hu5HTR7 digested by Sall, expected band sizes 4304, 2188 and 34 (not visible) bp. Restriction enzyme was obtained from Thermo Fisher Scientific.

## Supplemental Material



**Figure S 21: Plasmid card of pTet-NewMCS**



**Figure S 22: Plasmid card of Exp-pcDNA3.2delICMV(EF1 $\alpha$ -tTA/TetO-mCh-Rs1)**



## Supplemental Material

### PROCEDURE

1. Set up a 50 ml bacterial culture in appropriate selective media and incubate on a shaker (250 rpm) at 37°C overnight.
2. Transfer bacteria to a 50 ml tube and spin at 4000xg at 4°C for 10 min.
3. Discard supernatant and resuspend pellet in 2 ml resuspension buffer with 50 ug/ml RNase freshly added.
4. Add 2 ml of lysis buffer, invert 3-4 times and incubate for 3 min at RT.
5. Add 2 ml of neutralization buffer and invert 3-4 times.
6. Distribute lysate into 1.5 ml Eppendorf tubes (~4 tubes) by pouring, not pipetting.
7. Spin at 13,200xg at RT for 10 min.
8. Collect supernatants in a 15 ml tube and discard pellets.
9. Add 1x volume of 96% ethanol (~5 ml).
10. Mix thoroughly for 5 sec.
11. Load the sample-ethanol mix onto 5 spin-columns in three sequential ~700 µl aliquots--after the addition of each aliquot, spin the column 30 sec at 13,200xg.
12. Discard flow-through.
13. Repeat step 11 until the entire sample is run through the spin-columns.
14. Wash with 500µl washing buffer and spin at 13,200xg at RT for 30 sec.
15. Discard flow-through.
16. Repeat step 14-15.
17. Do a final spin at 13,200xg at RT for 1.5 min.
18. Discard the old tube and put the column onto a new tube.
19. Add 30-35µl of ddH<sub>2</sub>O and incubate for 2 min at RT.
20. Spin at 13,200xg for 2 min to elute the DNA from column.
21. Combine the eluted DNA from all 5 columns in one tube (~175µl).
22. Measure DNA concentration.
23. Store samples at -20°C.

**Figure S 25: Miraprep protocol**

# Supplemental Material

## Required Material

Note Please make sure that the entire supplement is added to the Nucleofector®Solution. The ratio of Nucleofector®Solution to supplement is 4.5:1. For a single reaction use 82 µl of Nucleofector®Solution plus 18 µl of supplement to make 100 µl of total reaction volume.

- Supplemented Nucleofector®Solution at room temperature
- Supplied certified cuvettes
- Supplied plastic pipettes
- Supplied pmaxGFP®Vector
- Substrate of interest, highly purified, preferably by using endotoxin-free kits; A260 : A280 ratio should be at least 1.8
- 6-well culture dish or culture system of your choice
- For detaching cells: 0.5 mg/ml Trypsin and 0.2 mg/ml EDTA in PBS and supplemented culture media or PBS/0.5%BSA
- Culture medium: Minimum Essential Medium [ATCC®Cat. No. 30-2003] supplemented with 10%FCS and 1 mM sodium pyruvate [Lonza, Cat. No. BEL3-115E]
- Prewarm appropriate volume of culture medium to 37°C (1.5 ml per sample)
- Appropriate number of cells (1 x 10<sup>6</sup> cells per sample; lower or higher cell numbers may influence transfection results)

## 1. Pre Nucleofection®

### Cell culture recommendations

- 1.1 Replace media every 2 days
- 1.2 Passage cells at 80 – 90% confluency
- 1.3 Seed out 5 x 10<sup>6</sup> cells/25 cm<sup>2</sup> flask
- 1.4 Subculture 2 – 3 days before Nucleofection®
- 1.5 HEK-293 cells should not be used for Nucleofection® after passage number 20.
- 1.6 Optimal confluency for Nucleofection® 80 – 90% Higher cell densities may cause lower Nucleofection® Efficiencies

### Trypsinization

- 1.7 Remove media from the cultured cells and wash cells once with PBS; use at least same volume of PBS as culture media
- 1.8 For harvesting, incubate the cells -5 minutes at 37 °C with indicated trypsinization reagent (please see required material)
- 1.9 Neutralize trypsinization reaction with supplemented culture medium or PBS/0.5%BSA once the majority of the cells (>90%) have been detached

## 2. Nucleofection®

### One Nucleofection® Sample contains

1 x 10 <sup>6</sup> cells
1 – 5 µg plasmid DNA (in 1 – 5 µl H <sub>2</sub> O or TE) or 2 µg pmaxGFP®Vector or 30 – 300 nM siRNA (3 – 30 pmol/sample)
100 µl Cell Line Nucleofector®Solution V

- 2.1 Please make sure that the entire supplement is added to the Nucleofector®Solution
- 2.2 Prepare 6-well plates by filling appropriate number of wells with 1 ml of supplemented culture media and pre-incubate/equilibrate plates in a humidified 37°C/5%CO<sub>2</sub> incubator
- 2.3 Harvest the cells by trypsinization (please see 1.7 – 1.9)
- 2.4 Count an aliquot of the cells and determine cell density
- 2.5 Centrifuge the required number of cells (1 x 10<sup>6</sup> cells per sample) at 200xg for 10 minutes at room temperature. Remove supernatant completely
- 2.6 Resuspend the cell pellet carefully in 100 µl room-temperature Nucleofector®Solution per sample

Note Avoid leaving the cells in Nucleofector®Solution for extended periods of time (longer than 15 minutes), as this may reduce cell viability and gene transfer efficiency

- 2.7 Combine 100 µl of cell suspension with 1 – 5 µg DNA, 2 µg pmaxGFP®Vector or 30 nM – 300 nM siRNA (3 – 30 pmol/sample) or other substrates
- 2.8 Transfer cell/DNA suspension into certified cuvette (sample must cover the bottom of the cuvette without air bubbles), close the cuvette with the cap
- 2.9 Select the appropriate Nucleofector®Program Q001 (Q01 for Nucleofector®Device)
- 2.10 Insert the cuvette with cell/DNA suspension into the Nucleofector®Cuvette Holder and apply the selected program by pressing the X-button
- 2.11 Take the cuvette out of the holder once the program is finished
- 2.12 Immediately add ~500 µl of the pre-equilibrated culture medium to the cuvette and gently transfer the sample into the prepared 6-well plate (final volume 1.5 ml media per well). Use the supplied pipettes and avoid repeated aspiration of the sample

## 3. Post Nucleofection®

- 3.1 Incubate the cells in humidified 37°C/5%CO<sub>2</sub> incubator until analysis. Gene expression or down regulation, respectively, is often detectable after only 4 – 8 hours

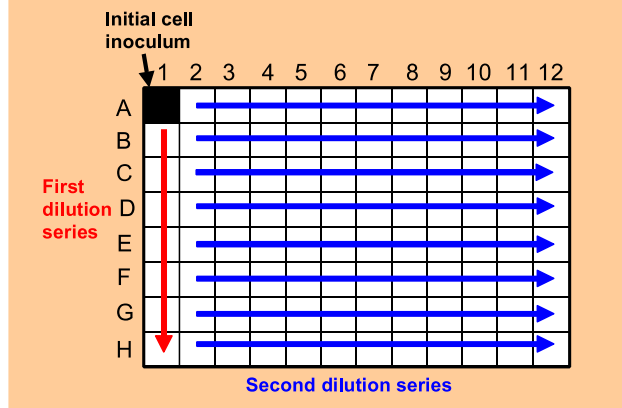
**Figure S 26: Electroporation protocol for HEK293 cells by amaxa GmbH.** For more detailed protocol visit: <https://knowledge.lonza.com/cell?id=46>

## Supplemental Material

### Procedure

1. Fill the reagent dispensing tray with 12mL of the appropriate culture medium, then using an 8-channel micropipettor add 100µL medium to all the wells in the 96 well plate except well **A1** (see diagram below) which is left empty.

**Figure 1. Initial plate setup.**



Adding 4000 cells in well A1 ( $2 \times 10^4$  cells/mL) is a good starting cell concentration. Increase this concentration for more difficult to grow cell lines.

Transferring clones directly from a well in a 96 well plate into a T-25 flask is not recommended. The cells may be unable to grow due to their inability to condition the larger volume of medium in the flask. Using some conditioned medium when subculturing the cells for the first time will also help them survive and grow.

2. Add 200µL of the cell suspension to well **A1**. (See Figure 1.) Then using a single channel pipettor quickly transfer 100µL from the first well to well B1 and mix by gently pipetting. Avoid bubbles. Using the same tip, repeat these 1:2 dilutions down the entire column, discarding 100µL from **H1** so that it ends up with the same volume as the wells above it.
3. With the 8-channel micropipettor add an additional 100µL of medium to each well in column 1 (giving a final volume of cells and medium of 200µL/well). Then using the same pipettor quickly transfer 100µL from the wells in the first column (**A1** through **H1**) to those in the second column (**A2** through **H2**) and mix by gently pipetting. **Avoid bubbles!**
4. Using the same tips, repeat these 1:2 dilutions across the entire plate, discarding 100µL from each of the wells in the last column (**A12** through **H12**) so that all the wells end up with 100µL of cell suspension.
5. Bring the final volume of all the wells to 200µL by adding 100µL medium to each well. Then label the plate with the date and cell type. Adding filtered conditioned medium (medium in which cells have been previously grown for 24 hours) to the wells can increase the success rate (cloning efficiency) for difficult to grow cells.
6. Incubate plate undisturbed at 37°C in a humidified CO<sub>2</sub> incubator.
7. Clones should be detectable by microscopy after 4 to 5 days and be ready to score after 7 to 10 days, depending on the growth rate of the cells. (See Figure 2 on page 3.) Check each well and mark all wells that contain just a single colony. These colonies can then be subcultured from the wells into

larger vessels. Usually each clone is transferred into a single well in a 12 well or 24 well plate.

**Figure S 27: Single-cell cloning protocol byCorning Inc.** For more detailed protocol visit: [https://www.corning.com/catalog/cls/documents/protocols/Single\\_cell\\_cloning\\_protocol.pdf](https://www.corning.com/catalog/cls/documents/protocols/Single_cell_cloning_protocol.pdf)



### 3. Nano-Glo® HiBiT Extracellular Assay Protocols

#### 3.A. Overview of the Nano-Glo® HiBiT Extracellular Detection System

The Nano-Glo® HiBiT Extracellular Detection System quantifies the amount of HiBiT tag that is accessible to the extracellular medium. The assay is compatible with most commonly used cell culture medium containing 0–10% serum and has been tested with DMEM, RPMI 1640, McCoy's 5A, MEM $\alpha$ , Opti-MEM® I, F-12 and CO<sub>2</sub>-Independent media. While the reagents have been designed to give a signal half-life of greater than 60 minutes at 22°C, different combinations of medium and serum may affect the background, signal, or signal decay rate (see Section 6.H). Additional information about the Nano-Glo® HiBiT Extracellular Detection System can be found in Section 6.

To achieve a linear assay performance at low light levels, the background luminescence must be subtracted from all readings. Background luminescence generally originates from two main sources: 1) reagent background from autoluminescence of the furimazine substrate and low levels of activity associated with the LgBiT protein, and 2) machine background from the luminometer. Reagent background can vary with media type, and is increased by both serum and cells (see Section 6.H). Therefore, for the most accurate measurements of low-abundance proteins, include a sample of untransfected or mock-transfected cells in the same medium to measure the assay background. For the greatest sensitivity, reduce the amount of serum by exchanging medium prior to the assay (see Section 6.I). Use an opaque, white tissue-culture plate to minimize cross-talk between wells and absorption of the emitted light. Ensure that the plates used are compatible with the instrument measuring luminescence.

#### 3.B. Preparing the Nano-Glo® HiBiT Extracellular Reagent

Calculate the amount of Nano-Glo® HiBiT Extracellular Reagent needed to perform the desired experiments. This usually constitutes a volume equal to the total amount of medium in wells, plus any extra required for dispensing. Dilute the LgBiT Protein 1:100 and the Nano-Glo® HiBiT Extracellular Substrate 1:50 into an appropriate volume of room temperature Nano-Glo® HiBiT Extracellular Buffer in a new tube. Mix by inversion.

For example, if 4ml of Nano-Glo® HiBiT Extracellular Reagent is needed, transfer 4ml of Nano-Glo® HiBiT Extracellular Buffer to a 15ml centrifuge tube and add 40 $\mu$ l of LgBiT Protein and 80 $\mu$ l of Nano-Glo® HiBiT Extracellular Substrate.

##### Notes:

1. The LgBiT Protein stock contains glycerol, which prevents it from freezing at –20°C. The viscosity of this solution may make accurate pipetting difficult. Pipet slowly and avoid excess solution clinging to the outside of the pipette tip. Use a positive displacement pipette, if possible.
2. If the Nano-Glo® HiBiT Extracellular Substrate or LgBiT Protein has collected in the cap or on the sides of the tube, briefly spin the tubes in a microcentrifuge.
3. We recommend preparing the Nano-Glo® HiBiT Extracellular Reagent fresh for each use. Once reconstituted, the reagent will lose about 15% activity over 8 hours and about 60% activity over 24 hours at room temperature. Unused reconstituted reagent may be stored at –80°C, –20°C or 4°C for later use, although there will be some loss of performance relative to freshly prepared reagent. At 4°C, the reconstituted reagent should lose less than 20% activity over 24 hours.

#### 3.C. General Protocol for Adding Nano-Glo® HiBiT Extracellular Reagent to Cells

1. Reconstitute the Nano-Glo® HiBiT Extracellular Reagent as described in Section 3.B.
2. Remove plates containing mammalian cells expressing a HiBiT-tagged protein from the 37°C incubator.  
**Optional:** To minimize well-to-well variability caused by differences in temperature, equilibrate the plate to room temperature (e.g., 5 minutes on a metal block).
3. Add a volume of Nano-Glo® HiBiT Extracellular Reagent equal to the culture medium present in each well, and mix. For example, add 100 $\mu$ l of Nano-Glo® HiBiT Extracellular Reagent to 100 $\mu$ l of cell culture medium.  
**Note:** Mix the samples by gently pipetting samples or placing the plate on an orbital shaker (300–500 rpm) for 3–10 minutes.
4. Measure luminescence 10 minutes after adding reagent. For a HiBiT tag placed within the protein sequence, longer incubation times may be necessary compared to terminal protein tagging. Measure luminescence using settings specific to your instrument. For 96-well plates on GloMax® instruments, integration times of 0.5–2 seconds are recommended. Longer integration times may improve data quality at lower levels of expression. The luminescence intensity will generally decay in a well-mixed sample with a signal half-life of 1–2.5 hours, depending on conditions (see Figure 8, Panel B; Figure 9 Panel B; and Figure 10, Panel B).

##### Notes:

1. To ensure luminescence is proportional to the amount of HiBiT-tagged protein present, subtract the assay background, especially when measuring low amounts of protein. Include untransfected or mock-transfected cells as background controls in your experiment (see Section 6.I).
2. Placing HiBiT in internal protein positions, like extracellular surface loops, may slow LgBiT and HiBiT equilibration. Increase reagent incubation times to compensate, if necessary.

**Figure S 28: Nano-Glo® HiBiT Extracellular Detection System protocol by Promega GmbH.** For more detailed protocol visit: <https://www.promega.com/-/media/files/resources/protocols/technical-manuals/500/nano-glo-hibit-extracellular-detection-system-technical-manual.pdf?la=en>

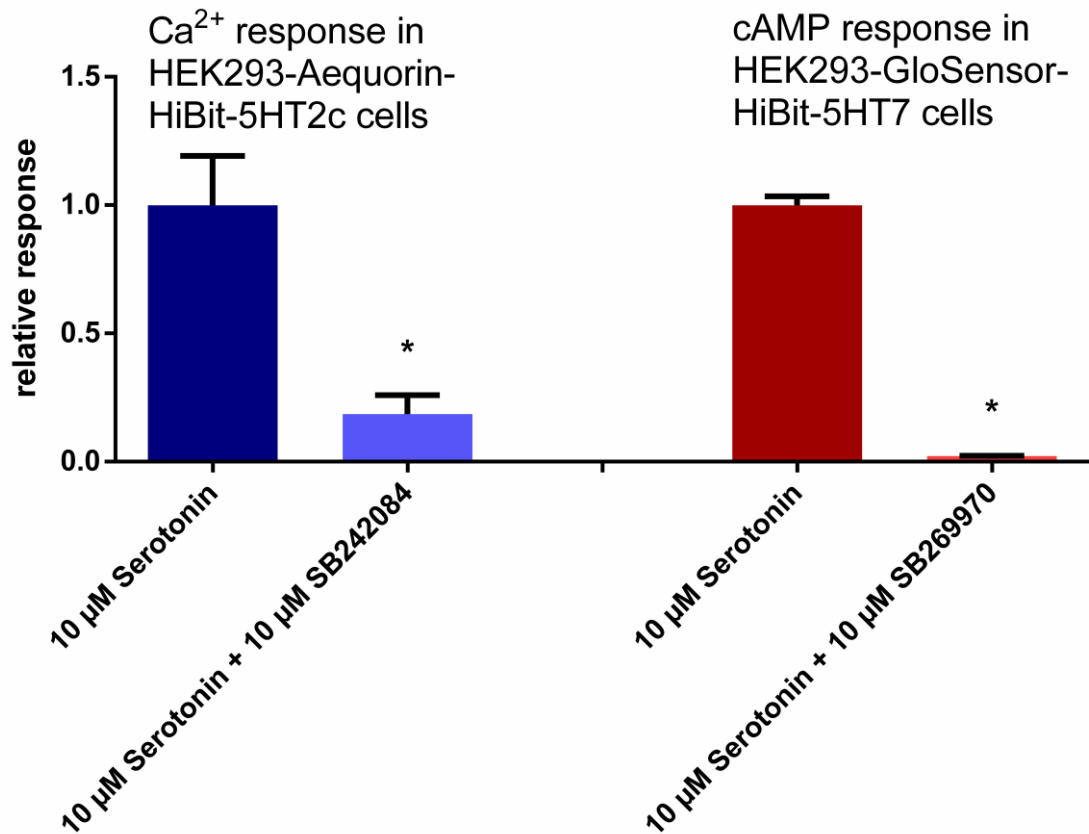


**Figure S 29: Determination of second messenger generation of 5-HT<sub>2c</sub> and 5-HT<sub>7</sub> receptors.** Stimulation was achieved with 10 μM Serotonin and blocking with selective antagonists (SB242084 for 5-HT<sub>2c</sub> and SB269970 for 5-HT<sub>7</sub>). Ca<sup>2+</sup> response was measured in HEK293-Aequorin-HiBit-5HT<sub>2c</sub> cells as described in 4.11 and cAMP response in HEK293-GloSensor-HiBit-5HT<sub>7</sub> cells described as followed. Data are shown as mean + SEM, n ≥ 10. Marked values with p ≤ 0.05 are significantly different from control, determined by Student's unpaired t-test.

## Supplemental Material

### Determination of cAMP response in HEK293-GloSensor-HiBiT-5HT7 cells

#### Experimental setup

Luminescence measurements were conducted on a Tecan Infinite® M200 PRO plate reader operated by Tecan i-control ver. 1.10.

#### Cell measurements

HEK293-GloSensor-HiBiT-5HT7 cells were seeded in a density of 25,000 cells per cm<sup>2</sup> on a white 96-well plate with a transparent flat bottom for luminescence measurements three days prior to the experiment. Beforehand, the plates were coated using 50 µl of 0.1 mg/ml PDL solution for 30 min at 37 °C and washed three times with 50 µl PBS. Two hours before assay start, the culture medium was replaced with 25 µl substrate solution (4% GloSensor™ cAMP reagent in 1:1 HEK293 culture medium : HEPES buffered Hanks' Balanced Salt Solution (HBSS)) with or without 20 µM SB269970. The cells were incubated for 1 h at 37 °C and 5% CO<sub>2</sub> and another 1 h at RT in the plate reader to reach the optimum temperature of 24 °C for the firefly luciferase. Basal chemiluminescence was measured for this hour. The measurement protocol was paused and stimulation with 25 µl of 20 µM Serotonin solution in 1:1 HEK293 culture medium: HEPES buffered HBSS was carried out. The measurement of chemiluminescence was continued for further 60 min in intervals of 2 min.

#### Data analysis

For the resulting measurement curve of RLU over time [min] the area under the curve (AUC) was determined via trapezoidal rule (exemplary calculation see section 4.11). AUC was calculated for the full measurement time of 120 min. Resulting AUC values for cells treated with 10 µM SB269970 were normalized to untreated cells. Statistical significance was determined by Student's unpaired t-test with a p-value < 0.05.

## Supplemental Material

### Determination of hyperoside and hyperforin in STW3-VI®

For both substances, the amounts of 0.5, 0.75 and 1 µg were analyzed using HPLC gradient 7 (Table 7). Peak integration resulted in the following peak areas (Table S 1).

**Table S 1: HPLC determination of hyperoside and hyperforin reference standards**

Substance	Amount [µg]	Mean peak area [mAu*s]
Hyperoside	0.5	3035.7
	0.75	4395.1
	1	5838.4
Hyperforin	0.5	345.2
	0.75	534.4
	1	703.8

Linear regression of those values resulted in the following equations:

Hyperoside:

$$y = 5605.2 * x + 219.2 \quad \text{with } R^2 = 0.9997$$

Hyperforin:

$$y = 717.2 * x - 10.1 \quad \text{with } R^2 = 0.9990$$

Injecting 20 µl of STW3-VI® in a concentration of 1 mg/ml yielded the following values for peak area. Using the equations displayed above the amount of hyperoside and hyperforin in STW3-VI® was calculated (Table S 2).

**Table S 2: Calculation of hyperoside and hyperforin in STW3-VI®**

Substance	Peak area [mAu*s]	Amount in 20 µl [µg]	Concentration in 1 mg/ml STW3-VI® [µM]
Hyperoside	3480.7	0.582	53.3
	2644.4	0.433	
	2856.9	0.471	
Hyperforin	370.7	0.531	36.8
	246.0	0.357	
	203.6	0.298	

A concentration of 0.02 mg/ml STW3-VI® roughly equals 1.0 µM for both hyperoside and hyperforin.

## 10. Danksagung

Ohne weitreichende Unterstützung wäre das Schreiben der Dissertationsschrift in dieser Form nicht möglich gewesen. Daher möchte ich diese Stelle nutzen, um mich ganz herzlich zu bedanken bei

Prof. Dr. Hanns Häberlein, für die Möglichkeit diese Arbeit unter seiner Leitung anfertigen zu dürfen, die unentwegte Unterstützung und die hervorragende Atmosphäre, die er in seinem Arbeitskreis geschaffen hat.

Prof. Dr. Gerd Bendas für die freundliche Übernahme des Koreferats.

PD Dr. Sebastian Franken für ein stets offenes Ohr, viele konstruktive und auch kritische Diskussionen, neue Denkansätze und kostbare Ratschläge.

der Firma Steigerwald Arzneimittelwerk GmbH (Bayer Consumer Health) aus Darmstadt und Frau Dr. Christiane Kolb für die finanzielle Unterstützung dieser Arbeit.

allen meinen Arbeitskolleginnen und -kollegen aus dem Arbeitskreis Häberlein für die Unterstützung und die herausragende Zeit bei und abseits der Arbeit.

Dr. Thomas Sorkalla für die außerordentliche Unterstützung bei Fluoreszenz-Korrelations-Spektroskopie Experimenten.

allen Mitarbeitern des Instituts für die gute Zusammenarbeit, von Lumineszenz-Messungen im Arbeitskreis von Prof. Dr. Voss bis hin zu massenspektrometischen Untersuchungen unter Anleitung von Dr. Marc Sylvester und PD Dr. Sebastian Franken.

meinen Eltern Elisabeth und Bernhard, meinem Bruder Michael und seiner Frau Lisa und allen weiteren Familienmitgliedern auf deren Unterstützung ich in jeder Lebenslage zählen kann.

meinen Freunden, egal an welchem Ort der Welt, für die schöne gemeinsame Zeit.

## 11. Publikationen und Poster

### Publikationen

Bussmann, H. Schulte-Michels, J. Bingel, M. Meurer, F. Aatz, S. Häberlein, F. Franken, S. Häberlein, H. A comparative study on the influence of an ivy preparation and an ivy/thyme combination on the  $\beta$ 2-adrenergic signal transduction. *Heliyon* **6**, e03960 (2020). doi: 10.1016/j.heliyon.2020.e03960

Schulte-Michels, J. Wolf, A. Aatz, S. Engelhard, K. Sieben, A. Martinez-Osuna, M. Häberlein, F. Häberlein, H.  $\alpha$ -Hederin inhibits G protein-coupled receptor kinase 2-mediated phosphorylation of  $\beta$ 2-adrenergic receptors. *Phytomedicine* **23**, 52–57 (2016). doi: 10.1016/j.phymed.2015.12.001

### Poster

- Nov. 2019 Aatz, S. Kolb, C. Häberlein, H. Influence of St. John's wort extract STW3-VI, hyperoside, and hyperforin on the agonist-induced internalization of 5-HT<sub>2A</sub> receptors  
DGPPN Congress, Berlin
- Nov. 2018 Aatz, S. Kolb, C. Häberlein, H. Influence of St. John's wort extract STW3-VI, hyperoside, and hyperforin on the binding behavior and lateral mobility of 5-HT<sub>2A</sub>-receptors  
DGPPN Congress, Berlin
- Mär. 2018 Aatz, S. Sorkalla, T. Kolb, C. Aziz-Kalbhenn, H. Franken, S. Häberlein, H. Synthesis and characterization of a novel, highly affine, and selective fluorescence-labeled 5-HT<sub>2A</sub> receptor agonist  
26th European Congress of Psychiatry, Nice
- Okt. 2017 Aatz, S. Sorkalla, T. Kolb, C. Aziz-Kalbhenn, H. Franken, S. Häberlein, H. Development of a selective fluorescence-labeled ligand for binding studies and characterization of lateral mobility of 5-HT<sub>2A</sub>-receptors on living cells  
WPA XVII World Congress of Psychiatry, Berlin